Doctoral School in Life and Humanoid Technologies
Course in “Neuroscience and Brain Technologies”
Cycle XXVII

Lamin B1 levels modulates cell specification during embryonal neurogenesis

PhD Student
Sameehan Uday Mahajani

Supervisor
Dr. Laura Gasparini

ISTITUTO ITALIANO
DI TECNOLOGIA

UNIVERSITÀ DEGLI STUDI
DI GENOVA

Dedicated to my father, Uday K Mahajani.

DECLARATION

I, Sameehan Uday Mahajani declare that this dissertation is my own work and all the sources have been quoted and acknowledged by means of complete references.

Sameehan Uday Mahajani

Acknowledgements

I would like to dedicate this thesis to my dad, Late Mr. Uday K Mahajani, who would have been extremely happy to see me doing quality research in a very reputed institute. With his memories forever with me, I hope to make him proud.

I would like to gratefully and sincerely thank Dr. Laura Gasparini, for her untiring support and guidance. Most importantly, she encouraged me to grow as a researcher and an independent thinker. I owe my gratitude to Dr. Caterina Giacomini for her constant motivation. I would like to thank her for teaching me several new techniques and helping me to understand how to better design experiments to get optimum results. I appreciate the fact that she explained me the simplest concepts with great enthusiasm and hope she would forgive me for any mistakes I may have made during my lab work. I have learned a lot under their guidance and would like to wish both of them the very best in the future.

I would also like to thank all the people working in the group, Nadia Mazzaro, Erica Barini, Nahuai Badiola and Denise Ferrera, for helping me with various experiments. I am indebted to my friends and flat-mates for supporting me throughout the process.

I would like to express my deepest appreciation to my mother, Dr. Sarita Uday Mahajani and my sister, Sameera Mahajani-Lonkar and my brother-in-law, Gajanan Lonkar for constantly encouraging me towards excellence.

I have saved the last words of acknowledgment for the most important person in my life, my better half Debia Wakhloo who has been by my side all these years. She has always been a part of intense scientific discussion and without her unwavering love and understanding this wouldn't have been possible.

Abstract

Lamin B1 (LMNB1) is a type V intermediate filament protein and is one of the major components of the nuclear lamina. It has been shown that LMNB1 acts as a modifier gene affecting the risk of Neural Tube Defects in mice and humans, in which synonymous and non-synonymous missense variants of LMNB1 resulting in protein loss-of-function have been observed. Consistently, it has been demonstrated that experimental ablation of LMNB1 deeply impairs neurogenesis during embryonic development in the mouse. However, how LMNB1 protein expression regulates cell fate commitment at the cellular and molecular levels is still undetermined. Here, we investigate whether LMNB1 influences neuronal and astrocyte differentiation in cultured Neural Stem Cells (NSCs) from the dorsal forebrain of E12 embryos of wild type (WT) and *Lmnb1*$^{\Delta/\Delta}$ mice. We find that LMNB1 protein levels play a key role in regulating the differentiation rate of NSCs into neurons and astrocytes but not oligodendrocytes. In fact, LMNB1 deficiency significantly reduces the number of neurons and increases the number of astrocytes originating from NSCs, without altering oligodendrocyte numbers. Conversely, LMNB1 overexpression significantly increases the rate of NSC differentiation into neurons, but does not change the numbers of both astrocytes and oligodendrocytes. Apoptotic features are undetectable in NSC-derived cells, indicating that the observed changes are not due to altered cellular survival. Nuclear abnormalities (i.e. reduced nuclear area and circularity) are present only in LMNB1-deficient NSC-derived neurons, but not astrocytes and oligodendrocytes, nor LMNB1 overexpressing neurons. We also find that LMNB1 protein levels affect the differentiation of NSCs derived neurons. In fact, both LMNB1-deficiency and overexpression significantly alter axonal length of NSCs-derived neurons, indicating that the protein levels of LMNB1 regulate axonal outgrowth. Moreover, using quantitative RT-PCR, we elucidate that a defective Notch signaling pathway is responsible for the impaired cell fate commitment observed in *Lmnb1*$^{\Delta/\Delta}$ mice. Expression levels of certain Notch transcription factors are significantly altered

when in Lmnb1 deficient NSCs during the course of differentiation. After determining the defects in NSC differentiation in *Lmnb1*$^{\Delta/\Delta}$ mice, we also evaluated if loss of LMNB1 can cause defects in neuronal migration. Using in utero electroporation, we observed a defect in neuronal migration when Lmnb1 was either absent or overexpressed. The *in vitro* data of astrocytic vs neuronal cell fate was also confirmed using *in vivo* immunohistochemistry analysis, where we observed a reduced cortical thickness due to significantly reduced number of glutamatergic neurons and increase in the area of astrocytic maker GFAP^{+} when Lmnb1 was knockdown down using in utero electroporation with Sh-Lmnb1. These results indicate that LMNB1 plays a key role in cell fate commitment and neuronal migration during embryonic neurogenesis and that finely tuned levels of the protein are required to achieve proper morphological properties of NSCs-derived neurons.

INDEX

LIST OF FIGURES

LIST OF TABLES

LIST OF ABBREVIATIONS

ABBREVIATION	DESCRIPTION
ADLD	Autosomal Dominant Leukodystrophy
bFGF	Basic Fibroblast Growth Factor
CNS	Central Nervous System
CP	Cortical Plate
DAPI	4’,6’-diamidino-2-phenylindole
DCX	Doublecortin
DIV	Days In Vitro
DLL4	Delta-Like Ligand 4
E11	Embryonic Day 11
EDFC	Embryonic stem cell-Derived Fibroblast-like Cells
EGF	Epidermal Growth Factor
EGFP	Enhanced Green Fluorescent Protein
ES/ESC	Embryonic Stem Cells
GE	Ganglionic Eminence
GFAP	Glial Fibrillary Acidic Protein
iPSC	Human Induced Pluripotent Stem Cells
IZ	Intermediate Zone
LIF	Leukemia Inhibiting Factor
LMNB1	Lamin B1
LV	Lateral Ventricle
MEF	Mouse Embryonic Fibroblasts

MGE	Medial Ganglionic Eminence
MRI	Magnetic Resonance Imaging
MZ	Marginal Zone
NEP	Neuroepithelial
NGN1	Neurogenin 1
NICD	Notch Intracellular Domain
NPC	Nuclear Pore Complex
NSC	Neural Stem Cells
NTD	Neural Tube Defects
NUP	Nucleoporins
PBS	Phosphate-Buffered Saline
PCR	Polymerase Chain Reaction
PDGFRα	Alpha-type Platelet-Derived Growth Factor Receptor
PFA	Paraformaldehyde
PLL	Poly-L-Lysine
PP	Pre-Plate
qRT-PCR	Quantitative Real Time Polymerase Chain Reaction
SHH	Sonic Hedgehog pathway
SP	Sub-Plate
SVZ	Sub-Ventricular Zone
VZ	Ventricular Zone
WT	Wild Type

INTRODUCTION

1.1 Lamins and associated disorders

Lamins are type V intermediate filament proteins which are the key structural components of the nuclear lamina. They form a meshwork which lies beneath the inner nuclear membrane giving structural integrity to the nucleus. Lamins also play an important role in nuclear architecture, DNA replication and gene expression *(Vergnes et al, 2004)*. Lamins contain a highly conserved α-helical central rod domain and head and tail domains (Fig. 1). Moreover, lamins contain the nuclear localization signals (NLS) in the tail domains *(Dauer and Worman, 2009).*

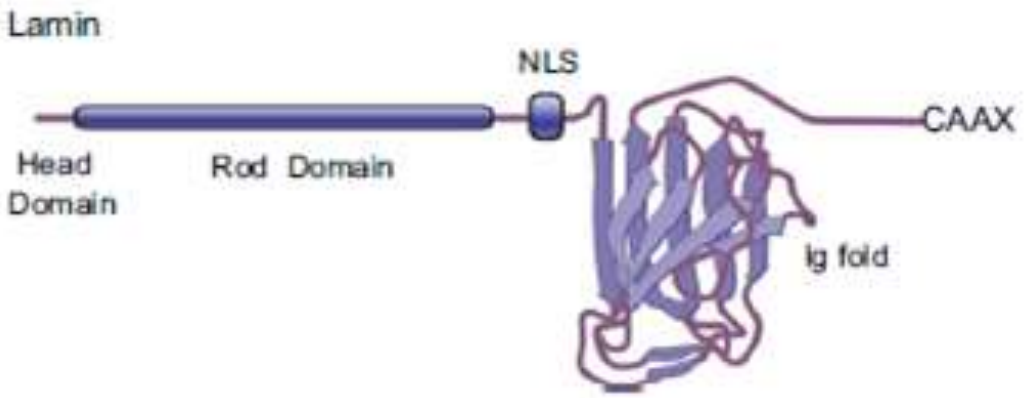

Figure 1. Structure of Lamins
Adapted from Dauer and Worman, 2009.

There are three genes which encode lamins namely; *LMNA* gene encodes Lamin A and Lamin C, by alternative RNA splicing, whereas *LMNB1* encodes Lamin B1 protein and *LMNB2* encodes Lamin B2 protein. There have been various disorders reported which are related to the mutation caused to Lamin A and Lamin C genes. Disorders like cardiomyopathy, peripheral neuropathy and progeria have been associated with mutations in LMNA gene *(Dauer and Worman, 2009)*. The mutation in LMNA gene is suggested to cause abnormal structure of the nucleus and is also implicated in DNA synthesis and transcription, further leading to various disorders.

It has been reported that the duplication in LMNB1 gene leads to adult-onset Autosomal Dominant Leukodystrophy (ADLD; *Padiath et al, 2006)*. ADLD is a demyelinating progressive fatal disease first described in an American-Irish kindred *(Eldridge et al, 1984)*. In 2006, it was reported that ADLD is caused by a duplication of the LMNB1 gene resulting in an increased expression of LMNB1 mRNA and protein (Fig. 2; *Padiath and Fu, 2010*; *Padiath et al, 2006*). Autonomic symptoms like bladder dysfunction, hypotension with decreased sweating is observed in the fourth-fifth decade of life, which is followed by cerebellar and pyramidal abnormalities and cognitive decline. These patients were frequently diagnosed as having chronic progressive multiple sclerosis *(Eldridge et al, 1984)*. However, magnetic resonance imaging (MRI) showed symmetric widespread demyelination of the central nervous system (CNS) occurring in the absence of an autoimmune response. ADLD disorders shows characteristic features of preservation of oligodendrocytes in the presence of demyelination *(Lin et al, 2014)*. Moreover, a variant form of disorder without autonomic symptoms at onset and sparing of cerebellar white matter with MRI was described in a single Italian family, in which LMNB1 expression was increased despite the absence of point mutations or copy number variations of LMNB1 gene *(Brussino et al, 2010)*. Most hereditary leukodystrophies were either autosomal recessive or X-linked recessive with an early disease onset age. However, ADLD was observed to be highly penetrant, autosomal dominant with an adult onset *(Coffeen et al, 2000).*

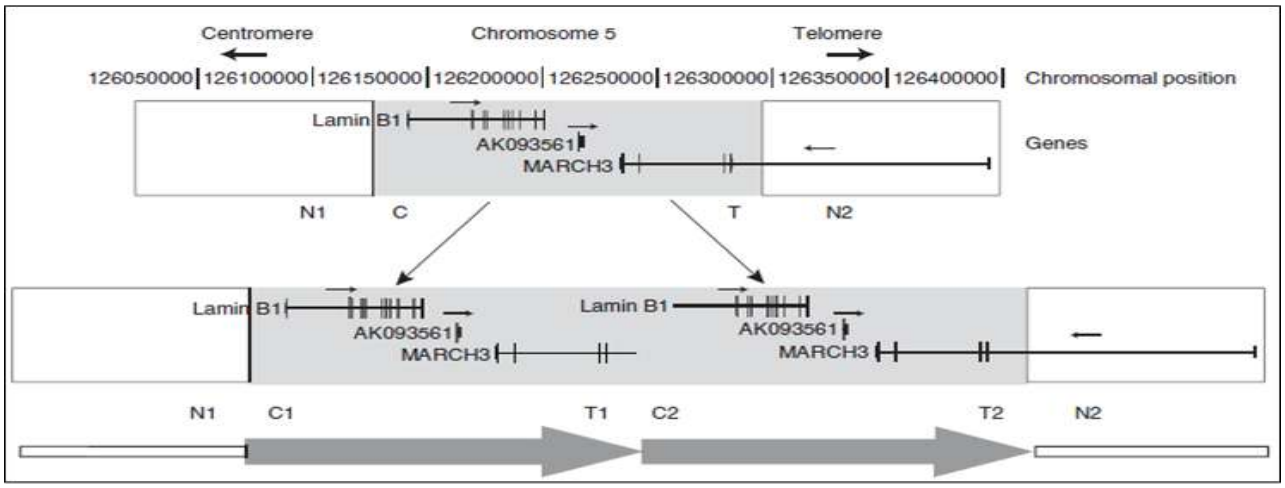

Figure 2. Duplication of LMNB1 causes ADLD.
Adapted from Padiath et al, 2006.

1.2 ADLD animal models

When LMNB1 gene was implicated in the ADLD, the authors decided to observe the effect of Lmnb1 overexpression in D. melanogaster and in vitro model systems *(Padiath et al, 2006)*. Transgenic flies were generated using *lamin* Dm_0 gene which shares 39% sequence identity to the human LMNB1. These transgenic flies showed high degree of lethality, however the ones that survived showed severely deformed eyes which were smaller size with almost complete lack of pigmentation. When the authors specifically expressed *lamin* Dm_0 in neuronal or glial tissues, it resulted in complete lethality. However, when they overexpressed LMNB1 in vitro using HEK293 cell lines, they observed an increase in the surface area of the nuclear envelope accompanied by extensive folding and blebbing of the nuclear membrane *(Padiath et al, 2006).*

In 2004, when the first knockout mouse model of Lmnb1 was generated, the authors observed that the Lmnb1 deficient mice survived embryonic development but died at birth with defects in lung and bone *(Vergnes et al, 2004).* This mouse model was also used in our project. This mouse model was generated by inserting a mutation in the intron 5 of *Lmnb1* resulting in an mRNA fusion

transcript containing the first five exons joined in-frame to a β-geo reporter gene. The mutant lamin B1 protein contained the amino-terminal head domain and a truncated α-helical central rod domain lacking the carboxyl-terminal 273 aa of lamin B1. The authors first generated an Embryonic Stem (ES) cell line containing this mutant Lmnb1, which was then injected into mouse blastocysts. The off-springs were then bred to produce heterozygous $Lmnb1^{+/\Delta}$ mice, which survived and used for further breeding to obtain a homozygous $Lmnb1^{\Delta/\Delta}$ mice. When the authors cultured primary fibroblasts from $Lmnb1^{+/+}$ and $Lmnb1^{\Delta/\Delta}$ embryos, they observed severe nuclear abnormalities in $Lmnb1^{\Delta/\Delta}$ cultured fibroblasts such as large blebs and de-localization of others lamins like Lamin A/C *(Vergnes et al, 2004).*

Various reports have been published suggesting that LMNB1 regulates nuclear mechanisms and integrity *(Lammerding et al, 2006)* and also interacts with chromatin determining chromosome segregation *(Guelen et al, 2008; Malhas et al, 2007).* It has also been reported to regulate gene expression through mRNA synthesis *(Malhas et al, 2007; Tang et al, 2008)* and splicing *(Jagatheesan et al, 1999).*

In rodent models, Lmnb1 is highly expressed in brain *(Broers et al, 1997; Tunnah et al, 2005)*, with varying expression during neurogenesis and neuronal differentiation. The expression of Lmnb1 has been reported to be at its peak during birth *(Lin and Fu, 2009; Takamori et al, 2007).*

It has been reported that LMNB1 is overexpressed in ADLD patient fibroblasts, with no change in other types of Lamins. The overexpression of LMNB1 is specifically at the nuclear lamina and it enhances nuclear stiffness *(Ferrera et al, 2014)*. When the authors transfected cell lines such as HEK293 and N2A, they observed that overexpression of LMNB1 causes similar mechanical phenotype as in the patient fibroblasts. In a type of rescue experiment, when they knockdown the levels of LMNB1 using ShRNA, they were capable of restoring the elasticity of the nuclei from patient

fibroblasts similar to the levels of control fibroblasts. The authors suggest that overexpression of LMNB1 may alter nuclear signaling as the cells display a reduced nuclear ion channel open probability on voltage-step application *(Ferrera et al, 2014)*.

Recently, it has also been published that deregulation of Lmnb1 expression might induce modified splicing of several genes, which could suggest an alteration of mRNA processing as one of the pathogenic mechanism in ADLD *(Bartoletti-Stella et al, 2015)*. In this study, the authors used ADLD patient fibroblasts to perform Gene Set Enrichment Analysis (GSEA), and observed that overexpression of LMNB1 is associated with dysregulation of genes involved in the immune system, neuronal and skeletal development. They observed that RAVER2, which codes a putative transcription regulator of the splicing repressor polypyrimidine tract binding protein (PTB), was upregulated in ADLD patient fibroblasts. Similar observations were made in mutant mice with different Lmnb1 expression levels confirming that *Raver2* expression was dependent on Lmnb1 in neural tissues *(Bartoletti-Stella et al, 2015)*.

It has been reported that a polarized mechanics of fibroblast cytoskeleton is essential for the directed cell migration *(Kole et al, 2005)*. The authors observed mechanical stiffening of both leading lamella and perinuclear region depends on the cytoskeleton reorganization produced by motility of the fibroblasts. When they disrupted the microtubule network of these fibroblasts, they observed an arrest of cell migration and loss of subcellular mechanical polarization, suggesting that cell migration is coordinated through microtubules *(Kole et al, 2005; Tobwin et al, 2009)*.

1.3 Lamin B1 role in embryonic development

Various studies over the past few years have reported the importance of Lmnb1 during embryonic development. In 2011, it was reported that Lmnb1-deficient embryos show abnormal cortical layering and reduced cortical size as compared to their wild type (WT) littermates *(Coffinier et al, 2011)*. The abnormal cortical layering was indicated based on the impaired position of layer specific neurons in Lmnb1-null ($Lmnb1^{\Delta/\Delta}$) cortical plate as compared to $Lmnb1^{+/+}$ embryos. However, the reason for abnormal cortical layering is not known. The authors suggest that it might be due to impaired neuronal migration *(Coffinier et al, 2011)*.

It has also been reported that type B- Lamins are not required for self-renewal and pluripotency by mouse Embryonic Stem Cells (ESCs), but are essential for proper organogenesis *(Kim et al, 2011)*. They also suggest that defects in spindle orientation in neural progenitor cells and migration of neurons are most likely causes of brain disorganization observed in $Lmnb1^{\Delta/\Delta}$ embryos.

Moreover, the role of Lmnb1 in development was further illustrated in 2012 and 2013, where it was published that Lmnb1 gene acts a modifier gene for the risk of Neural Tube Defects (NTDs) in mice *(De Castro et al, 2012)* and in humans *(Robinson et al, 2013)*. After performing DNA sequencing on 239 NTD patients, they authors identified 5 synonymous and 3 non-synonymous (missense) variants of Lmnb1. They suggest that reduction of one glutamic acid residue in Lmnb1 can cause significant reduction in the stability of Lmnb1 interaction with the nuclear lamina *(De Castro et al, 2012; Robinson et al, 2013)*.

1.4 Neural Stem Cells

NSCs are defined as multipotent, self-renewing progenitor cells. However, in the CNS these cells can generate neurons, astrocytes or oligodendrocytes *(Anderson, 2001).* In vitro, these NSCs are

obtained from the forebrain of E11.5 embryos and then cultured to obtain clump of cells called neurospheres with the addition of growth factors. Usually, differentiation can be initiated in these cells based on the plating conditions or medium conditions provided. For example, to obtain a higher percentage of neurons, these neurospheres are triturated and plated on Laminin coated coverslips. To induce astrocyte differentiation, these neurospheres have to be cultured in the presence of Leukemia Inhibiting Factor (LIF), whereas oligodendrocytes differentiation is generally done using poly-L-Lysine (PLL) coated coverslips, but the differentiation takes a longer time. NSCs remain in their proliferative state if the medium is supplemented with growth factors like Epidermal Growth Factor (EGF) and basic Fibroblast Growth Factor (bFGF) (Fig. 3).

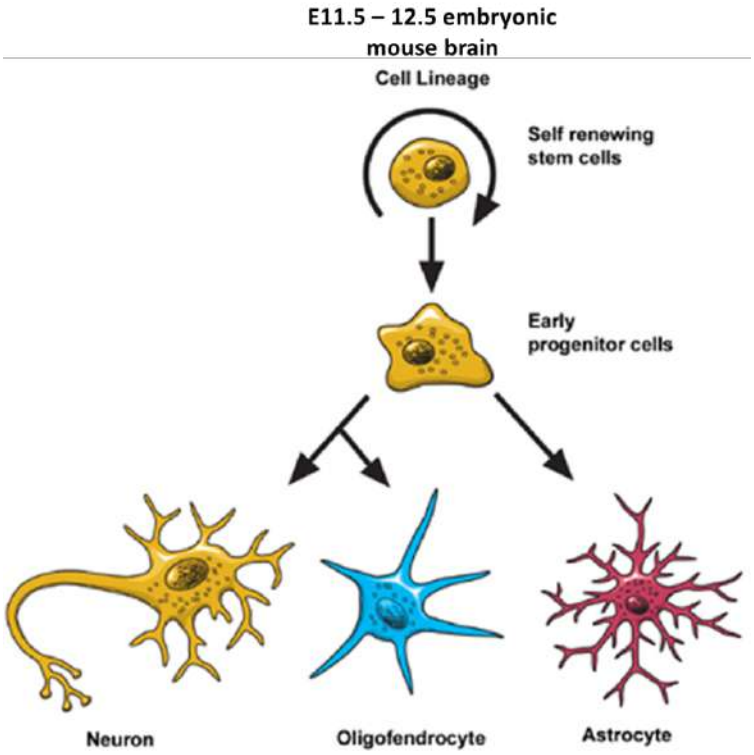

Figure 3. Stem cells differentiate to produce various type of nerve cells.
Adapted from ninds.nih.gov.

In 2010, it was reported that NSCs show higher deformability which is dependent on intracellular connectivity. The authors performed micropipette aspiration to test the mechanics of the nuclei of two type of stem cells namely, CD34+ hematopoietic stem cells and bone marrow stromal cells. They observed the nuclei of the CD34+ cells are stiffer than the nuclei of the bone marrow stromal cells, which represents higher nuclear volume per cell volume ratio *(Ribeiro and Dahl, 2010).*

It has been known that stem cell differentiation during embryonic development involves changes in gene expression structural reorganization within the nucleus. It was reported that the nuclei of newly generated stem cells are physically plastic and are more pliable than the nuclei of differentiated cells. The authors observe that the nuclei of ESCs are highly deformable and stiffen 6-fold through terminal differentiation, whereas the nuclei from hematopoietic stem cells possess an intermediate stiffness and deform irreversibly. When they knockdown Lamin A/C in human epithelial cells, they observe that the nuclei of these lamin-deficient cells are mostly fluid-like. The authors, therefore, conclude that the nucleus of stem cells are set by nucleoplasm/chromatin structure, whereas the extent of deformation is modulated by the lamina *(Pajerowski et al, 2007)*.

It has been reported that defects in nuclear envelope can cause stem cell dysfunction in old mice. The authors hypothesized that as aging is associated with abnormal stem cell homeostasis, the nuclear envelope alterations could impact the stem cell compartment. They used *Zmpste24*-null mice, which is one of the model for progeria and exhibits nuclear lamina defects. They observe an aberrant nuclear architecture in epidermal stem cells from these mice, which leads to defect in the number and proliferative capacity of these stem cells. They also observe signaling pathways like Wnt are altered in *Zmpste24*-deficient mice, thereby indicating at a link between age-related nuclear envelope defects and stem cell dysfunction *(Espada et al, 2008)*.

Culture conditions in vitro or physiological conditions in vivo causes various signaling pathways to become active and further lead to proliferation or differentiation of these NSCs *(Wen et al, 2009)*.

1.5 Signaling pathways involved in differentiation

Few important pathways involved during the course of differentiation are mentioned below as they have been studied in this project.

1.5.1 Wnt Signaling pathway. Wnt signaling pathway plays a crucial role in the control of cell growth and differentiation during CNS development *(Zechner et al, 2003)*. Various reports have showed that active Wnt signaling induces neuronal and astrocytic differentiation but inhibits oligodendrocyte differentiation *(Zechner et al, 2003; Kasai et al, 2005; Machon et al, 2007).* Wnt signaling is also essential for the normal proliferation of NSCs *(Hirsch et al, 2007).*

1.5.2 Notch Signaling pathway. One of the most important and most studied pathways involved in the regulation of cell fate commitment is Notch signaling. This pathway has been reported to promote astrocyte differentiation by inhibiting neurogenesis and oligodendrocyte differentiation *(Louvi et al, 2006)*. This pathway was mainly studied in this project. Notch signaling is triggered by cell to cell contact, where a ligand (Delta1 or Jagged1) present on the membrane of one cell interacts with the Notch1 receptor on the other cell membrane. The ligand binding triggers a series of proteolytic events which leads to cleavage of Notch to generate Notch intracellular domain (NICD). This active NICD contains nuclear import signals, thereby translocates inside the nucleus through importins alpha 3,4 and 7 with the help of Nuclear Pore Complexes (NPCs) *(Lai, 2002; Huenniger et al, 2010)*. After translocation inside the nucleus, Notch signaling activates expression of various transcription factors like HES1 and HES5 (Fig. 4), which is further responsible

for promoting astrocyte differentiation and inhibiting neuronal differentiation *(Grandbarbe et al, 2003).* Notch signaling also influences various downstream factors like Neurogenin1 which is responsible for promoting neurogenesis *(Grandbarbe et al, 2003)*.

1.5.3 JAK-STAT Signaling pathway. STAT3 mediated signaling is known to be one of the main mechanisms which promotes astrocyte differentiation by inhibiting neurogenesis *(Yanagisawa et al, 1999)*. However, it has been reported that STAT3 signaling can only induce astrogenesis in the presence of an active Notch signaling pathway *(Taylor et al, 2007)*. However, this pathways plays an important role in promoting NSCs proliferation *(Fukuda et al, 2007)*.

1.5.4 SHH Signaling pathway. Sonic hedgehog signaling pathway has been reported to promote neuronal as well as astroglial differentiation *(Hatton et al, 2006)*. More importantly, Shh signaling is reported to control cell death by regulating the expression of downstream genes such as N-Myc and cyclin D1 which promotes cell survival *(Fuccillo et al, 2006).*

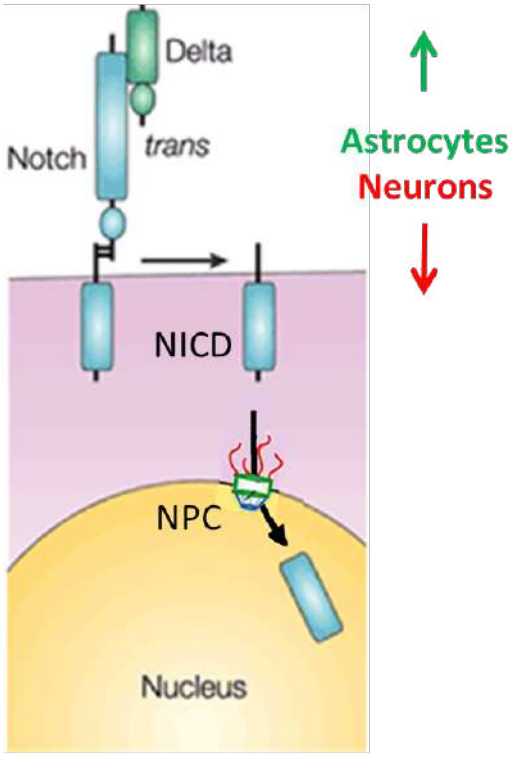

Figure 4. Notch signaling in NSCs.
Modified from Meshorer and Gruenbaum, 2008 and Huenniger et al, 2010.

1.6 Neocortex in mouse

These signaling pathways also play similar roles in vivo. The neocortex is a very complex, organized structure that contains hundreds of different neuronal cell types and a diverse range of glial cells *(Peters and Jones, 1984; Cajal, 1995)* This region is mainly responsible for cognitive function, sensory perception and consciousness *(Molyneaux et al, 2007)*. The neurons present in the cortical (CP) are mainly of glutamatergic pyramidal neurons and GABAergic interneurons. However, the majority of the CP comprises of glutamatergic neurons (approx. 80%), whereas the rest is made up of GABAergic interneurons. The differentiation and migratory route of these two subtypes of neurons is different from each other. In case of glutamatergic neurons, the neurons differentiate from the progenitor cells of the sub-ventricular zone (SVZ) and migrate to different neocortical layers in a tightly controlled temporal order from embryonic day 11.5 (E11.5) till birth in mouse *(Angevine et al, 1961; Caviness et al, 1995; Rakic, 1974)*. The neurons which are born earliest form the preplate, which is late split into the more superficial marginal zone and deeply located subplate (SP). The CP, which gives rise of the multilayered neocortex, develops between these two layers *(Bayer and Altman, 1991)*, in a way that neurons which are born later migrate through the neurons born earlier *(Molyneaux et al, 2007)* (Fig. 5A).

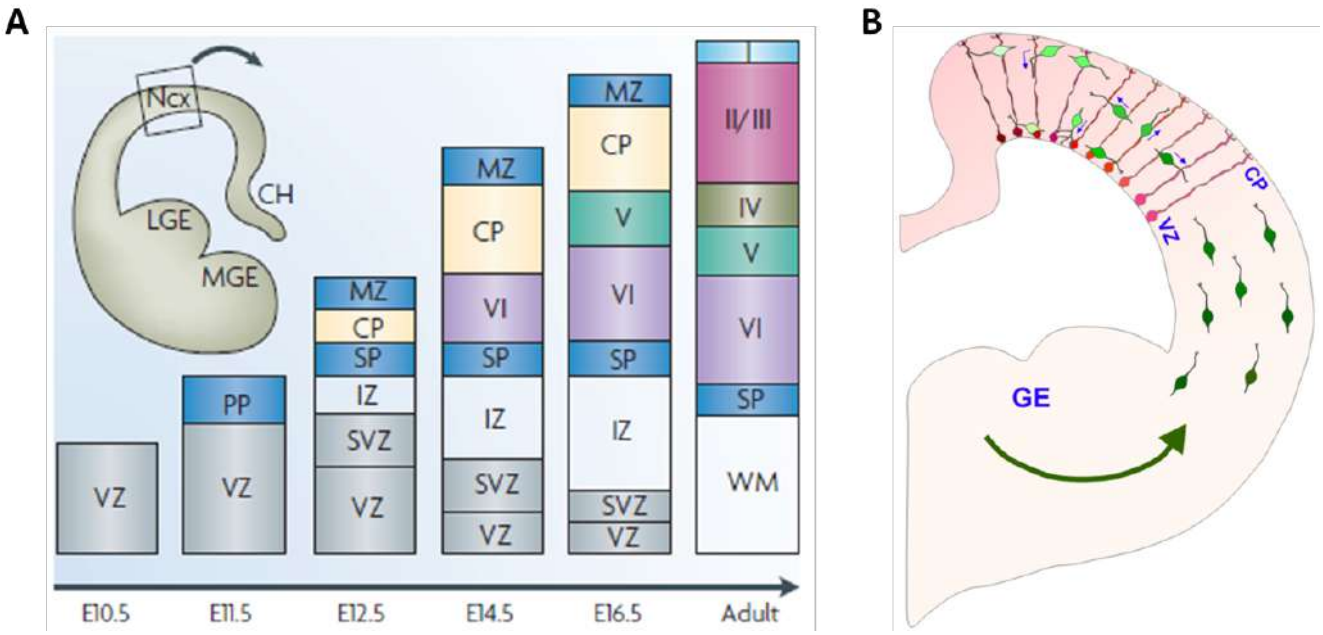

Figure 5. Glutamatergic and GABAergic neuronal migration.
A-B. Glutamatergic neuronal differentiation (A) adapted from Molyneaux et al, 2007.
GABAergic neuronal migration (B) *adapted from Yokota et al, 2007.*
[VZ – Ventricular zone; CP – Cortical plate; SVZ – Subventricular zone; MZ – Marginal zone; SP – Subplate; PP – Preplate; IZ – Intermediate zone; I-VI – Cortical layers I to VI; GE – Ganglionic Eminence]

The GABAergic interneurons are differentiated from the progenitor cells present in the Medial Ganglionic Eminence (MGE) and later migrate tangentially (Fig. 5B) to arrive in the CP *(Hevner et al, 2004)*. These interneurons demonstrate similar 'inside-out' migration once they arrive at the CP *(Hevner et al, 2004).* However for in vitro differentiation, authors have used Shh in the medium for efficient generation of GABAergic interneurons from human induced pluripotent stem cells (iPSCs) *(Maroof et al, 2013).*

1.7 In utero electroporation

To understand whether reduction or overexpression of Lmnb1 can cause defects in neuronal migration, it was necessary to perform in utero electroporation using Sh-Lmnb1 or pCAGS-LMNB1-EGFP plasmid. In utero electroporation is a method where we can inject a specific plasmid containing the gene of interest into the ventricle of embryo while inside the uterus of the mouse and pass electric impulses in such a way as to only target the progenitor cells present in a specific region (Fig. 6). In this project, we have injected Lmnb1 specific plasmids or their controls into the ventricle of E14.5 embryos and passed electric impulse in order to electroporated the progenitor cells present in the SVZ which would later differentiate and migrate upwards into the CP forming layer V. The entire protocol of this experiment is mentioned in the Methods.

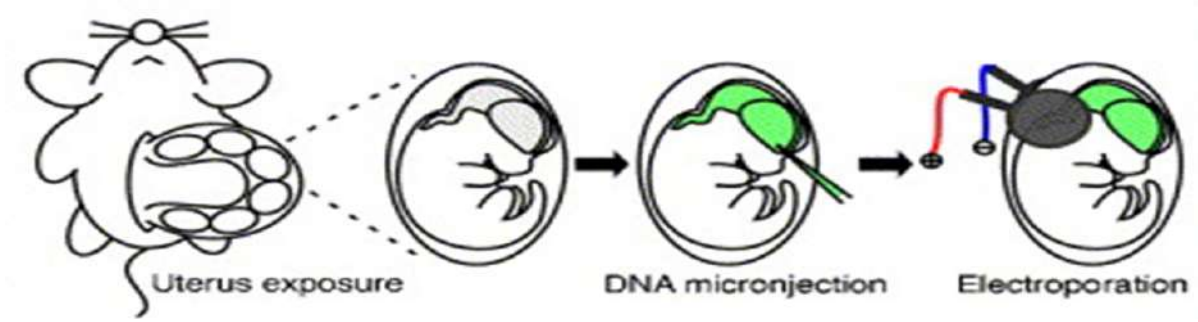

Figure 6. In utero electroporation
Adapted from Okada et al, 2007.

MATERIALS AND METHODS

2.1 Animals

Transgenic (*Lmnb1*$^{\Delta/\Delta}$) mice *(Vergnes et al, 2004, Giacomini C et al, 2016)* were obtained from the MMRRC Mutant Mouse Regional Resource Center (Univ. of California, Davis, CA, USA). Animal health and comfort were veterinary-controlled. The mice were housed in cages with filters in a temperature-controlled room with a 12:12 hour dark/light cycle with *ad libitum* access to water and food. All of the animal experiments were performed in accordance with the European Community Council Directive dated November 24, 1986 (86/609/EEC) and were approved by the Italian Ministry of Health and by the IIT Ethical Committee.

2.2 Genotyping

The genotypes of new born pups or embryos were determined using primers specific for the wild type *Lmnb1* allele (forward, 5'-TCCGTGTCGTGTGGTAGGAGG-3'; reverse, 5'-GCAGGAGGGTTGGGAAAGCC-3') and for the mutant allele carrying the gene-trap insertion (forward, 5'-TCCGTGTCGTGTGGTAGGAGG-3'; reverse, 5'-CACTCCAACCTCCGCAAACTC-3'). The primers were obtained from Sigma. The DNA was extracted from the embryo's tail by incubating them in 50mM NaCl at 99 °C for 1 hour. Then, 10% Tris (1M) was added and centrifuged at 14000 rpm at room temperature for 8 minutes. The DNA was then obtained from the supernatant and further used for genotyping. The kit used for genotyping was obtained from Promega. The composition of the master mix and the PCR cycle is listed in Table 1 and 2. After the PCR cycle was completed, the samples were then run on 2% agarose gel (with Ethidium Bromide) and analyzed using Image Quant 300 with UV transillumination. Comparing with 1Kb DNA ladder (Euroclone), the wild type embryos showed one band around 750 bp whereas the knockout embryos showed one band around 500 bp.

Table 1. Composition of master mix used to genotyping embryos from *Lmnb1*$^{+/\Delta}$ mice.

Genotyping Mix (20µl)	Volume (µl)
DNA (Sample)	2
PCR Buffer (5X)	4
Primers (Forward and Reverse; 10µM)	1
DNTPs (10mM)	0.40
GoTAQ Polymerase	0.25
DNase free H_2O	12.35

Table 2. PCR cycle used to genotyping embryos from *Lmnb1*$^{+/\Delta}$ mice.

Genotyping PCR cycle	Time (mins)
1) 95.0 °C	3:00
2) 94.0 °C	1:00
3) 60.0 °C	0:45
4) 72.0 °C	1:00
5) Cycle to step 2	40 times
6) 72.0 °C	5:00
7) 4.0 °C	Forever

2.3 Antibodies and reagents

The following primary antibodies were used: mouse monoclonal antibodies against *LMNB1* (Abcam; 1:100), EGFP (Millipore; 1:250), NPC (Covance; 1:100), Notch1 (Abcam; 1:1000), rabbit polyclonal antibodies against β-III Tubulin (Sigma; 1:250), GFAP (Dako; 1:100), PDGFR-α (SantaCruz; 1:100), GluR1 (Millipore; 1:250), GABA (Sigma; 1:250), Sox2 (Millipore; 1:100), TBR1 (Abcam; 1:250), FoxP2 (Abcam; 1:250), TPR1 (Abcam; 1:250) and Rat monoclonal antibody against Ctip2 (Abcam; 1:100). Secondary antibodies conjugated with Alexa 488 or Alexa 546 or Alexa 647 were used (Invitrogen; 1:500). For nuclear counterstaining, DAPI (Invitrogen; 1:500) or Hoechst 33342 (Sigma; 1:1000) were used.

For Western blot analysis, horseradish-peroxidase conjugated secondary antibodies (Bio-Rad Laboratories) were used. Unless otherwise specified, the general reagents and chemicals were from Sigma and the reagents for the cell cultures were from Invitrogen.

2.4 Culture and differentiation of Neural Stem Cells (NSCs)

NSCs were obtained from the dorsal forebrain of *Lmnb1* homozygous (*Lmnb1*$^{+/+}$) or *Lmnb1*-null (*Lmnb1*$^{\Delta/\Delta}$) E11.5-12.5 embryos. The forebrain was dissected in sterile Phosphate-buffered saline (PBS; Invitrogen) pH 7.4, dissociated using Accutase® solution (Sigma) at 37°C for 6 minutes, triturated into single cells and seeded into Neurobasal medium (Gibco) containing B-27 (Gibco; 1:50 v/v), Pen-Strep (Gibco; 1%), Glutamax (Gibco; 1% w/v), 20ng/ml Epidermal Growth Factor (EGF; Sigma) and 10ng/ml basic Fibroblast Growth Factor (bFGF; PeproTech). NSCs were grown at 37°C in a humidified incubator with 5% CO_2. Free floating spherical shaped clumps of cells known as 'neurospheres' formed in 3 days (Fig. 1). Neurospheres were passaged every 3 days. After 2 passages, to induce differentiation into neurons, astrocytes and oligodendrocytes, neurospheres were triturated into single cells using Accutase® solution, followed by 6 minutes incubation at 37C and centrifugation at

1200 rpm for 5 minutes. The cell pellet was then resuspended in complete Neurobasal medium and plated on glass coverslips coated with 0.1mg/ml Poly L-Lysine (Sigma) for 2-6 days in medium without EGF and bFGF. Half of the medium was changed every 3 days when the cells were kept longer for differentiation *(Currle et al, 2007, Mahajani et al, 2017)*. For the activation of notch signaling, we added DLL4 (500ng/ml; Life Technologies) in the medium after trituration of the neurospheres. The DLL4 containing medium was kept for 4 days.

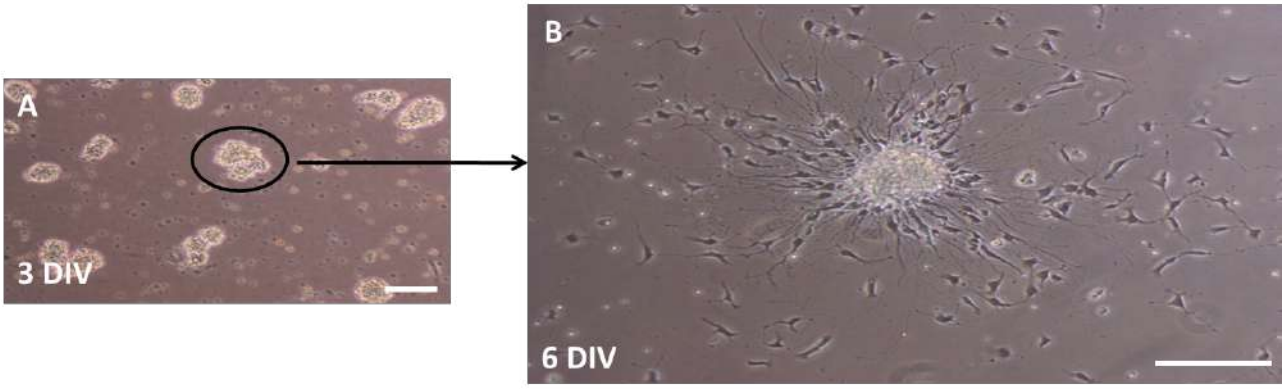

Figure 1. NSCs differentiation from neurospheres to dividing cells.
A-B. Representative images of *Lmnb1*$^{+/+}$ derived NSCs forming neurospheres (A; circled) and actively differentiating cells (B) observed by phase contrast microscopy. Scale bars 50 µm.

2.5 Plasmids and transfection

The pCAGGS-LMNB1-ires-EGFP (pLMNB1-EGFP) was generated by cloning human LB1 cDNA (NM_005573.3) into the pCAGGS-ires-EGFP (pEGFP) plasmid using two of the multiple restriction sites available. The design of the plasmids is shown in Figure 2. The purification of both the plasmids was performed using NucleoBond® Xtra Maxi kits (Macherey-Nagel) as described by the company protocol. The DNA pellet was dissolved in TE-Buffer (provided in the kit) and then quantified at Nanodrop-1000 Spectrophotometer (NanoDrop Technologies, Inc).

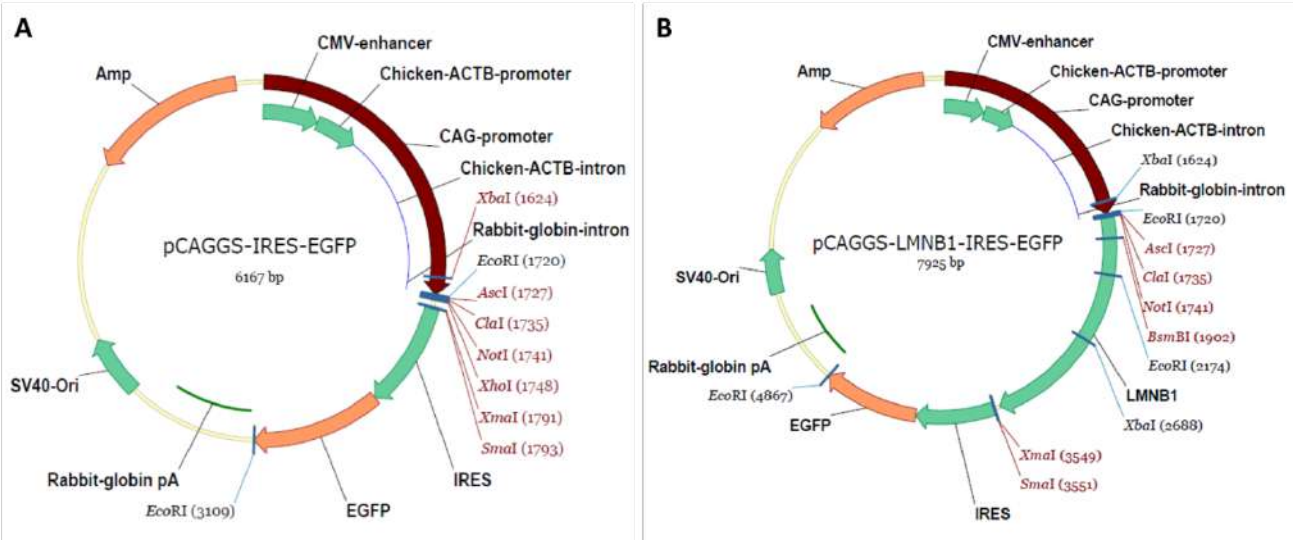

Figure 2. Plasmid design for pEGFP (A) and pLMNB1-EGFP (B).

When the NSCs derived from *Lmnb1*$^{+/+}$ embryos formed neurospheres, they were dissociated as mentioned above and single cells were transfected using either pLMNB1-EGFP or pEGFP plasmids with Amaxa P4 transfection kit (Lonza) using Amaxa 4D-Nucleofector X Unit (Lonza) and the DS-113 program. The efficiency of transfection was determined by counting the number of EGFP positive cells over total number of cells.

Knockdown of *Lmnb1 in vivo* was performed using Sh-*Lmnb1* with Sh-Scrambled used as a control. *Lmnb1* was cloned within pLKO.1-CMV-tGFP (Sigma) backbone. ShRNA efficiency was verified by Western blot analysis and sequencing. Lmnb1 shRNA and scramble shRNA plasmids containing the EGFP reporter were custom ordered from Sigma. The target sequences for Lmnb1 silencing were as follows: *Lmnb1:* CCGGGCGTCAGATTGAGTATGAGTACTCGAGTACTCATACTCAATCTGACGCTTTTTG (Clone ID: NM_010721.1 – 956s1c1).

2.6 Rate of differentiation and morphological analysis

The rate of differentiation of *Lmnb1*$^{\Delta/\Delta}$ and *Lmnb1*$^{+/+}$ NSCs-derived differentiated cells was quantified as a percentage of cells positive for neuronal (βIII-tubulin), astrocytic (GFAP) or oligodendrocytic (PDGFR-α) markers over the total number of cells identified by staining with DAPI. Approximately, 1000 DAPI^{+} cells for each staining condition were quantified in 3 independent experiments.

When *LMNB1* was overexpressed, the number of differentiated cells positive for one of the cellular markers and EGFP were calculated over the total number of EGFP-positive (EGFP^{+}) cells to determine the rate of differentiation. Differentiation rate is expressed as percentage throughout the text. Approximately, 400 EGFP^{+} cells were quantified for each staining condition in three independent experiments.

Axonal elongation of *Lmnb1*$^{\Delta/\Delta}$ and *Lmnb1*$^{+/+}$ NSCs-derived differentiated neurons was performed at 4 days in vitro (DIV). The cells were fixed, stained and quantified using NIH ImageJ program. Approximately, 180 βIII-tubulin^{+} neurons were analyzed for axonal length elongation in three independent experiments.

Similar axonal length quantification was performed in *Lmnb1*$^{+/+}$ NSCs-derived differentiated neurons expressing EGFP after transfecting with pEGFP and pLMNB1-EGFP. Approximately, 115 βIII-tubulin^{+} EGFP^{+} neurons from 3 independent experiments were used to measure the axonal length for each transfection condition.

Nuclei from *Lmnb1*$^{+/+}$ and *Lmnb1*$^{\Delta/\Delta}$ NSCs-derived neurons, astrocytes and oligodendrocytes were analyzed for nuclear size and circularity using NIH ImageJ program. The differentiated cells were first stained for DAPI and then the nuclear morphology was quantified manually. Approximately, 400 cells of each cell type were quantified for each genotype in three independent experiments.

For the nuclear morphology quantification when LMNB1 was overexpressed, *Lmnb1*$^{+/+}$ NSCs were transfected with either pLMNB1-EGFP or pEGFP and quantification was performed on neurons,

astrocytes or oligodendrocytes expressing EGFP. Approximately, nuclei of 200 $EGFP^+$ cells of each cell type for each transfection conditions were quantified in three independent experiments.

2.7 In Utero Electroporation

Overexpression of *LMNB1* in vivo was carried out by in utero electroporation using pLMNB1-EGFP, pEGFP, Lmnb1 shRNA or scramble-ShRNA plasmids. The plasmids were purified using NucleoBond® Xtra Maxi kits (Macherey-Nagel) and the DNA pellet was dissolved in sterile PBS at a concentration of 0.1-1mg/ml. The micropipettes used for in utero electroporation were of 10cm length with outer diameter of 1.2mm and inner diameter of 0.69mm (Sutter Instruments).

The pregnant mouse (E14) was anesthetized using Isoflurane (Merial Italia S.p.a). The mouse was continuously exposed to Isoflurane during the course of the surgery. The hair on the stomach of the mouse was first shaved and then cleaned using 70% ethanol and 10% Betadine® solution (Meda). The skin and the abdominal tissue was cut along a vertical axis. The uterus was then carefully taken out along with the embryos with a curved blunt forceps. The uterus was kept wet by adding pre-warmed (37°C) PBS during the entire surgery. DNA (3 µg) containing 1% Fast-Green dye (Sigma) was injected in the ventricle of each embryo brain. The injected embryos were held in parallel along its antero-posterior axis and electric pulses (5x, 30mV for 50ms) were passed through the brain. After electroporation, the uterus was carefully repositioned in the abdominal cavity. The cavity was filled with warm PBS and stitched using a 45cm Vicryl suture (Ethicon). The stomach of the mouse was then again cleaned with 70% ethanol and 10% Betadine® solution. The mouse was then administered diclofenac (0.5mg/kg) (Voltaren, Novartis) by i.p. injection and kept warm until awake. The mouse was sacrificed at E18 by cervical dislocation and the brains from the electroporated embryos were collected for immunohistochemistry *(Saito T, 2006)*.

For *Lmnb1* knockdown studies, electroporated pups were born and immediately transferred to a foster CD-1 mother. The pups were sacrificed at P7 and the brains collected for immunohistochemistry.

2.8 Quantitative Real-Time PCR (qRT-PCR)

Neurospheres were collected before plating them on PLL (Undifferentiated NSCs) or after differentiation for 1 or 4 days. RNA was extracted using RNeasy Micro Kit (Qiagen) and quantified with a Nanodrop-1000 Spectrophotometer. After DNase treatment, RNA was reverse transcribed using the QuantiTect Reverse Transcription kit (Qiagen). Complementary DNA was analyzed by qRT-PCR (5ng RNA equivalent/reaction) using 0.2 µM target-specific primers and QuantiFast SYBR Green (Qiagen). Primers were validated by qRT-PCR analysis on serial dilutions of a positive control complementary DNA to assess their specificity and efficiency. Forty qRT-PCR cycles were performed on 7900HT instrument (Applied Biosystems) equipped with the Sequence Detection Systems (SDS) 2.3 software. Data were normalized using the expression of housekeeping genes Actin and HPRT1. C_t values were converted into fold-expression values relative to the control using qBase^{PLUS} software (Biogazelle) *(Ferrera et al, 2014, Mahajani et al, 2019, Pan et al, 2019).* The master mix composition and the qRT-PCR cycle used in this experiment is listed in Table 3 and 4 along with the sequence of the primers in Table 5.

Table 3. Composition of master mix used for qRT-PCR analysis.

Quantitative RT-PCR Master Mix (120µl)	Volume (µl)
SyBr Green	60
Primers (0.1 - 0.5µM)	1.2 - 6.0
Template	40
H_2O	14 - 18.8

Table 4. PCR cycle used for qRT-PCR analysis.

Quantitative RT-PCR Cycle	Time (seconds)
1) Denaturation (95.0 °C)	30
2) Annealing (95.0 °C to 72.0 °C)	20
3) Extension (72.0 °C)	20
4) Cycle to Step 2	40 times
5) Denaturation (95.0 °C)	60
6) Annealing (95.0 °C to 72.0 °C)	30
7) Extension (72.0 °C)	30

Table 5. Primers used for qRT-PCR analysis

Gene	Forward primer	Reverse primer	Efficiency
Actin	AAGTGGTTACAGGAAGTCC	ATAATTTACACAGAAGCAATGC	2.09
HPRT1	TGAGGCGGCGAGGGAGAG	AAGCGGTCTGAGGAGGAAGC	2.08
GFAP	GATCTATGAGGAGGAAGTTC	CGTATTGAGTGCGAATCT	2.05
β III Tubulin	GCCTTTGGACACCTATTCAGG	TTCTTTCCTCAGGACATCCAG	2.07
DCX	GCCCTTCCTCCTCACTTTCACA	GTCTCAATGCCTCCCTCTCCTT	2.01
Sox2	CCACCAATCCCATCCAAATTAACG	GATCTATACATGGTCCGATTCCC	1.76
HES1	GTCTACACCAGCAACAGT	CATGGAGTCCGAAGTGAG	2.02
HES5	TCATAGGAAAGCACTCAG	TTAAGGATCATCGTGGAG	2.07
β-Catenin	CAATGGCTTGGAATGAGACT	CCGTATCCACCAGAGTGAA	1.97
GSK3β	CATCCTTATCCCTCCACAT	CGGTCTCCAGCATTAGTA	1.99
SHH	AGCGGCAGGCAAGGTTAT	GCTCGGCTCGTTCGTTCC	1.87
Neurogenin1	GTAGTCCCTCGGCTTCAG	TGTGGAGCAGGTCTTTGG	1.95
STAT3	CCTGAGACTGGCAACTGT	GAAGCAAGCAAGCGACAT	2.04
WNT3	AATCTACCGCAACAGAACAG	CATCTTGGAATGTCACGAGTAG	1.92

Key: qRT-PCR, quantitative real time polymerase chain reaction.

2.9 Immunocytochemistry

Immunocytochemistry was performed as previously described with minor *modifications (Ferrera et al, 2014, Colombi et al, 2013, Psol et al, 2021)*. Briefly, cells were fixed with 4% paraformaldehyde (PFA) dissolved in PBS, washed three times using PBS. Composition of PBS and PB buffer is listed in Table 6 and 7 respectively. The cells were then washed three time with low salt solution followed by three washes with high salt solution. The composition of low and high salt solution is listed in Table 8

and 9. The cells were then blocked and permeabilized with 12% normal serum (Euroclone) in PBS containing 0.25% Triton X-100 for 1 hour. Coverslips were further incubated with primary antibodies diluted in blocking solution for 3 hours at room temperature or overnight at 4°C. After removal of the primary antibody, the cells were washed three time with high salt solution for 5 minutes each. They were then blocked for another 10 minutes using the same blocking solution described above. Alexa dye-conjugated secondary antibodies diluted in blocking solution was then added to the cells and kept covered at room temperature for 2 hours. Coverslips were mounted using Prolong Gold antifade reagent (Invitrogen) containing DAPI (4',6'-diamidino-2-phenylindole). Fluorescence images were collected using an automated Olympus BX51 microscope, equipped with a MBF Optonic CX9000 camera and 40X UPLFLN semi-apo fluorite NA 0.3 objective and MBF Neurolucida V11 software. Confocal imaging was performed using a Leica TCS SP5 AOBS TANDEM inverted confocal microscope that was equipped with a HCX PL APO 40 x 1.25 Oil and a HCX PL APO blue 63 x 1.4 NA Oil objective lenses.

Table 6. Composition of PBS buffer used for immunocytochemistry and immunohistochemistry.

PBS Buffer (10X; 1L)	Amount (gms)
Sodium Chloride (NaCl)	80
Potassium Chloride (KCl)	2
Sodium Hydrogen Phosphate Dihydrate (Na_2HPO_4, $2H_2O$)	18.05
Potassium Phosphate monobasic (KH_2PO_4, anhydrous)	2.4
H_2O	1 liter

Table 7. Composition of PB buffer used for immunocytochemistry and immunohistochemistry.

PB Buffer (0.12 M; 1L)	Amount (gms)
Sodium Hydrogen Phosphate Dihydrate (Na_2HPO_4, anhydrous)	34.07
Sodium Phosphate monobasic monohydrate (NaH_2PO_4, H_2O)	33.91
H_2O	1 liter

Table 8. Composition of low salt solution used in immunocytochemistry.

Low Salt solution (1X; 1L)	Amount (gms)
Sodium Hydrogen Phosphate Dihydrate (Na_2HPO_4, anhydrous)	17.03
Sodium Phosphate monobasic monohydrate (NaH_2PO_4, H_2O)	16.95
Sodium Chloride (NaCl)	8.76
H_2O	1 liter

Table 9. Composition of high salt solution used in immunocytochemistry.

High Salt solution (1X; 1L)	Amount (gms)
Sodium Hydrogen Phosphate Dihydrate (Na_2HPO_4, anhydrous)	17.03
Sodium Phosphate monobasic monohydrate (NaH_2PO_4, H_2O)	16.95
Sodium Chloride (NaCl)	29.2
H_2O	1 liter

2.10 Immunohistochemistry

Embryonic or neonatal brains were fixed in 4% PFA overnight. The brains were cryopreserved in 30% sucrose (Sigma) dissolved in PBS overnight at 4°C. They were then embedded in Tissue Tek OCT compound (Societa' Italiana Chimici) and stored at -80°C for at least one night. Cryosections (10µm, 40 µm or 80µm) were cut using Leica CM 3050S cryostat and they sections were kept in PBS with 0.02% Sodium azide until used *(Wakhloo et al, 2020)*. The bregma selected for quantification was approximately 0.14mm with interaural plane at 3.94mm. Before the staining protocol, the sections were incubated in 4% PFA for 20 minutes at room temperature. PFA was then washed off from the sections using PBS for 5 minutes followed by wash with PB for 15 minutes. Sections were then blocked in 5% normal goat serum in PBS containing 0.25% Triton X-100 for 1 hour and incubated with primary antibodies in blocking solution overnight at 4°C. The blocking solution containing the primary antibody was removed and the sections were first washed with PBS for 5 minutes and then with PB for 15 minutes. The sections were also blocked using the blocking solution for 20 minutes followed by incubation with appropriate Alexa dye-conjugated secondary antibodies (Invitrogen) diluted in blocking solution for 2 hours at room temperature. Fluorescence and confocal imaging was performed as described above.

Cortical thickness for *Lmnb1*$^{\Delta/\Delta}$ and *Lmnb1*$^{+/+}$ embryos at different developmental stages was measured on slices collected at the same bregma for both genotypes and stained with Hoechst 33342 dye as the reference. A straight line was drawn from the SVZ to the MZ of the cortical plate and the length was measured after setting the correct scale for the images using ImageJ NIH software.

For the measurement of CP and the VZ thickness, sections from E13.5 *Lmnb1*$^{\Delta/\Delta}$ and *Lmnb1*$^{+/+}$ embryos collected at the same bregma were immunostained against βIII-tubulin (neuronal marker) to identify the CP and counterstained with Hoechst 33342 to visualize the entire cortex. The portion

of the cortical plate devoid of βIII-tubulin staining, but with Hoechst positive cells was considered as the VZ.

For counting the number of cells in the VZ or CP, a width of 1000 µm was set for both *Lmnb1*$^{\Delta/\Delta}$ and *Lmnb1*$^{+/+}$ brain section collected at the same bregma. Cells counted throughout the VZ (Hoechst+; βIII-tubulin negative) or CP (positive for Hoechst and βIII-tubulin) and normalized on the respective area determined using the ImageJ NIH software.

For the quantification of glutamatergic (GluR1^{+}) and GABAergic (GABA^{+}) neurons, sections (5 sections/brain) were collected from E19.5 *Lmnb1*$^{\Delta/\Delta}$ and *Lmnb1*$^{+/+}$ embryos (n=4/genotype) at the same bregma (0.14mm) for both genotypes. The number of GluR1^{+} glutamatergic neurons in the CP was counted within a 2mm^2 area containing layer V. The number of GABA^{+} neurons was counted within the entire cortical plate comprised in a width of 1000 µm.

For the quantification of number of electroporated cells located in the cortical layers after Lmnb1 silencing, we divided the cortical plate into 10 equal bins as previously described *(Hevner, et al 2004)*. According to this method, in P7 normal rodent cortex, bins correspond to marginal zone (MZ; bin1), cortical layers II-IV (bins 2-4), cortical layer V (bins 5-6) and cortical layer VI (bins 7-9). The last bin (bin10) corresponds to the sub-plate (SP) with additional bins for the intermediate zone (IZ; bin11) and sub-ventricular zone (SVZ; bin12). The number of EGFP^{+} cells were quantified based on their position in the bins.

For studies of neuronal migration, coronal sections (40 µm) of electroporated brains were stained for Ctip2, which is a marker of layer V of the cortical plate, and EGFP. Total numbers of EGFP^{+} cells present within, above or below the Ctip2 layer were quantified. More than 1200 and 980 EGFP^{+} neurons were analyzed for pEGFP and pLMNB1-EGFP electroporated brains, respectively, in 4 independent experiments. For the knockdown experiments, GFAP^{+} area was analyzed in electroporated brains.

2.11 Western blotting

Lmnb1$^{+/+}$ and *Lmnb1*$^{\Delta/\Delta}$ E18.5 brains were lysed in RIPA lysis buffer supplemented with protease and phosphatase inhibitors (Sigma) by sonication. Samples were spun at 10,000g for 20 minutes at 4°C. The supernatant was collected and protein concentration was measured using the BCA assay (Pierce). Equal amount of proteins were separated on 10% bis-tris polyacrylamide gels. Gels were transferred to nitrocellulose Protran™ 0.2µm NC membranes (Amersham). The list and composition of the buffers used are listed below. The blotting efficiency was monitored using Ponceau S and equal loading was verified using MemCode (Thermo Scientific), which was imaged by ImageQuant to be used for normalization. The membranes were blocked for 1 h in 5% milk in Tris-buffered saline (10 mM Tris, 150 mM NaCl, pH 8.0) containing 0.1% Triton X-100 (TBST) and incubated overnight at 4°C with primary antibodies, followed by horseradish peroxidase-conjugated anti-mouse (1:5000; BioRad) or anti-rabbit (1:5000; BioRad) secondary antibodies for 1 hour at room temperature and visualized using Super Signal West Pico Chemiluminescent Substrate (Thermo Scientific). Chemiluminescent signals were acquired using films (Hyperfilm ECL, Amersham) or an image Quant LAS 4000 mini (GE Healthcare). Densitometric analysis was performed using the NIH ImageJ program. Protein levels were expressed as a percentage of the ratio with MemCode or Actin. Buffers prepared are listed below and in *(Mahajani et al, 2010, Wakhloo et al, 2013)*.

Table 10. Composition used to prepare running gel for Western blot.

Running gel (10%; 30ml)	Volume (ml)
Acrilammide 30%	10
Lower Buffer 4X	7.5
H_2O	12.5
Ammonium persulfate (APS)	150 µl
Temed	15 µl

Table 11. Composition used to prepare stacking gel for Western blot.

Stacking gel (20ml)	Volume (ml)
Acrilammide 30%	2.5
Upper Buffer 4X	5
H_2O	12.5
Ammonium persulfate (APS)	220 µl
Temed	15 µl

Table 12. Composition of lower buffer used to prepare running gels.

Lower Buffer (4X; 1L)	Amount (gms)
Tris (Trizma® Base) 1.5 M	181.7
Sodium Dodecyl Sulfate (SDS) 0.4%	4
Final Volume (H_2O)	1 Liter
pH 8.8	

Table 13. Composition of upper buffer used to prepare stacking gels.

Upper Buffer (4X; 1L)	Amount (gms)
Tris (Trizma® Base) 0.5 M	60.4
Sodium Dodecyl Sulfate (SDS) 0.4%	4
Final Volume (H_2O)	1 Liter
pH 6.8	

Table 14. Composition of running buffer used in Western blot.

Running buffer (10X; 1L)	Amount (gms)
Sodium Dodecyl Sulfate (SDS)	10
Glycine	144.7
TRIS (Trizma® base)	30.3
Final Volume (H_2O)	1 Liter
pH 8.3 - 8.6	

Table 15. Composition of transfer buffer used in Western blot.

Transfer buffer (1X; 1L)	Amount (gms)
TRIS (Trizma® base)	3.02
Glycine	14.4
Methanol (10%)	100 ml
Final Volume (H_2O)	1 Liter

Table 16. Composition of stripping buffer used for Western blot.

Stripping buffer (1X; 100ml)	Volume (ml)
Tris – HCl (0.5M; pH – 6.8)	12.5
Sodium Dodecyl Sulfate (SDS) 10%	10
Final Volume (H_2O)	100 ml
β - Mercaptoethanol	0.8 µl

Table 17. Composition of wash buffer used for Western blot.

TBST buffer (1X; 1L)	Amount (gms)
Tris – HCl (50mM; pH – 7.5)	6.05
Sodium Chloride (NaCl; 150mM)	8.76
Final Volume (H_2O)	100 ml
Triton X-100 (0.25%)	2.5 ml

Table 18. Composition of RIPA lysis buffer used in Western blot.

RIPA Lysis buffer (1X; 100ml)	Volume (ml)
Tris (Trizma® Base) 50mM; pH – 8.0)	5
Sodium Dodecyl Sulfate (SDS) 0.5%	0.5
Sodium Chloride (NaCl) 150mM	3
Nonidet P-40 (1%)	1
Sodium DeoxyCholate (DOC) 0.5%	0.5 gms
Final Volume (H_2O)	100ml
Protease and Phosphatase inhibitors (50X)	2ml

Table 19. Composition of blocking buffer used in Western blot.

Blocking buffer (1X; 100ml)	Amount (gms)
Tris – HCl (50mM; pH – 7.5)	0.6
Sodium Chloride (NaCl; 150mM)	0.87
Non Fat Dried Milk (Bovine; 5%) OR Bovine Serum Albumin (BSA; 5%)	5 gms
Triton X-100 (0.25%)	2.5 ml
Final Volume (H_2O)	100 ml

2.12 Statistical analysis

The results in the text are presented as the mean ± SEM. Statistical analysis was performed using GraphPad Prism software. For dataset with normal distribution, Student's t-test was used for comparison between two groups. ANOVA test followed by Bonferroni post hoc test was used for comparing more than two groups. The differences between groups were considered to be statistically significant when $p < 0.05$.

RESULTS

3.1 Lamin B1 levels tilts the balance of neuronal versus astrocytic differentiation in cultured murine NSCs

It has been reported that Lmnb1 deficiency impairs embryonic brain development leading to reduced brain size and abnormal layering of neurons in the mouse cortex *(Coffinier et al, 2011)*. However, it remains unclear how Lmnb1 deficiency regulates cell fate commitment during embryonic neurogenesis. To investigate whether Lmnb1 regulate cell fate commitment, we generated primary multipotent neural stem cells (NSCs) from *Lmnb1*$^{\Delta/\Delta}$ and *Lmnb1*$^{+/+}$ embryo and differentiated them into neurons, astrocytes or oligodendrocytes using specific culture conditions for 2, 4 or 6 days *(Elkabetz and Studer, 2009).* Differentiated cells were identified by immunostaining for cell-specific markers, including neuronal β-III Tubulin, GFAP for astrocytes and PDGFRα for oligodendrocyte precursors. The percentage of NSC-derived neurons was significantly reduced (-20%) in *Lmnb1*$^{\Delta/\Delta}$ cultures (Fig. 1A-F; G), while the number of astrocytes was increased (+18%) compared to *Lmnb1*$^{+/+}$ cells (Fig. 1C-E). The percentage of NSC-derived oligodendrocytes was similar in *Lmnb1*$^{\Delta/\Delta}$ (10.77% ± 4.43) and *Lmnb1*$^{+/+}$ cultures (12.60% ± 4.93, n=3, *p<0.5; **p<0.01; Student's t-test).

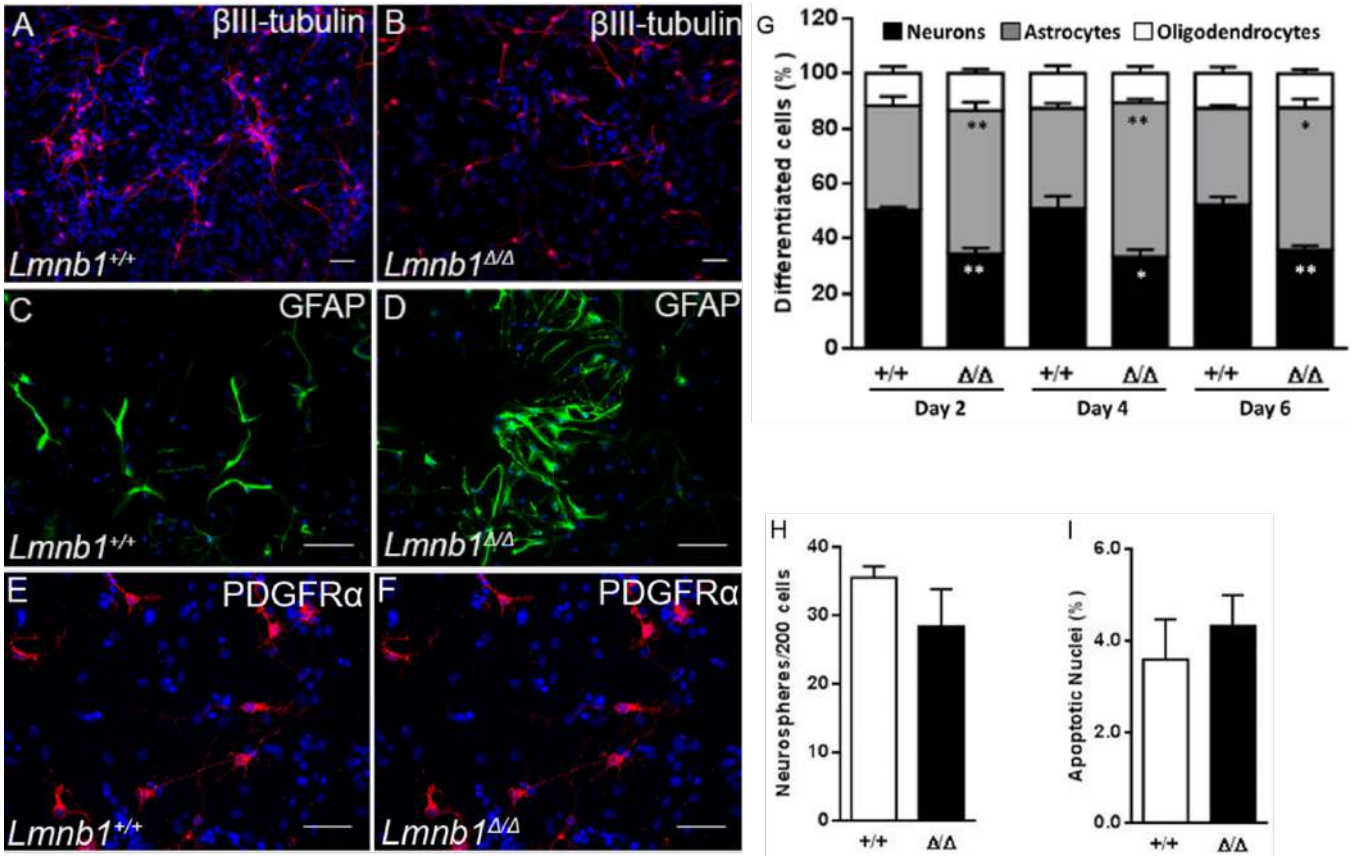

Figure 1. *Lmnb1* deficiency alters the NSC differentiation rate into neurons and astrocytes.
NSCs from *Lmnb1*$^{+/+}$ and *Lmnb1*$^{\Delta/\Delta}$ embryos were differentiated for 2, 4 or 6 days as described in the methods.

A-F. Representative fluorescence images of immunoreactivity for neuronal βIII-tubulin (A-B; red), astrocytic GFAP (C-D; green) and oligodendrocyte precursor PDGFRα (E-F; red) proteins in differentiated NSCs. Nuclei are counter-stained with DAPI (blue). Scale bars 50 µm.

G. Quantitative analysis of differentiated cells. The numbers of neurons (βIII-tubulin^{+}), astrocytes (GFAP^{+}) and oligodendrocytes (PDGFRα^{+}) were counted. Data is expressed as percentage of the total number of cells identified by DAPI nuclear staining. Graph bars represent the average percentage ± SEM. *p<0.05, **p<0.01 vs Lmnb1$^{+/+}$ at respective differentiation time, Student's t–test. Approximately, 1000 DAPI^{+} cells consisting for each staining condition were quantified in 3 independent experiments.

H. Quantitative analysis of NSCs self-renewal. Total number of neurospheres obtained after plating equal number of NSCs from *Lmnb1*$^{+/+}$ and Lmnb1$^{\Delta/\Delta}$ embryos were counted. Graph bars represent the average number of neurospheres ± SEM.

I. Quantitative analysis of NSC viability. Apoptotic nuclei with condensed chromatin were counted in *Lmnb1*$^{+/+}$ and *Lmnb1*$^{\Delta/\Delta}$ NSC cultures as described in the methods. Graph bars represent the average percentage ± SEM.

To investigate whether Lmnb1 absence could affect progenitors' proliferation, we examined NSC ability of generating neurospheres. We seeded equal number of NSCs of each genotype and quantified the number of neurospheres produced over 72 h. We found that the number of neurospheres were similar in *Lmnb1*$^{+/+}$ (Fig. 1H) and *Lmnb1*$^{\Delta/\Delta}$ (n=3, p=0.2404, Student's t-test), indicating that NSC self-renewal properties are conserved in the absence of Lmnb1.

To investigate potential effects on cell survival, we examined the occurrence of apoptosis in undifferentiated cells in *Lmnb1*$^{\Delta/\Delta}$ and *Lmnb1*$^{+/+}$. We found that deficiency of Lmnb1 does not affect the number of apoptotic cells (Fig. 1I).

Consistently, through gene expression analysis by qRT-PCR, we found that in *Lmnb1*$^{\Delta/\Delta}$ differentiated cells, the expression of GFAP and βIII-tubulin was increased and decreased, respectively as compared to *Lmnb1*$^{+/+}$ differentiated cells (Fig. 2A-B). Levels of GFAP and βIII-tubulin were comparable in both *Lmnb1*$^{\Delta/\Delta}$ and *Lmnb1*$^{+/+}$ undifferentiated cells.

We next investigated whether Lmnb1 levels affect different neuronal progenitors through analysis of the expression of specific markers such as Sox2 and doublecortin (DCX) in undifferentiated NSCs and cells differentiated for 4 days. Sox2 identifies proliferating progenitors such as radial glia, intermediate and neuronal progenitors *(Hutton and Pevny, 2011)* and its levels vary during astrocytogenesis *(Falcone et al, 2015)*. Instead DCX marks late neuronal progenitors and postmitotic neurons in the first 2-3 weeks of differentiation *(Couillard-Despres et al, 2005)*. In undifferentiated NSCs, the expression of both DCX and Sox2 was compared in both genotypes (Fig. 2C, D). In *Lmnb1*$^{+/+}$ NSCs, the expression of DCX increased during differentiation, while Sox2 was reduced, indicating changes in the number of progenitor cells during the course of differentiation. In *Lmnb1*$^{\Delta/\Delta}$ differentiating cells, the expression of DCX was reduced while Sox2 mRNA was increased (Fig. 2C,

D). These results indicate that *Lmnb1* depletion tilts the balance of neuronal versus astrocytic differentiation in vitro, without affecting NSC self-renewal properties.

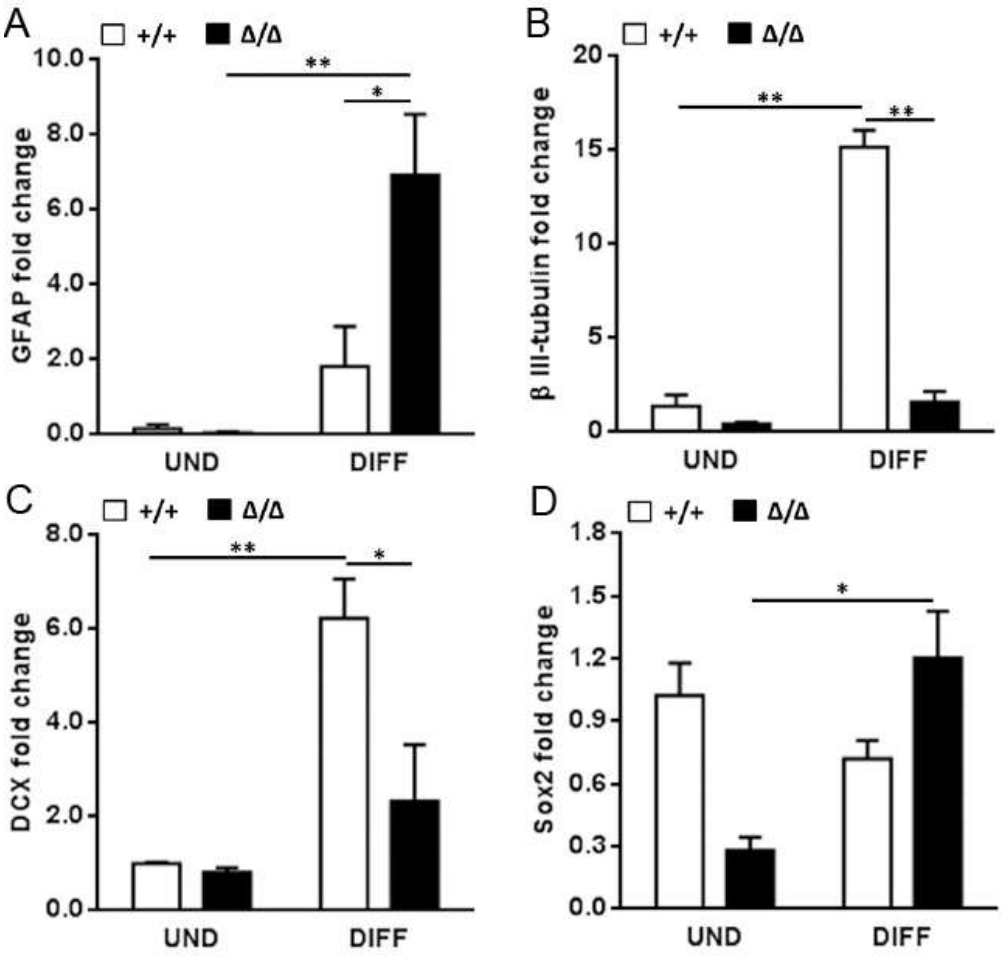

Figure 2. Lmnb1 deficiency alters expression of cellular markers.
Quantitative real time PCR of *Lmnb1*$^{+/+}$ and *Lmnb1*$^{\Delta/\Delta}$ undifferentiated and differentiated NSCs revealed altered gene expression.
A-D. Quantitative analysis of cellular markers. *Lmnb1*$^{+/+}$ and *Lmnb1*$^{\Delta/\Delta}$ undifferentiated and 4 DIV differentiated NSCs were analyzed for expression patterns of astrocytic marker GFAP (A), neuronal marker β III tubulin (B), actively diving neuronal marker Doublecortin (DCX; C) and progenitor marker Sox2 (D), by qRT-PCR. Graph bars represent the average fold change ± SEM. *p<0.05, **p<0.01 vs *Lmnb1*$^{+/+}$ at respective differentiation time, two-way ANOVA followed by Bonferroni test.

To examine the specific contributions of Lmnb1 to cell fate determination, we transfected undifferentiated WT NSCs with human Lamin B1 (LMNB1) together with the EGFP reporter or with EGFP alone using Axama P4 transfection kit. The first step was to determine the transfection conditions of NSCs using pLMNB1-EGFP or pEGFP plasmids.

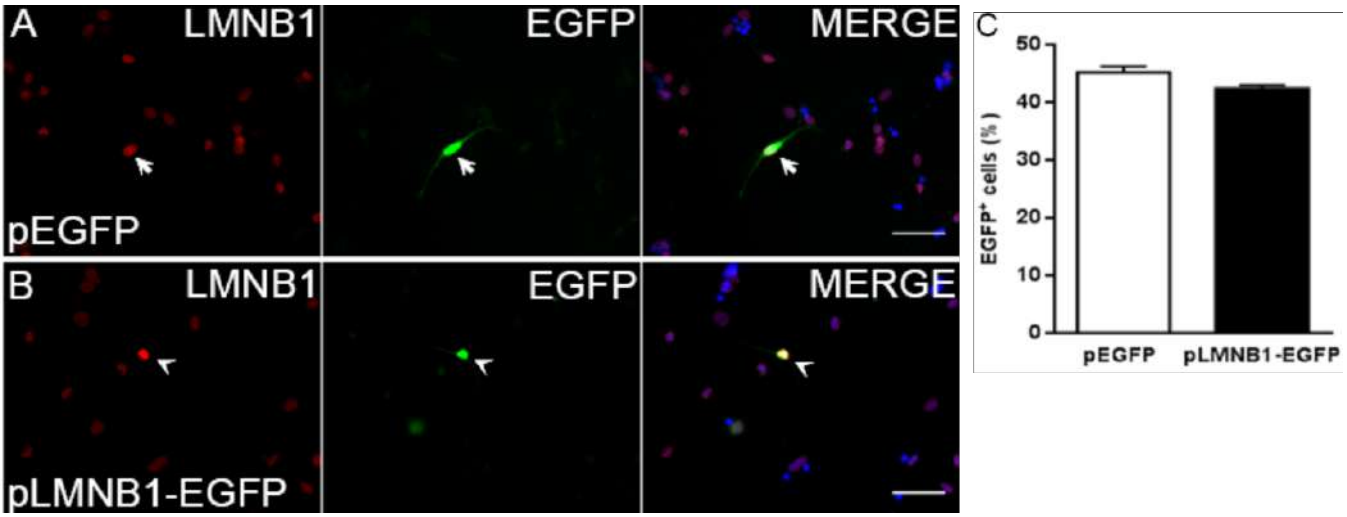

Figure 3. LMNB1 overexpression in NSCs using pLMNB1-EGFP plasmid.
Lmnb1$^{+/+}$ derived NSCs were transfected using pLMNB1-EGFP or pEGFP and cultured as described in the methods.
A-B. Representative fluorescence images of immunoreactivity for LMNB1 (A-B; red) and EGFP (A-B; green) in *Lmnb1*$^{+/+}$ NSCs transfected with pEGFP (A) or pLMNB1-EGFP (B). Nuclei are counter-stained with DAPI (blue). Scale bars 50 µm.
C. Transfection efficiency. Total number of EGFP^{+} cells obtained after transfecting *Lmnb1*$^{+/+}$ NSCs with pEGFP or pLMNB1-EGFP were counted. Graph bars represent the percentage of EGFP^{+} cells ± SEM.

This confirmed that overexpression of LMNB1 specifically co-localizes with the expression of EGFP in pLMNB1-EGFP (Fig. 3B; arrowhead), but not in pEGFP (Fig. 3A; arrow) transfected NSCs. Moreover, the similar transfection efficiency (Fig. 3C) confirms that overexpression of LMNB1 does not lead apoptosis in NSCs.

After transfection, we plated the NSCs in differentiating conditions for 2, 4 or 6 days and quantified the number of EGFP-positive differentiated neurons (Fig. 4A-B), astrocytes (Fig. 4C-D) and oligodendrocytes (Fig. 4E-F). We found that LMNB1 overexpression significantly enhanced the percentage of neurons (+12%, Fig. 4G) with only a slight, but insignificant reduction of astrocyte (-8%) and oligodendrocyte (-4%) proportion compared to the control NSCs-derived differentiated cells expressing EGFP alone (n=3; **$p<0.01$; Student's t-test).

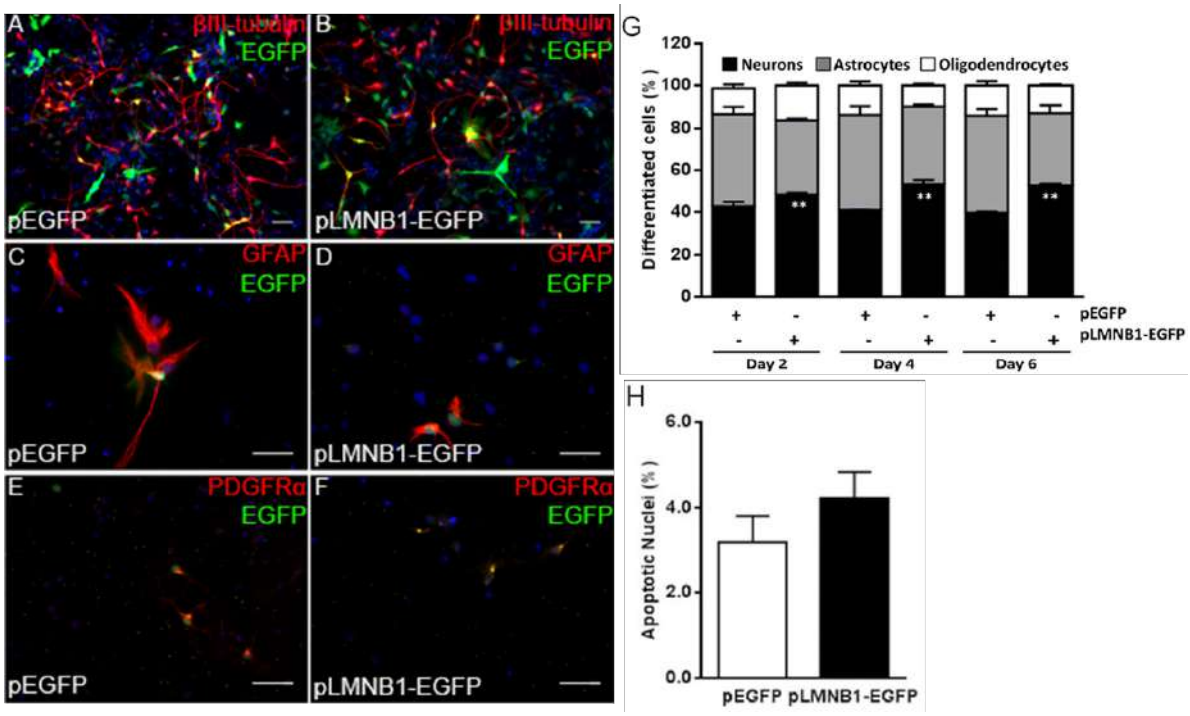

Figure 4. LMNB1 overexpression increases the NSC rate of differentiation into neurons.

NSCs from *Lmnb1*$^{+/+}$ embryos were transfected with pEGFP or pLMNB1-EGFP and differentiated for 2, 4 or 6 days as described in the methods.

A-F. Representative fluorescence images of immunoreactivity for βIII-tubulin (A-B; red), GFAP (C-D; red), PDGFRα (E-F; red) and EGFP (A-F; green) in differentiated NSCs transfected with pEGFP or pLMNB1-EGFP. Nuclei are counter-stained with DAPI (blue). Scale bars 50 µm.

G. Quantitative analysis of differentiated cells. The numbers of neurons (βIII-tubulin^{+}), astrocytes (GFAP^{+}) and oligodendrocytes (PDGFRα^{+}) co-expressing EGFP were counted and expressed as percentage of the total number of EGFP^{+} cells. Graph bars represent the average percentage ± SEM. *p<0.05, **p<0.01 vs pEGFP transfected cells at respective differentiation time, Student's t–test. Approximately, 400 EGFP^{+} cells were quantified for each staining condition in 3 independent experiments.

H. Quantitative analysis of NSC viability. The number of apoptotic nuclei of *Lmnb1*$^{+/+}$ NSCs transfected with pEGFP or pLMNB1-EGFP were counted as described in the methods. Graph bars represent the average percentage ± SEM.

We also checked for the effect of LMNB1 overexpression on cell survival by examining the occurrence of apoptosis in undifferentiated cells in pLMNB1-EGFP transfected NSCs as compared to the control pEGFP transfected NSCs. We found that overexpression of Lmnb1 does not affect the

number of apoptotic cells (Fig. 4H), indicating that the Lmnb1 expression levels do not affect the survival of differentiating progenitors from E12.5 embryos.

Lastly, we also checked for the differentiation rate in *Lmnb1*$^{+/\Delta}$ derived NSCs as compared to *Lmnb1*$^{+/+}$ NSCs (Fig. 5A). We observed a significant increase in the number of differentiated astrocytes from *Lmnb1*$^{+/\Delta}$ NSCs as compared to *Lmnb1*$^{+/+}$ NSCs. However, when we checked for GFAP expression levels in the cortical plate of *Lmnb1*$^{+/\Delta}$ (Fig. 5C) mice at 3 months of age, we did not observe any significant difference as compared to age matched *Lmnb1*$^{+/+}$ (Fig. 5B) mice (Fig. 5D).

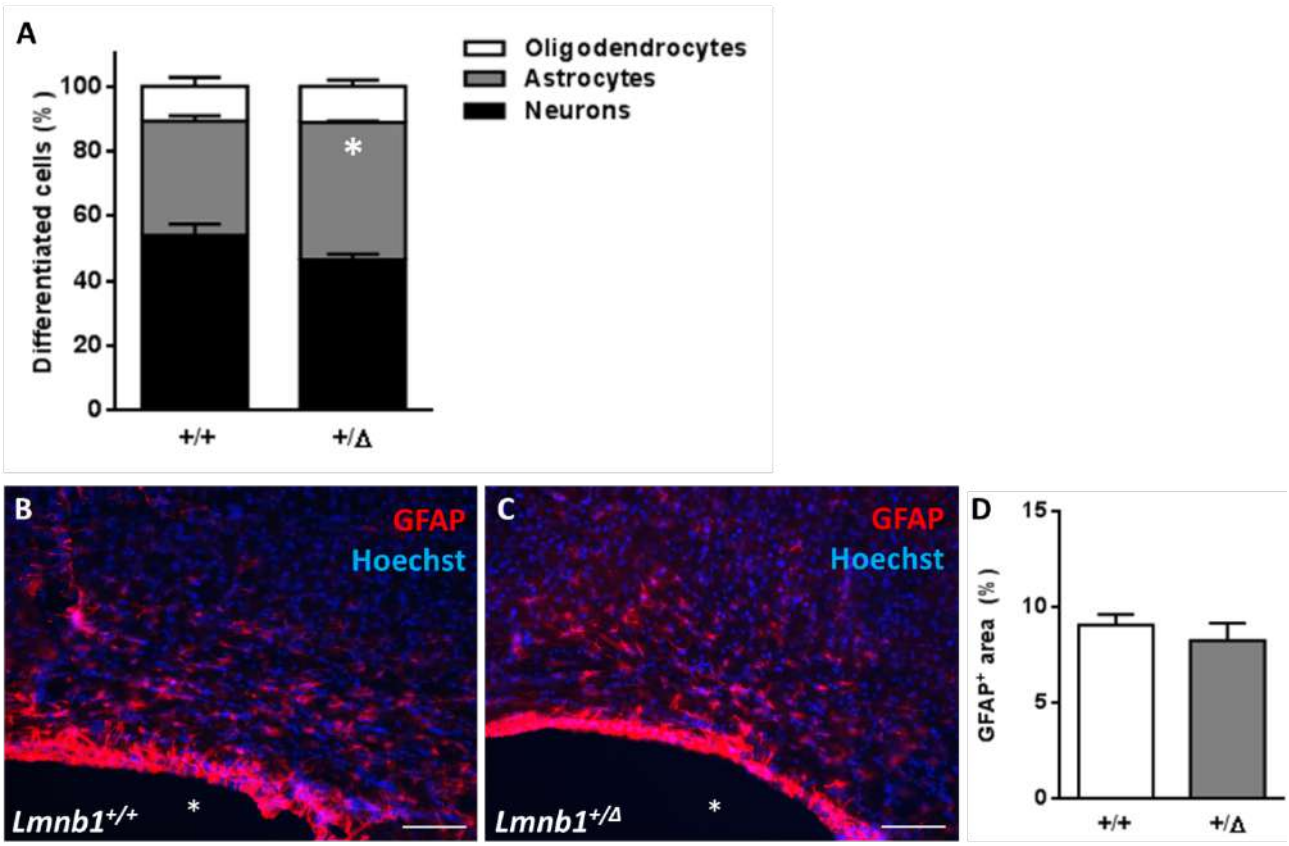

Figure 5. Quantification of astrocytic differentiation in *Lmnb1$^{+/\Delta}$* *in vitro* and *in vivo*.

A. Quantification of NSCs differentiation. Rate of differentiation of neurons, astrocytes and oligodendrocytes from *Lmnb1$^{+/\Delta}$* NSCs and *Lmnb1$^{+/+}$* NSCs. Graph bars represent the average percentage ± SEM. *p<0.05, Lmnb1$^{+/+}$ NSCs at 4 DIV, Student's t–test.

B-C. Representative fluorescence images for immunoreactivity of astrocytic marker (GFAP; B-C; red) in the cortical plate of *Lmnb1$^{+/+}$* (B) and *Lmnb1$^{+/\Delta}$* (C) mice at 3 months of age. Nuclei are counter stained using Hoechst 33342 dye (blue). Scale bars 50 µm. Ventricles are marked with (*).

D. Quantification of GFAP^{+} area. Total area covered by GFAP was quantified in cortical plate of *Lmnb1$^{+/+}$* and *Lmnb1$^{+/\Delta}$* mice at 3 months of age. Graph bars represent the average percentage of GFAP^{+} area ± SEM.

3.2 Altered levels of *Lmnb1* causes morphological abnormalities

After observing the effect of *Lmnb1* absence or overexpression on cell fate commitment, we decided to determine if altered levels of *Lmnb1* had any effect on the development and maturation of these differentiated neurons.

It has been reported that Lamin B plays a key role in axon maintenance in Xenopus retinal ganglion cells *(Yoon et al, 2012).* However, the role of LMNB1 in axonal development is not known. Therefore, we decided to evaluate the effect of altered LMNB1 levels on neuronal differentiation through the analysis of axonal elongation during the maturation of $Lmnb1^{+/+}$ (Fig. 6A), and $Lmnb1^{\Delta/\Delta}$ NSCs-derived neurons (Fig. 6B). We stained 4 DIV neurons against βIII-tubulin antibody and measured axonal length observing a significant decrease in $Lmnb1^{\Delta/\Delta}$ NSCs-derived as compared to $Lmnb1^{+/+}$ NSCs-derived neurons (Fig. 6C). To evaluate the effect of LMNB1 overexpression on axonal elongation, we performed the same measurements on differentiation neurons from WT NSCs transfected with pLMNB1-EGFP (Fig. 6E) or pEGFP (Fig. 6D). We observed a significant decrease in axonal length measurement in pLMNB1-EGFP transfected neurons as compared to the pEGFP transfected neurons differentiated from WT NSCs (Fig. 6F). These results, thereby, indicate that an alteration in the level of Lmnb1 can cause deleterious effect on axonal elongation during the maturation of these differentiated neurons.

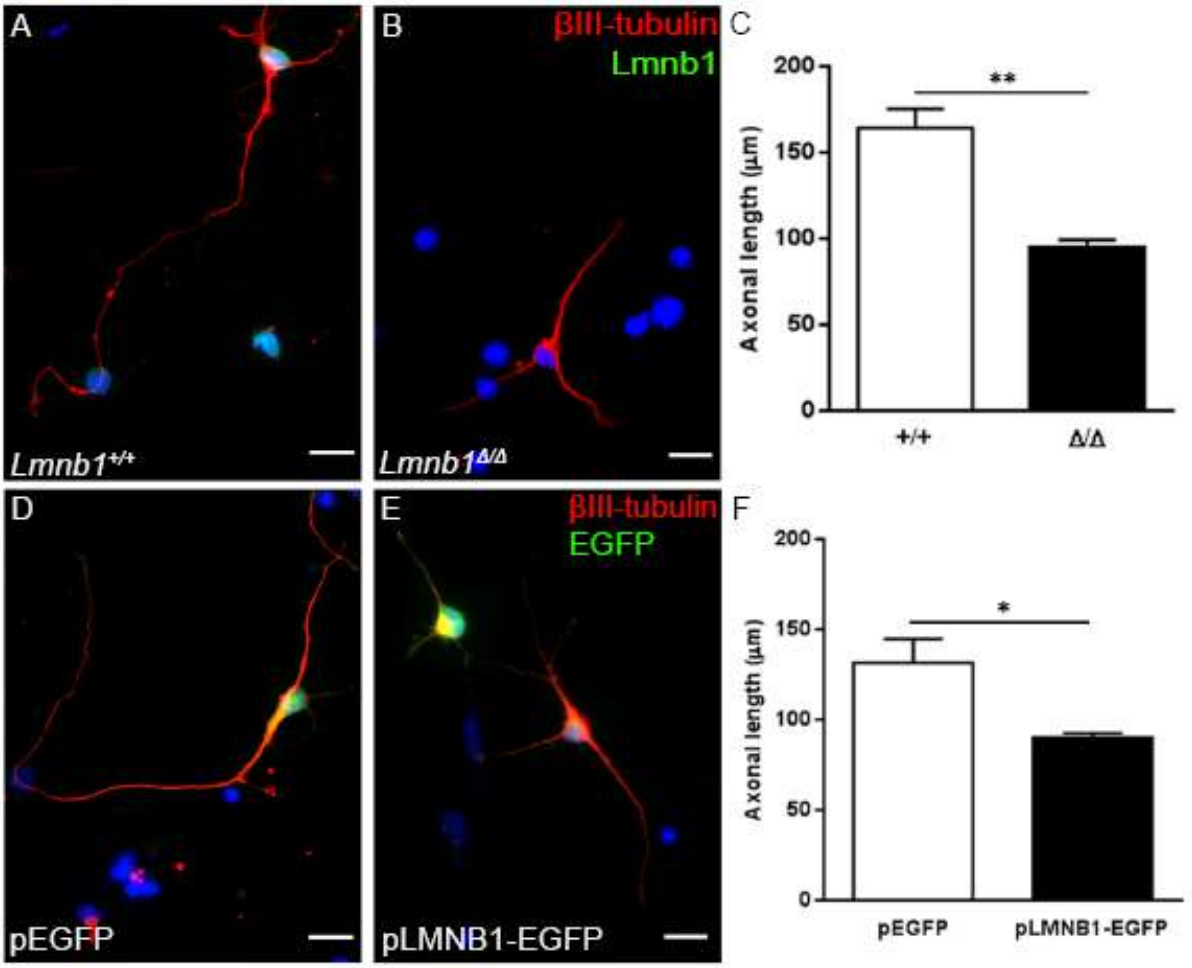

Figure 6. Abnormal levels of Lamin B1 reduce axonal length.
Axonal elongation in 4 DIV neurons differentiating from *Lmnb1*$^{\Delta/\Delta}$ and *Lmnb1*$^{+/+}$ NSCs or from NSCs overexpressing LMNB1 was measured as described in the methods.
A-C. Representative fluorescence images and quantitative analysis (C) of axonal length in neurons differentiated from *Lmnb1*$^{+/+}$ and *Lmnb1*$^{\Delta/\Delta}$ NSCs immuno-stained against for βIII-tubulin (red) and Lmnb1 (green).
D-F. Representative fluorescence images and quantitative analysis (F) of axonal length in neurons differentiated from NSCs transfected with pEGFP (D) or pLMNB1-EGFP (E) and immuno-stained for βIII-tubulin (red) and EGFP (green). In all fluorescence images, nuclei are counter-stained with DAPI (blue). Scale bars 20 µm. In panel C and F, bars represent the mean axonal length ± SEM. *p<0.05, **p<0.01, Student's t–test. Approximately, 180 βIII-tubulin^{+} neurons and 115 βIII-tubulin^{+} EGFP^{+} neurons from 3 independent experiments were used to measure the axonal length for each genotype (C) or transfection condition (F) respectively.

Lmnb1 is required to provide structural integrity to the nucleus. Therefore, we decided to evaluate the effect of altered level of LMNB1 on the nucleus of the differentiated neurons, we checked for the nuclear area and circularity. We observed a significant reduction in the nuclear area of the *Lmnb1*$^{\Delta/\Delta}$ NSCs-derived neurons (62.42 µm^2 ± 6.11 vs 76.47 µm^2 ± 2.29) as compared to the *Lmnb1*$^{+/+}$ NSCs-derived neurons (Fig. 7A) whereas no difference was observed in the nuclear area of the *LMNB1* overexpressing EGFP$^+$ neurons as compared to the control pEGFP transfected neurons (Fig. 7B). Even the nuclear circularity of the *Lmnb1*$^{\Delta/\Delta}$ NSCs-derived neurons was significantly reduced (0.54 ± 0.04 vs 0.72 ± 0.02) as compared to *Lmnb1*$^{+/+}$ NSCs-derived neurons (Fig. 7A), with no difference in the nuclear circularity after LMNB1 was overexpressed as compared to the control pEGFP transfected neurons (Fig. 7B). These results indicate that LMNB1 deficiency affect nuclear morphology in differentiated neurons derived from NSCs.

The nuclear area and circularity of *Lmnb1*$^{\Delta/\Delta}$ NSCs-derived astrocytes did not show any difference to the nuclear area and circularity of *Lmnb1*$^{+/+}$ NSCs-derived astrocytes respectively (Fig. 7C). We also did not observe any difference in the nuclear area and circularity in *LMNB1* overexpressing astrocytes after transfecting with pLMNB1-EGFP plasmid as compared to the control pEGFP transfected astrocytes (Fig. 7D).

Similar nuclear area and circularity quantifications were carried out on *Lmnb1*$^{\Delta/\Delta}$ NSCs-derived oligodendrocytes and we did not observe any difference as compared to the *Lmnb1*$^{+/+}$ NSCs-derived oligodendrocytes (Fig. 7E). The nuclear area and circularity of differentiated oligodendrocytes was not altered when *LMNB1* was overexpressed as compared to the control (Fig. 7F).

The quantification of nuclear area and circularity of differentiated neurons, astrocytes and oligodendrocytes from NSCs lacking LMNB1 or overexpressing LMNB1 suggest that loss of LMNB1 affects the nuclear area and circularity of only the differentiated neurons, but not astrocytes and

oligodendrocytes. No significant difference in the nuclear morphology was observed when LMNB1 was overexpressed in neurons, astrocytes or oligodendrocytes (Marotta et al, 2016, Pietro et al, 2015).

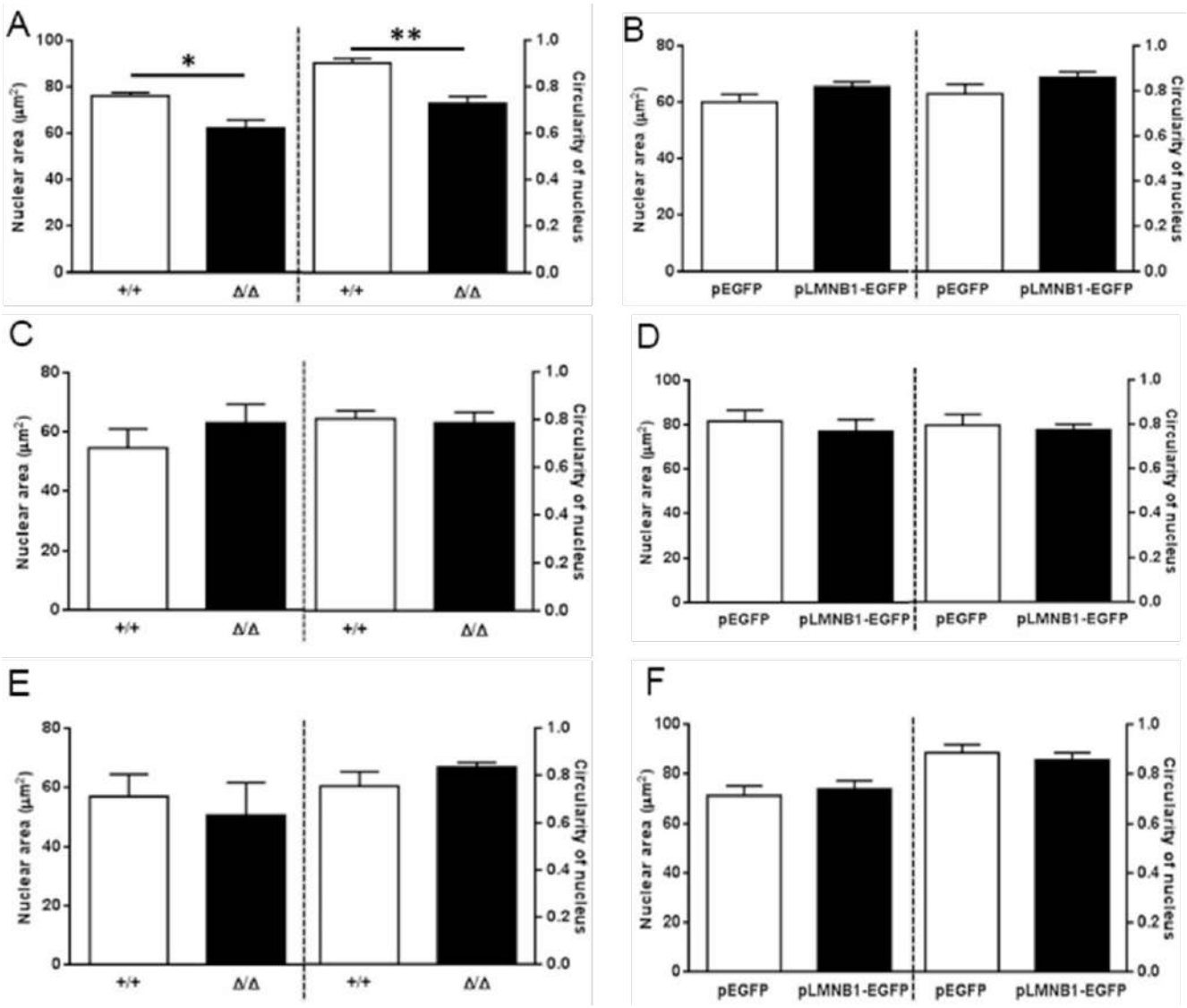

Figure 7. Altered levels of Lmnb1 affects the nuclear morphology of differentiated neurons, but not astrocytes and oligodendrocytes.

Nuclear area and circularity of differentiated neurons, astrocytes and oligodendrocytes derived from *Lmnb1*$^{+/+}$ or *Lmnb1*$^{\Delta/\Delta}$ NSCs and *Lmnb1*$^{+/+}$ NSCs transfected with pEGFP or pLMNB1-EGFP was quantified as previously described.

A,C,E. Quantitative analysis of nuclear size and shape in neurons (A), astrocytes (C) and oligodendrocytes (E) derived from *Lmnb1*$^{+/+}$ or *Lmnb1*$^{\Delta/\Delta}$ NSCs.

B,D,F. Quantitative analysis of nuclear size and shape in neurons (B), astrocytes (D) and oligodendrocytes (F) from *Lmnb1*$^{+/+}$ NSCs transfected with pEGFP or pLMNB1-EGFP. In all panels, graph bars represent the average nuclear area or circularity ± SEM. *p<0.05, **p<0.01 vs *Lmnb1*$^{+/+}$, Student's t-test.

3.3 Lmnb1 deficiency reduces cortical thickness in the developing embryonic brain

In the mouse, neuronal progenitors of the ventricular zone (VZ) start differentiating into neurons at embryonic day 11 (E11), populating the cortical plate (CP) *(Molyneaux et al, 2007)*. Consistent with previous findings *(Coffinier et al, 2011)*, we found that in *Lmnb1*$^{\Delta/\Delta}$ embryos the cortical thickness is reduced (Fig. 8A-B). This phenotype was observed from E13.5 (Fig. 8B). To investigate how Lmnb1 affects neuronal progenitors and neurogenesis in vivo, we analyzed the VZ and CP in *Lmnb1*$^{\Delta/\Delta}$ and *Lmnb1*$^{+/+}$ embryos at E13.5. Brain sections were immunodecorated against the neuronal marker βIII-tubulin to visualize the cortical plate and counterstained with Hoechst 33342 dye. The VZ was identified as the region close to the ventricle and devoid of βIII-tubulin. We found that the thickness of both CP and VZ was reduced in E13.5 *Lmnb1*$^{\Delta/\Delta}$ brain (Fig. 8C-D). The percentage reduction of CP was greater (-41%) than that of VZ (-22%). This, together with the finding that *Lmnb1*$^{\Delta/\Delta}$ NSC-derived neurons had reduced nuclear size (Nuclear Area; *Lmnb1*$^{\Delta/\Delta}$: 62.4 ± 6.1 µm^2; *Lmnb1*$^{+/+}$: 76.5 ± 2.3 µm2; n=3/group, *p<0.05, Student's t-test), suggest a possible impairment of neuron generation in *Lmnb1*$^{\Delta/\Delta}$ brain with relative preservation of progenitors. To test this hypothesis, considering the reduced size of *Lmnb1*$^{\Delta/\Delta}$ neuronal nuclei *(Giacomini et al, in preparation)*, we counted the number of cells present in the CP and VZ at E13.5. We found that in the VZ, *Lmnb1*$^{\Delta/\Delta}$ and *Lmnb1*$^{+/+}$ had similar number of cells (Fig. 8E). However, *Lmnb1*$^{\Delta/\Delta}$ embryos displayed a significant reduction of βIII-tubulin$^+$ neurons in the CP (Fig. 8F). This indicates that the absence of Lamin B1 impairs neurogenesis in vivo without affecting the number of VZ progenitors.

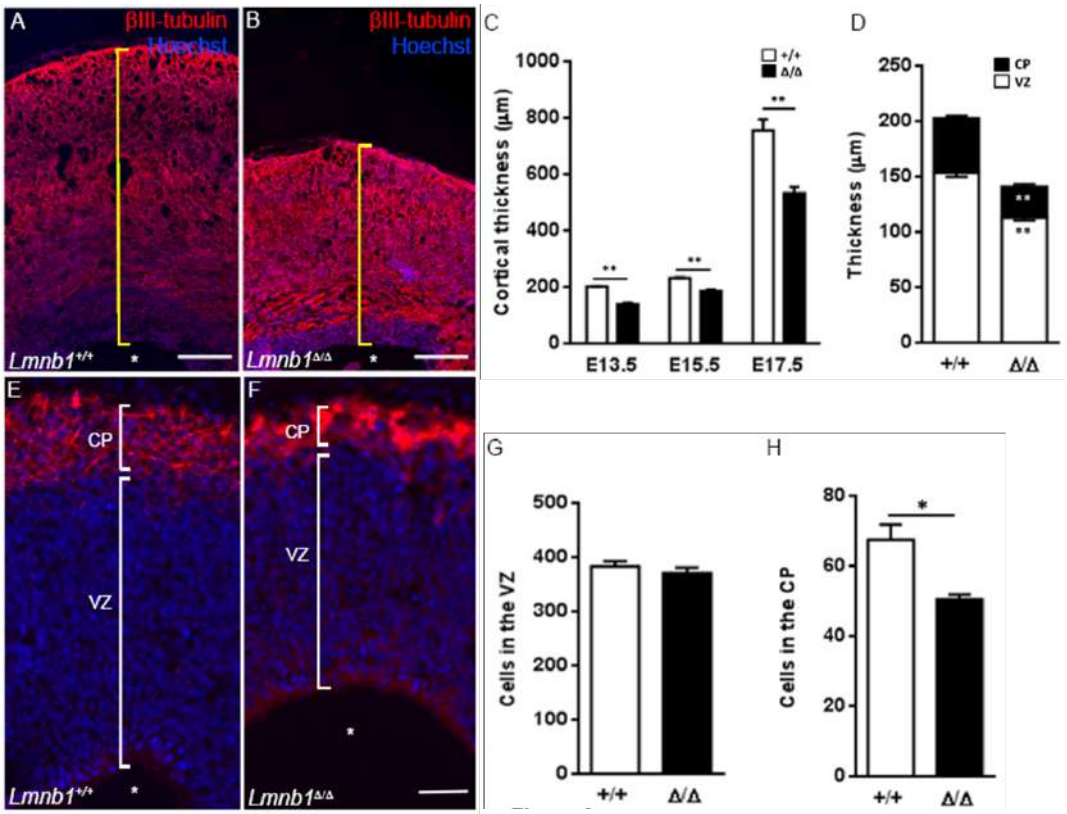

Figure 8. Lmnb1 deficiency significantly reduces the cortical thickness during embryonic development.

Brain sections from *Lmnb1*$^{+/+}$ and *Lmnb1*$^{\Delta/\Delta}$ embryos at E13.5, E15.5 and E17.5 were stained as described in the methods.

A-B. Representative fluorescence images of cortical coronal sections from E17.5 *Lmnb1*$^{+/+}$ and *Lmnb1*$^{\Delta/\Delta}$ brains immuno-stained against βIII-tubulin (red). Nuclei are counter-stained with Hoechst 33342 (blue). Scale bar 20 µm.

C. Quantitative analysis of cortical thickness in E13.5, E15.5 and E17.5 brains of *Lmnb1*$^{+/+}$ and *Lmnb1*$^{\Delta/\Delta}$ embryos. Graph bars represent the average cortical thickness ± SEM. **p<0.01, Student's t-test, from 3 independent experiments.

D. Quantitative analysis of thickness of cortical plate (CP) and ventricular zone (VZ) in E13.5 brains of *Lmnb1*$^{+/+}$ and *Lmnb1*$^{\Delta/\Delta}$ embryos. Graph bars represent the average thickness ± SEM. **p<0.01, Student's t-test, from 3 independent experiments.

E-F. Representative fluorescence images of cortical coronal sections of E13.5 *Lmnb1*$^{+/+}$ and *Lmnb1*$^{\Delta/\Delta}$ brains immuno-stained against βIII-tubulin (red). Nuclei are counter-stained with Hoechst 33342 (blue). Scale bar 20 µm.

G-H. Quantitative analysis of number of cells present in the VZ and the CP in E13.5 brains of *Lmnb1*$^{+/+}$ and *Lmnb1*$^{\Delta/\Delta}$ embryos. Graph bars represent the average number of cells ± SEM. *p<0.05, Student's t-test, from 3 independent experiments.

3.4 Lmnb1 deficiency alters the balance between glutamatergic and GABAergic neurons in the embryonic cortical plate

In the cortex, the majority of neurons are glutamatergic *(Rakic, 2009)* and originate from progenitors located in the subventricular zone (SVZ) in the lateral ventricle (LV). A proportion of cortical neurons are GABAergic neurons, which originate in the medial ganglionic eminence (MGE) and migrate to the cortical plate *(Molyneaux et al, 2007)*. To investigate whether the reduced number of neurons in the cortical plate was related to differential effects of Lmnb1 on the generation of specific types of neurons, we analyzed the number of glutamatergic and GABAergic neurons in the cortex of E19.5 embryos of $Lmnb1^{\Delta/\Delta}$ and $Lmnb1^{+/+}$ (Fig. 9A-B; D-E). We found that the number of glutamatergic neurons in the cortical plate of $Lmnb1^{\Delta/\Delta}$ (Fig. 9C) embryos was significantly reduced (-20%) as compared to the age matched $Lmnb1^{+/+}$ (n=3; **p<0.01; Student's t-test). However, we observed that the number of GABAergic neurons was significantly increased (+15%) in the cortex of $Lmnb1^{\Delta/\Delta}$ (Fig. 9F) compared to $Lmnb1^{+/+}$ (n=3; **p<0.01; Student's t-test). Magnified fluorescence images of $GluR1^{+}$ neurons and $GABA^{+}$ neurons are shown in panels 9A'-B' and 9D'-E' for $Lmnb1^{+/+}$ and $Lmnb1^{\Delta/\Delta}$ brain sections respectively.

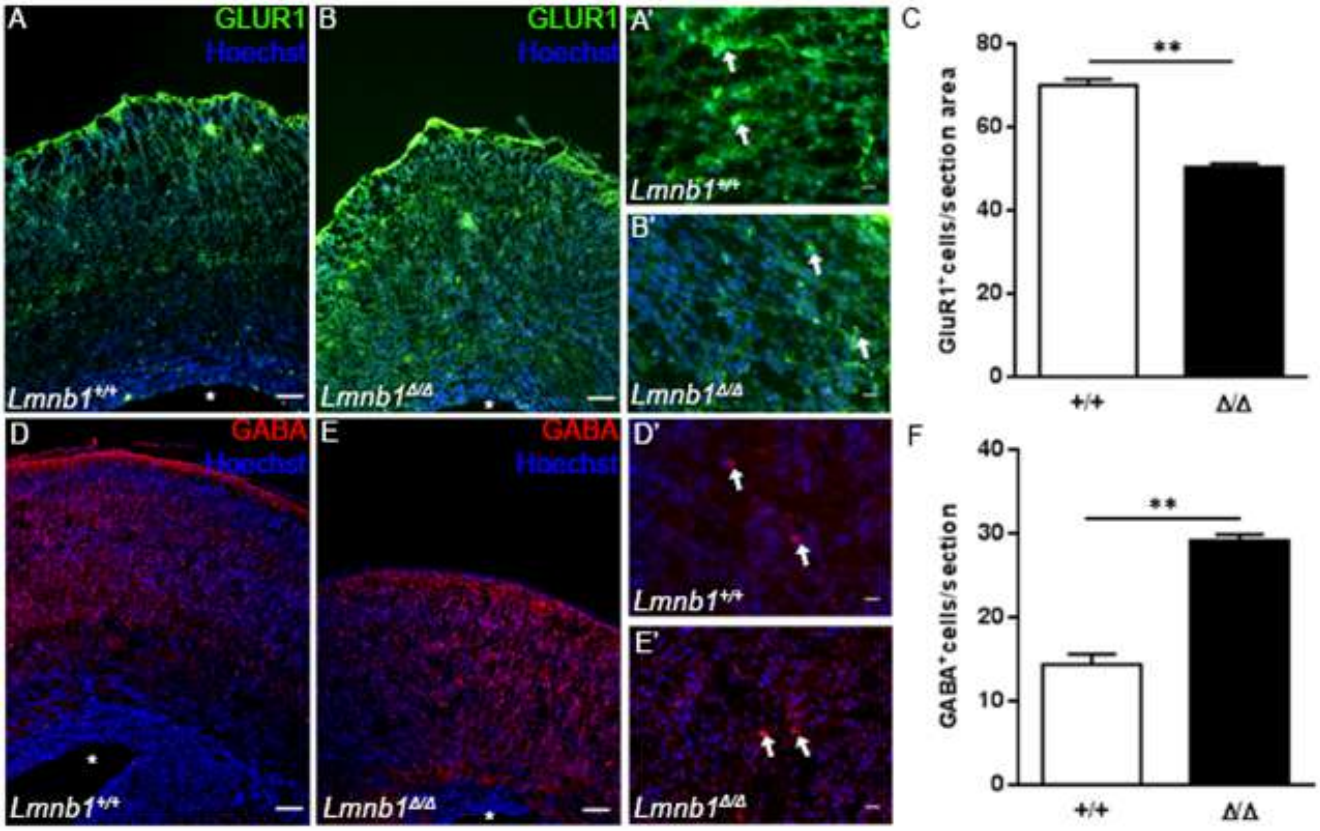

Figure 9. *Lmnb1* deficient embryonic brain has reduced number of Glutamatergic neurons and an increased number of GABA$^+$ neurons.

Sections of E19.5 embryonic brain of *Lmnb1*$^{+/+}$ and *Lmnb1*$^{\Delta/\Delta}$ were stained for GluR1 (glutamatergic neurons) and GABA (GABAergic neurons) as described in the methods.

A-C. Representative fluorescence images of immunoreactivity and quantification for GluR1 (green) in the cortex.

D-F. Representative fluorescence images of immunoreactivity and quantification for GABA (red) in the cortex. for GABA (red) in the cortex. Nuclei are counter-stained with Hoechst 33342 (blue). Magnified views of GluR1$^+$ and GABA$^+$ neurons (arrows) are shown in panel A'-B' and D'-E'. Scale bars: 100 µm (A-B; D-E); 20 µm (A'-B'; D'-E'). Graph bars represent the average number of GluR1$^+$ or GABA$^+$ cells/section ± SEM. **p<0.01, Student's t-test, from 3 independent experiments.

3.5 Lmnb1 deficiency leads to impaired neuronal differentiation at later developmental stages

As the reduced cortical thickness and reduction in the number of neurons in the absence of Lmnb1 could be due to a defect in neuronal differentiation, we analyzed the number of $Sox2^+$ cells in *Lmnb1*$^{+/+}$ and *Lmnb1*$^{\Delta/\Delta}$ littermates at E17.5. Sox2 marks the progenitor cells, and the number gradually decreases as most of the progenitor cells differentiate into neurons which migrate into the cortical plate. It has been reported that there is no significant difference in the number of $Sox2^+$ cells in *Lmnb1*$^{+/+}$ and *Lmnb1*$^{\Delta/\Delta}$ cortical plate at E17.5 *(Coffinier et al, 2011)*. When we performed the quantification of $Sox2^+$ cells at E17.5, we did not observe a significant difference in *Lmnb1*$^{+/+}$ (Fig. 10A) and *Lmnb1*$^{\Delta/\Delta}$ cortical plate (Fig. 10B). At a later stage of development (E19.5), we observed a significantly higher number of $Sox2^+$ cells (Fig. 10E) in *Lmnb1*$^{\Delta/\Delta}$ (Fig. 10D) as compared to the *Lmnb1*$^{+/+}$ (Fig. 10C) brain sections. This result might suggest that *Lmnb1*-deficient progenitors remain in a proliferative, undifferentiated state longer as compared to the *Lmnb1*$^{+/+}$ progenitor cells.

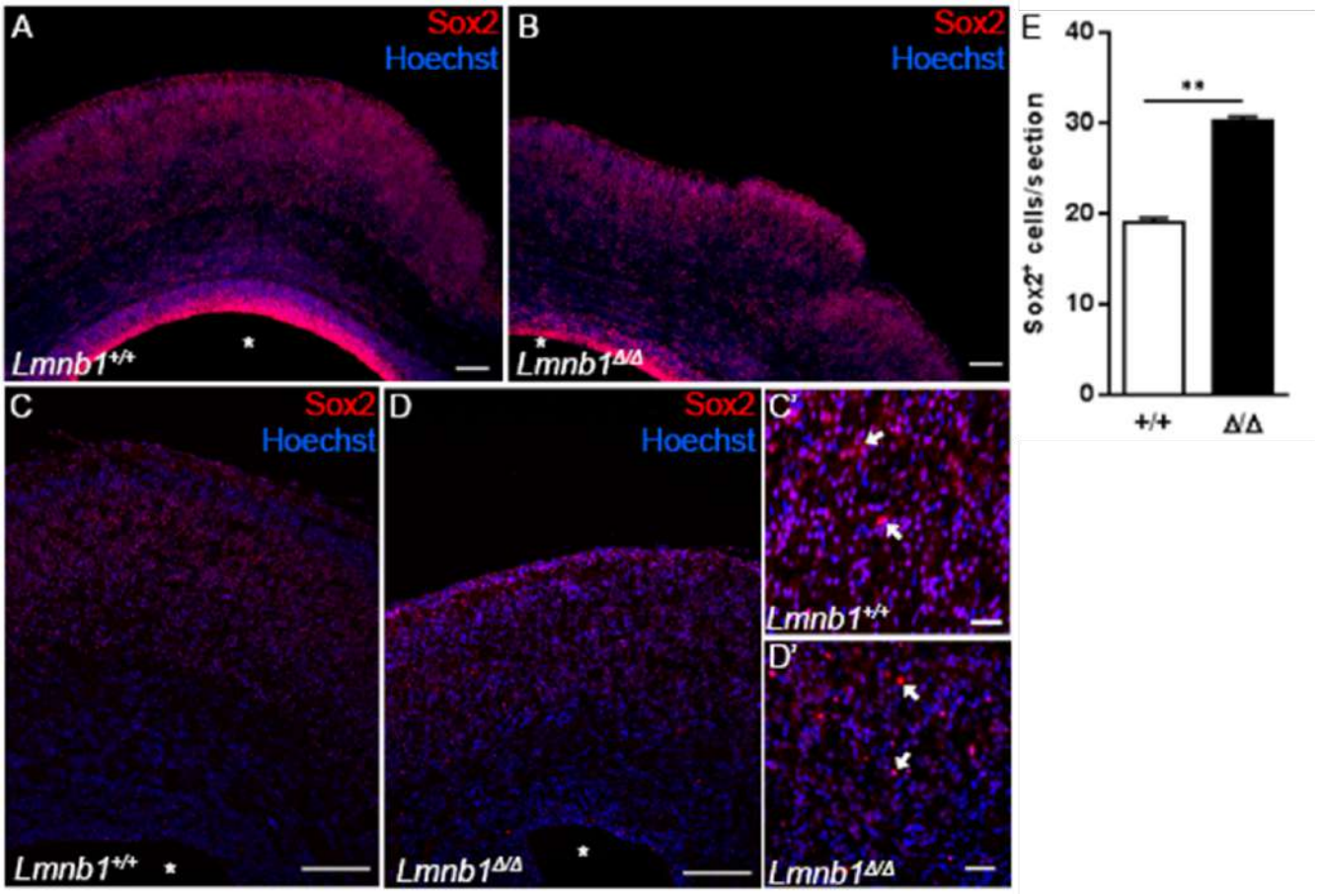

Figure 10. The number of Sox2$^+$ cells are increased in Lmnb1 deficient embryonic brain.
Sections of E17.5 and E19.5 embryonic brains of *Lmnb1$^{+/+}$* and *Lmnb1$^{\Delta/\Delta}$* were stained for Sox2 as described in the methods.

A-D. Representative fluorescence images of immunoreactivity for Sox2$^+$ progenitor cells (red) in E17.5 (A-B) and E19.5 (C-D) *Lmnb1$^{+/+}$* and Lmnb1$^{\Delta/\Delta}$ brain. Magnified views of Sox2$^+$ progenitors (arrows) in E19.5 brains are shown in panels C' and D'. Nuclei are counter-stained with Hoechst 33342 (blue). Scale bars: 100 µm (A-D); 10 µm (C'-D').

E. Quantitative analysis of Sox2$^+$ cells. Total numbers of Sox2$^+$ cells in the cortical plate of *Lmnb1$^{+/+}$* and Lmnb1$^{\Delta/\Delta}$ were counted. Graph bars represent the average number of Sox2$^+$ cells/section ± SEM. **p<0.01, Student's t-test, from 3 independent experiments.

However, when we looked for other progenitor markers like TBR2 and RC2 (radial glial marker), we observed a defective localization of RC2^{+} cells in E17.5 Lmnb1$^{\Delta/\Delta}$ (Fig. 11B) cortical plate as compared to *Lmnb1*$^{+/+}$ cortical plate (Fig. 11A). We did not observe any difference in the immunohistochemistry obtained from TBR2 staining in Lmnb1$^{\Delta/\Delta}$ and *Lmnb1*$^{+/+}$ (Fig. 11A-B). Magnified images are shown in panels (a-a' for *Lmnb1*$^{+/+}$; b-b' for Lmnb1$^{\Delta/\Delta}$).

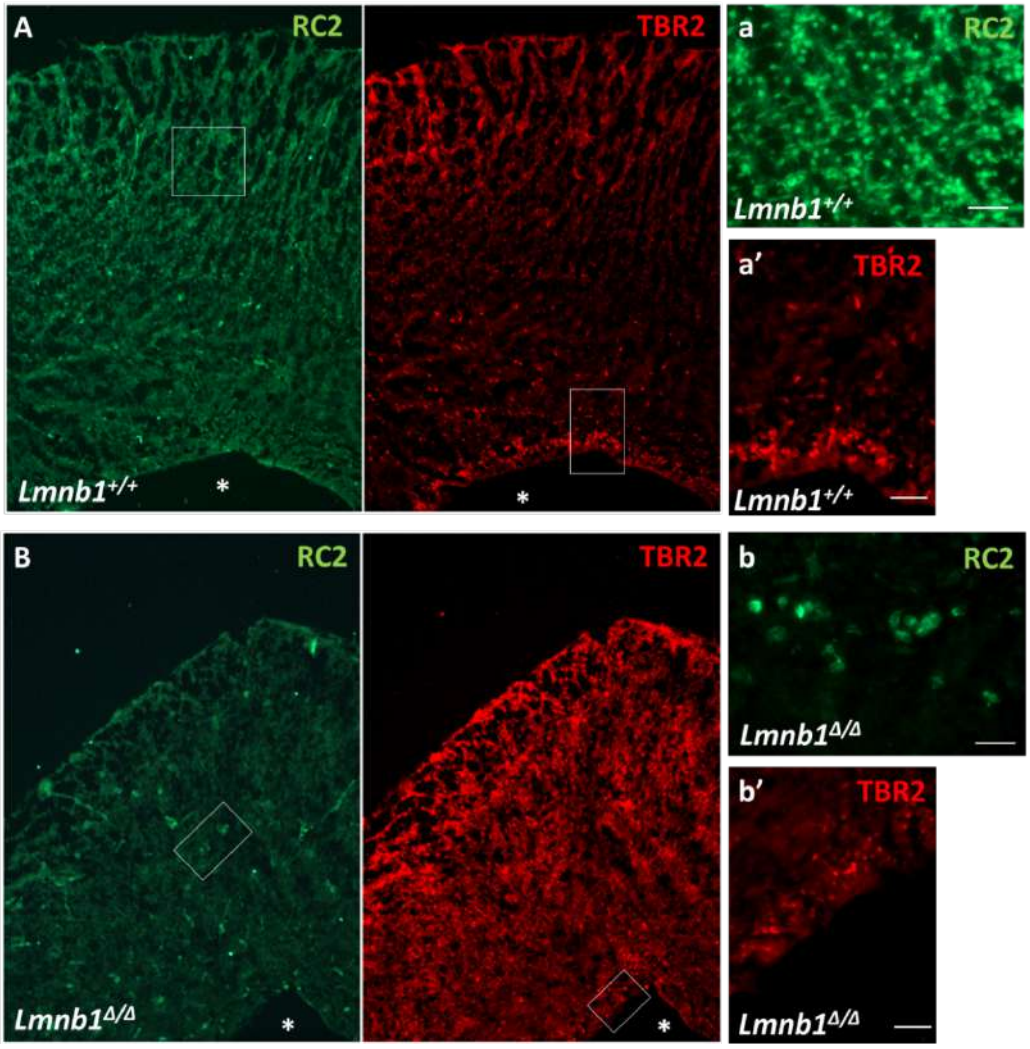

Figure 11. RC2^{+} cells delocalized in the cortical plate of *Lmnb1*$^{\Delta/\Delta}$ at E17.5.
Sections of E17.5 embryonic brains of *Lmnb1*$^{+/+}$ and *Lmnb1*$^{\Delta/\Delta}$ were stained for TBR2 and RC2 as described in the methods.
A-B. Representative fluorescence images of immunoreactivity for RC2 (green) and TBR2 (red) in E17.5 *Lmnb1*$^{+/+}$ (A) and Lmnb1$^{\Delta/\Delta}$ (B) brain. Magnified views are shown in panels a-a' and b-b'. Nuclei are counter-stained with Hoechst 33342 (blue). Scale bars: 100 µm (A-D); 10 µm (a-a'; b-b').

3.6 Knockdown of *Lmnb1* in vivo increases the number of astrocytes

In order to confirm that Sh-Lmnb1 can knockdown LMNB1 in vivo, we first quantified the expression of Lmnb1 in vitro by transfecting Sh-Lmnb1 or Sh-Scrambled plasmids in N2A cell line. By Western blot analysis, we observed that the level of Lmnb1 was significant reduced (-50%) when Sh-Lmnb1 was transfected (Fig. 12A-B) as compared to the Sh-Scrambled transfected or even against the untransfected cells.

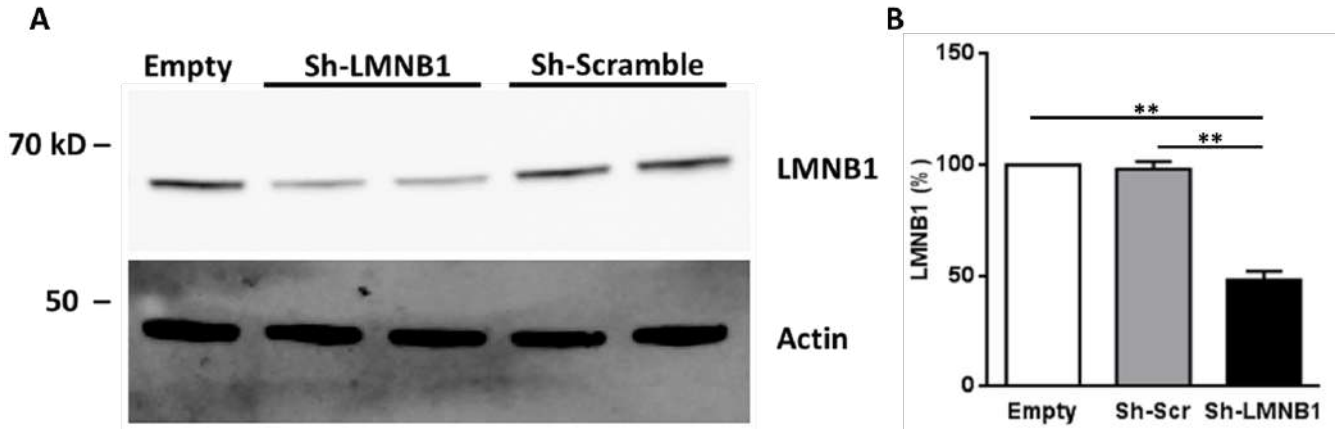

Figure 12. Knockdown of Lmnb1 using Sh-Lmnb1 plasmid in vitro.
A-B. Western blot analysis for LMNB1 expression in N2A cells transfected with Sh-Lmnb1 or Sh-Scrambled plasmids (A) and quantification as normalized to the expression level of actin (B). Graph bars represent the percentage of expression of LMNB1 ± SEM. **p<0.01, One-way ANOVA via Bonferroni test.

We next explored whether Lmnb1 deficiency was associated with increased astrocytic differentiation *in vivo*, by analyzing the protein expression of GFAP in brains of $Lmnb1^{\Delta/\Delta}$ and $Lmnb1^{+/+}$ E17.5 embryos. GFAP levels were significantly increased in $Lmnb1^{\Delta/\Delta}$ brain lysates as compared to the $Lmnb1^{+/+}$ as demonstrated by Western blot analysis (Fig. 13A-B). This suggests that Lmnb1 deficiency induces a potential increase of either astrocytes or radial glia, which also expresses GFAP at this developmental stage and act as astrocyte progenitors *(Mamber et al, 2013,*

*Raina et al, 2020)***.** We also observed a significant reduction in the expression level of neuronal marker βIII-tubulin in *Lmnb1*$^{\Delta/\Delta}$ brain lysates as compared to the *Lmnb1*$^{+/+}$ (Fig. 13C; n=3; *p<0.05; Student's t-test).

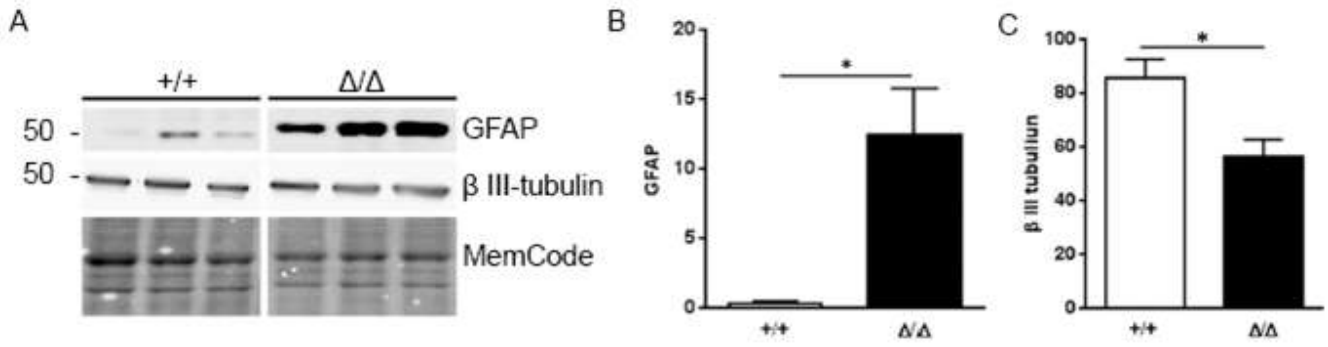

Figure 13. *Lmnb1*$^{\Delta/\Delta}$ embryo brains show increased GFAP expression and reduced βIII-tubulin expression.
A-C. Western blot analysis and quantification to determine the expression of GFAP (A-B) and βIII-tubulin (A;C) in E17.5 *Lmnb1*$^{\Delta/\Delta}$ brain lysates as compared to the *Lmnb1*$^{+/+}$. Normalization was performed using MemCode as described in the methods. Graph bars represent the average expression of GFAP or βIII-tubulin ± SEM. *p<0.05; Student's t-test.

To investigate whether in vivo astrocytic differentiation was specifically triggered by deficiency of Lmnb1, we knocked down expression in SVZ progenitors of WT embryonic brain by using in utero electroporation of *Lmnb1* specific sh-RNA (Sh-Lmnb1) or scramble (Sh-Scramble) control sh-RNA plasmids which contain the EGFP reporter. After electroporation, pups were born and analyzed at P7. The expression of endogenous Lmnb1 was effectively reduced by Sh-Lmnb1 (Fig. 14B), but not with Sh-Scramble (Fig. 14A). In brains electroporated with Sh-scrambled (Fig. 14D), GFAP expression was very low and limited to a few cells in the ventricular part of the SVZ similar to WT unelectroporated P7 pups (Fig. 14C) with a few scattered cells and processes through the cortex

with no overlap with EGFP$^+$ cells. Lmnb1 silencing by Sh-Lmnb1 electroporation results in a strong increase of GFAP immunoreactivity adjacent to EGFP$^+$ cells (Fig. 14E). Consistently, the area of GFAP immunoreactivity was significantly increased by 3-fold in brains where Lmnb1 was silenced (Fig. 14F). Overall, these results indicate that absence of Lmnb1 promotes astrocytes differentiation over neurogenesis during cortical development in vivo.

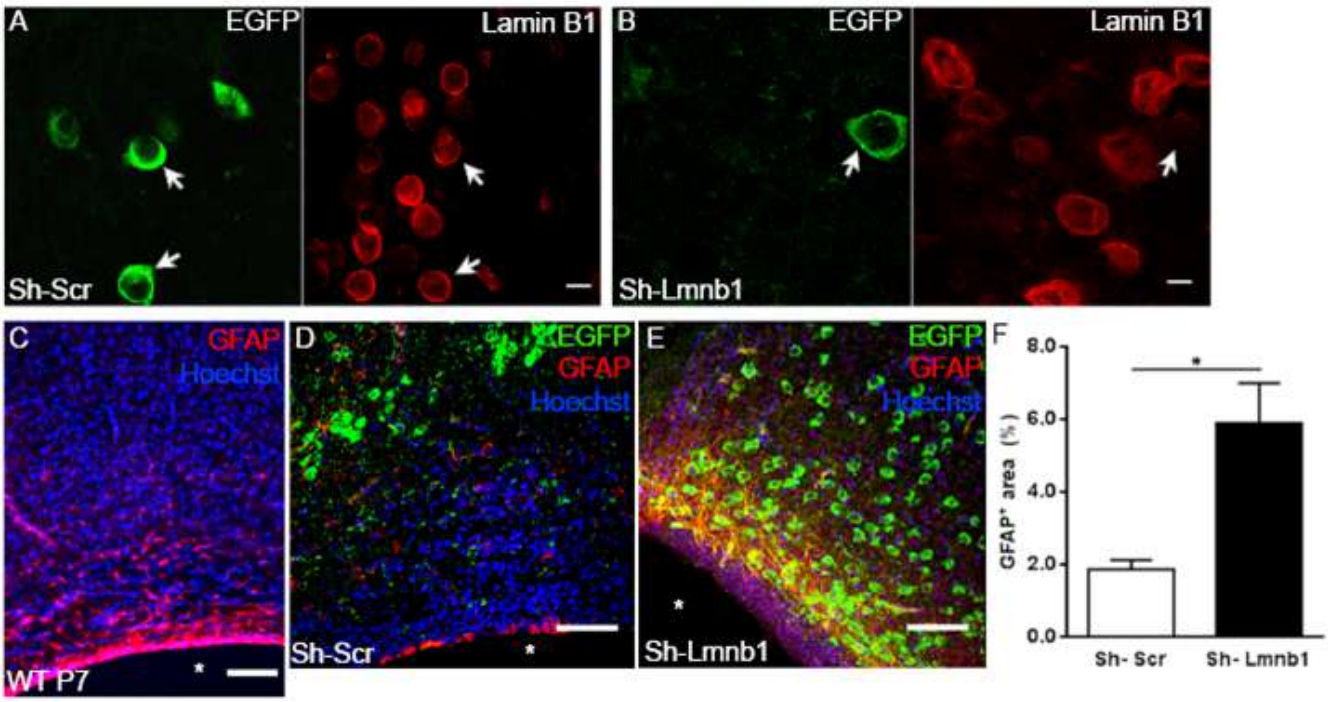

Figure 14. Knockdown of Lmnb1 increases GFAP$^+$ area *in vivo*.
A-B. Representative fluorescence confocal images of immunoreactivity for Lamin B1 (A-B; red) and EGFP (A-B; green) in Sh-Lmnb1 (B) and Sh-Scr (A) electroporated brains at P7.
C-D. Representative fluorescence confocal images of immunoreactivity for GFAP (C-D; red) and EGFP (C-D; green) in Sh-Lmnb1 (D) and Sh-Scr (C) electroporated brains at P7. Nuclei are counter-stained with Hoechst 33342 (blue). Scale bars: 5 µm (A-B); 10 µm (C-D).
E. Quantitative analysis of GFAP$^+$ area in P7 electroporated brains. Total GFAP$^+$ area was quantified after Sh-Lmnb1 or Sh-Scr electroporation in the cortex of P7 pups. Graph bars represent the average percentage of GFAP$^+$ area ± SEM. *p<0.05; Student's t-test.

To investigate the origin of the surplus GABAergic neurons, we knocked down Lmnb1 in SVZ progenitors of WT embryos using Sh-Lmnb1 plasmid and analyzed whether EGFP$^+$ cells were also positive for GABA. GABA immunoreactivity was never detected in EGFP$^+$ cells of brains electroporated with both Sh-Lmnb1 or Sh-Scramble (Fig. 15A,B), excluding the possibility that absence of Lmnb1 could switch the cell fate of glutamatergic progenitors into GABAergic precursors.

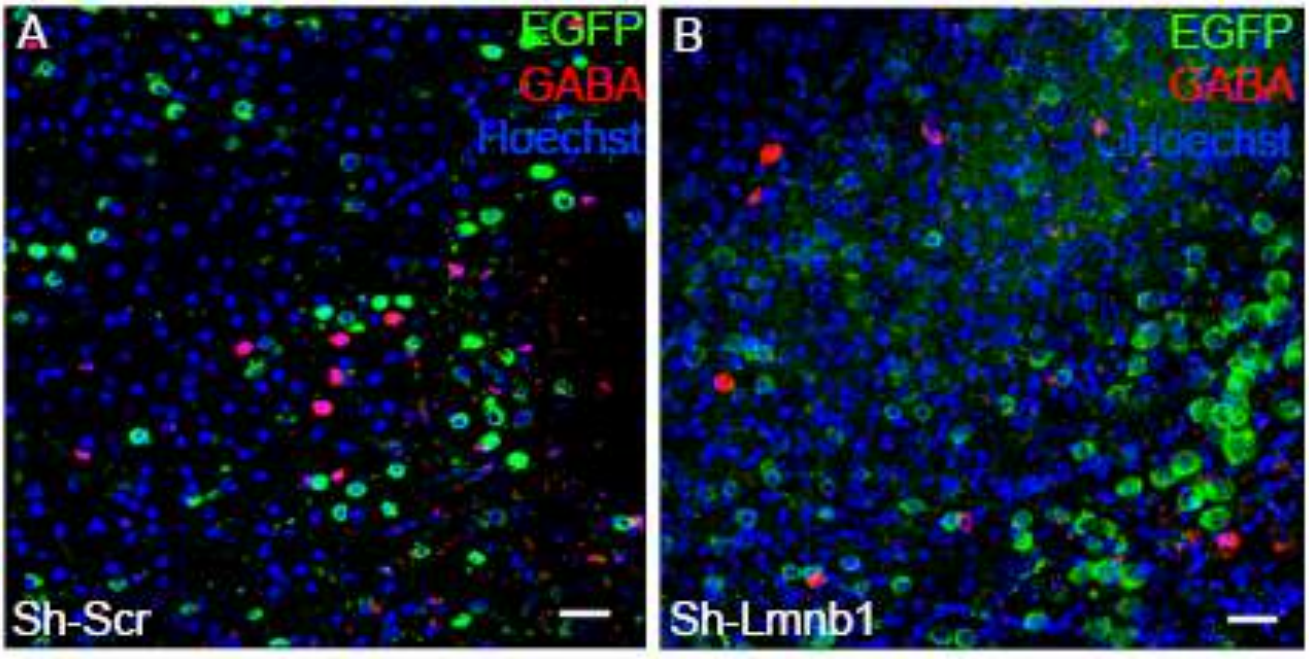

Figure 15. GABA expression does not co-localize with EGFP$^+$ electroporated cells.
A-B. Representative fluorescence confocal images of immunoreactivity for EGFP (A-B; green) and GABA (A-B; red) in Sh-Scrambled (A) or Sh-Lmnb1 (B) electroporated brains at P7. Nuclei are counter-stained with Hoechst 33342 dye (blue). Scale bars 5 µm.

3.7 Altered Lmnb1 levels cause defective neuronal migration in vivo

Deficiency of *Lmnb1* leads to abnormal cortical layering during embryonic development *(Coffinier et al, 2011)*. Indeed, consistent with previous findings *(Coffinier et al, 2011)*, we found that, in *Lmnb1*$^{\Delta/\Delta}$ E17.5 brain sections, layer VI neurons identified by Tbr1 (Fig. 16A-B) and FoxP2 (Fig. 16C-D) markers were scattered throughout the cortical plate and the majority of them positioned in more superficial layers than in *Lmnb1*$^{+/+}$ embryos (Fig. 16A-D). These findings suggest that abnormal levels of Lmnb1 could affect neuronal migration in the developing mouse brain.

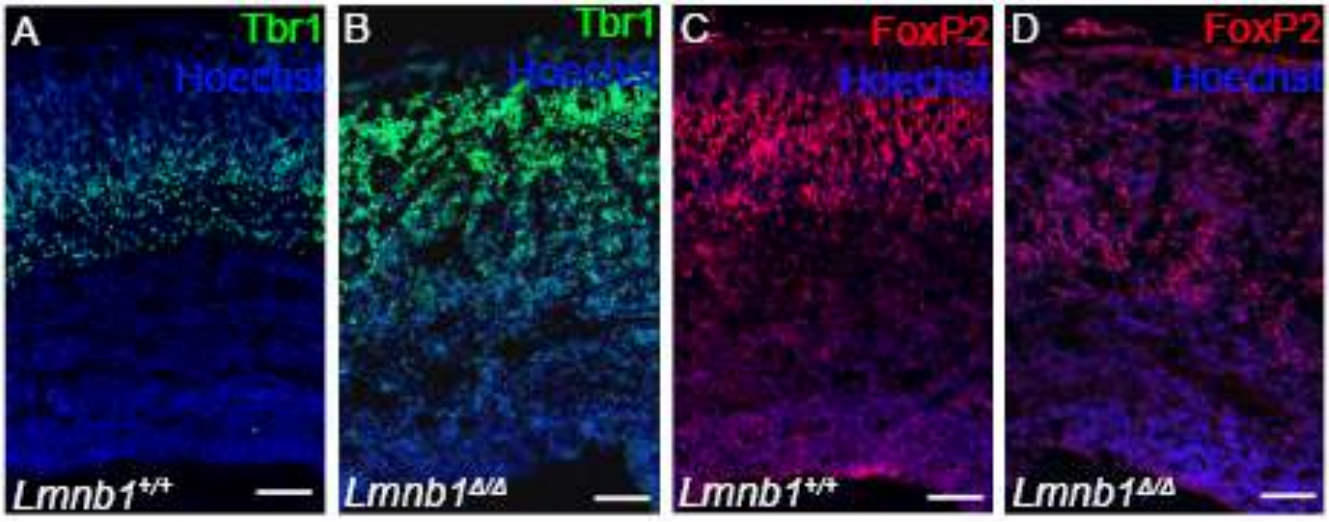

Figure 16. Abnormal localization of cortical layer markers in *Lmnb1*$^{\Delta/\Delta}$ E17.5 embryos.
A-B. Representative fluorescence images of immunoreactivity for Tbr1 (A-B; green) in E17.5 *Lmnb1*$^{+/+}$ (A) and *Lmnb1*$^{\Delta/\Delta}$ (B) cortex.
C-D. Representative fluorescence images of immunoreactivity for FoxP2 (C-D; red) in E17.5 *Lmnb1*$^{+/+}$ (C) and *Lmnb1*$^{\Delta/\Delta}$ (D) cortex. Nuclei were counter-stained using Hoechst 33342 dye (blue). Scale bars 50 µm.

To explore this assumption, we either knocked down or overexpressed Lmnb1 in the brain of WT embryos by in utero electroporation. We first silenced endogenous Lmnb1 by electroporating sh-Lmnb1 or sh-scramble plasmids in E14.5 embryos and analyzed the position of electroporated

neurons at P7. Neurons born at E14 typically localize in the layer IV-V *(Takahashi et al, 1999)*. Accordingly, in mice electroporated with sh-scramble control plasmid (Fig. 17A), EGFP$^+$ cells correctly localized in layers V (Fig. 17C). Conversely, in mice where Lmnb1 was silenced by sh-Lmnb1 (Fig. 17B), the majority of EGFP$^+$ neurons localized in the SVZ or the sub-plate (SP), with only a small percentage of EGFP$^+$ cells positioning in layer V of the cortical plate (Fig. 17C; n=3; *p<0.05; **p<0.01; Student's t-test). These results indicate that reduced levels of Lmnb1 strongly impairs neuronal migration during embryonic brain development in the mouse.

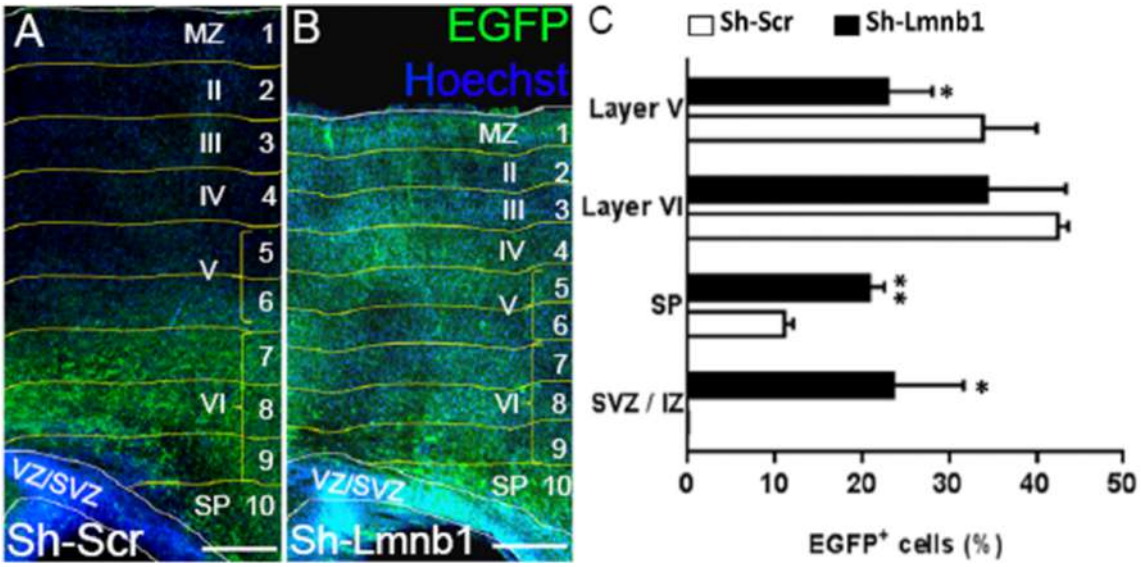

Figure 17. Knockdown of Lmnb1 leads to defective neuronal migration *in vivo*.
A-B. Representative fluorescence confocal images of immunoreactivity for EGFP (A-B; green) in Sh-Scrambled (A) and Sh-Lmnb1 (B) electroporated brains. Nuclei were counter-stained by Hoechst 33342 dye (blue). Scale bars 50 µm.
C. Quantitative analysis of location of electroporated cells. The total number of EGFP$^+$ electroporated cells were quantified with regards to their location in the cortex in Sh-Scrambled and Sh-Lmnb1 electroporated brains. Graph bars represent the average percentage of EGFP$^+$ cells ± SEM. *p<0.05; **p<0.01; Student's t-test. [MZ – Marginal Zone; I-VI – Cortical layers 1-6; VZ – Ventricular Zone; SVZ – Subventricular Zone; SP – Subplate].

We next overexpressed LMNB1 using the pLMNB1-EGFP and pEGFP control plasmids. Embryos were electroporated in utero at E14.5 and brains were analyzed at E18.5 (Fig. 18C-D). To confirm the overexpression, LMNB1 levels were analyzed by immunohistochemistry. As expected, LMNB1 levels were increased in $EGFP^+$ cells of embryos electroporated with pLMNB1-EGFP (Fig. 18B), but not with pEGFP (Fig. 18A). We thus quantified the number of $EGFP^+$ cells in the cortical plate based on their position with regards to a reference marker Ctip2 that is expressed in layer V neurons of the cortical plate *(Molyneaux et al, 2007, Raina et al, 2021)*. In brains overexpressing EGFP alone, over 70% of $EGFP^+$ neurons were located in the $Ctip2^+$ layer, i.e. layer V (Fig. 18E), with only a minor fraction locating above (13%) or below (15%). In brains overexpressing LMNB1, the percentage of EGFP+ neurons present within the layer V of the cortical plate was significantly reduced (53%) of neurons mislocalizing either above (28%) or below (18%) Ctip2 layer (Fig. 18E).

Altogether, these results indicate that Lmnb1 levels are critical to achieve correct neuronal migration in the developing embryonic brain and define the proper layer structure of the cortex.

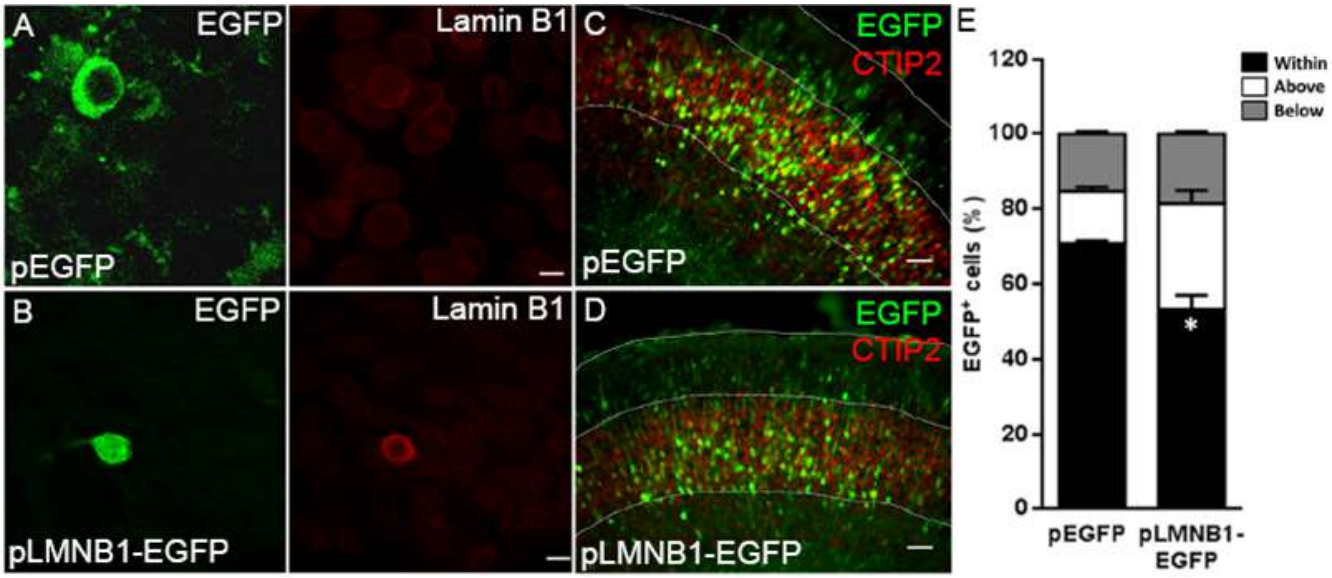

Figure 18. Overexpression of LMNB1 leads to defective neuronal migration *in vivo*.

A-B. Representative maximal projections of z-stack confocal images of cortical plate cells electroporated with pEGFP (A) or pLMNB1-EGFP (B) and immuno-stained against EGFP (A-B; green) and Lamin B1 (A-B; red).

C-D. Representative maximal projections of z-stack magnified images of cortical plate of E18.5 *Lmnb1*$^{+/+}$ brains electroporated with pEGFP (C) or pLMNB1-EGFP (D) and immuno-stained against EGFP (C-D; green) and Ctip2 (C-D; red). Scale bars 5 µm (A-B); 50 µm (C-D).

E. Quantitative analysis of the position of electroporated cells in the cortical plate with respect to V layer containing Ctip2^{+} neurons. Graph bars represent the average percentage of EGFP^{+} cells within, below or above the Ctip2 layer ± SEM. *p<0.05, Student's t–test.

3.8 Lmnb1 deficiency causes abnormal localization of Nuclear Pore Complexes (NPCs)

We next investigated the molecular mechanisms by which Lmnb1 induces changes in astrocytic and neuronal fate commitment. The balance and timing of neurogenesis vs astrocytic differentiation is regulated by gene expression programs induced by signaling molecules shuttling between cytosol and nucleus. The transport of such molecules occurs through nuclear pore complex (NPCs) *(Huenniger et al, 2010)*, whose distribution at the nuclear envelope is regulated by lamin binding *(Chen et al, 2013; Guo et al, 2014; Smythe et al, 2000; Al-Haboubi et al, 2011)*. Lmnb1 deficiency lead to de-localization of NPC in embryonic stem cell-derived fibroblast-like cells (EDFCs) and mouse embryonic fibroblasts (MEFs) *(Guo et al, 2014)*. We therefore investigated the localization of NPCs in differentiated cells from NSCs of $Lmnb1^{+/+}$ and $Lmnb1^{\Delta/\Delta}$ embryos. NPCs were evenly distributed on the nuclear envelope of $Lmnb1^{+/+}$ NSCs – derived cells (Fig. 19C), while they were irregularly spaced with asymmetric, polarized distribution in $Lmnb1^{\Delta/\Delta}$ cultures (Fig. 19D). Similar findings were obtained from the analysis of NPC in brain sections of E17.5 $Lmnb1^{+/+}$ and $Lmnb1^{\Delta/\Delta}$ embryos (Fig. 19A-B). Moreover, to understand if Lmnb1 deficiency affected the amount of nucleoporins (Nup) present within the NPCs in the brain, along with the localization, we performed a Western blot of E17.5 brain lysates of $Lmnb1^{+/+}$ and $Lmnb1^{\Delta/\Delta}$ embryos (Fig. 19E). We observed a significant decrease in the level of NUP 153 and Nup98 when Lmnb1 was absent as compared to their respective levels in $Lmnb1^{+/+}$ E17.5 brain lysates (Fig. 19F; **$p<0.01$; Student's t-test). These results indicate that there is a reduction in the level as well as de-localization of NPCs when Lmnb1 is absent.

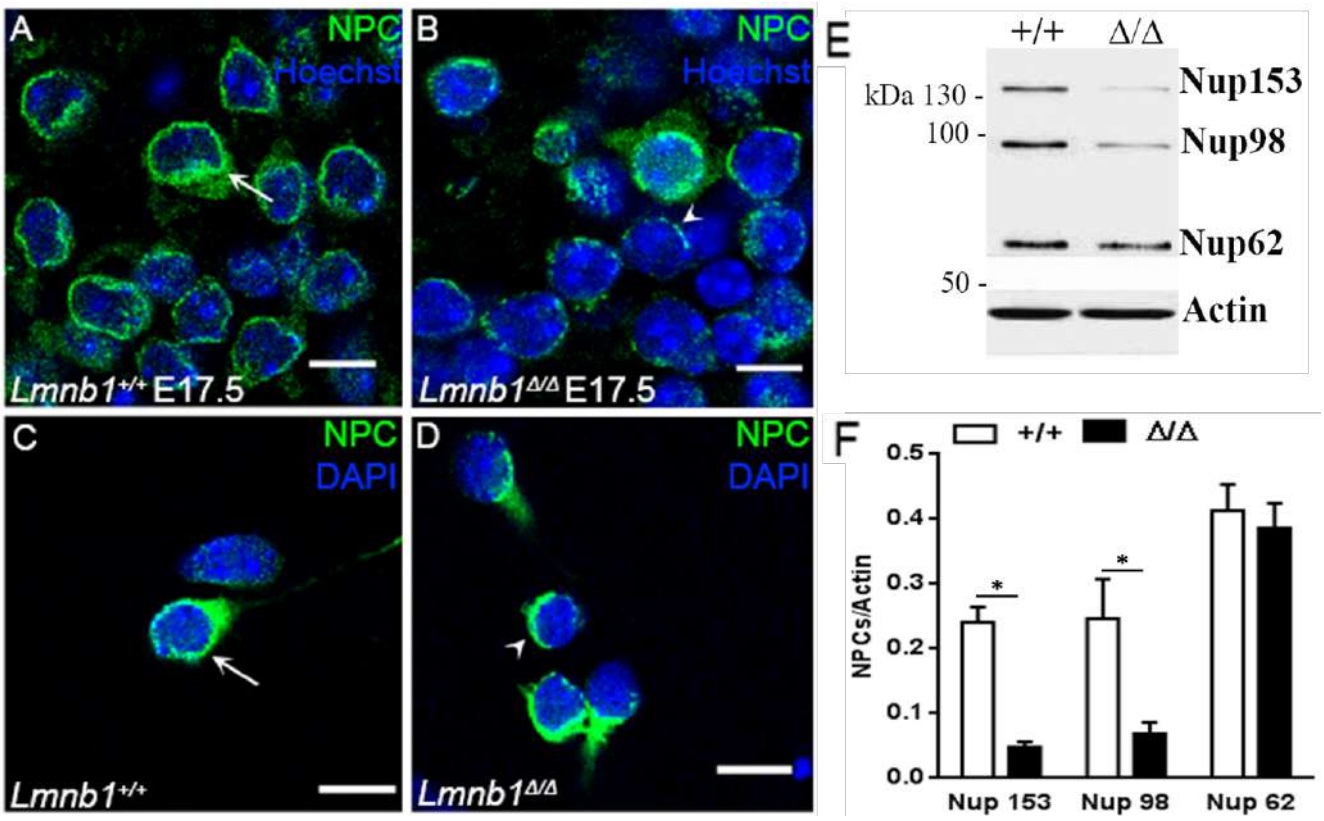

Figure 19. Lmnb1 deficiency is associated with NPC delocalization in the mouse embryo and in cultured NSCs.

A-D. Representative maximal projections of z-stack confocal images of cortex from E17.5 *Lmnb1*$^{+/+}$ and *Lmnb1*$^{\Delta/\Delta}$ embryonic brains (A-B) and NSCs (C-D) stained against NPC (green). Nuclei are counter-stained with Hoechst 33342 (A-B; blue) or DAPI (C-D; blue). Scale bars 10µm. In B and D, arrowheads indicate nuclei with clusterized, asymmetrical NPC localization.

E. Representative Western blot of Nup153, Nup98 and Nup62 in total lysates of brain from E17.5 *Lmnb1*$^{+/+}$ and *Lmnb1* $^{\Delta/\Delta}$ embryos.

F. Quantitative analysis of Nup153, Nup98 and Nup62 expression. NPC was normalized to MemCode. Graph bars represent the normalized values ± SEM. **p<0.01, Student's t-test.

We also checked for the localization of TPR1 in E17.5 *Lmnb1*$^{+/+}$ and *Lmnb1*$^{\Delta/\Delta}$ brain sections. TPR1 is a protein which is localized in the intranuclear filaments associated with the nucleoplasmic side of the NPC *(Cordes et al, 1997)*. We observed similar delocalization of TPR1 in *Lmnb1*$^{\Delta/\Delta}$ brain sections (Fig. 20B) as compared to the expression in *Lmnb1*$^{+/+}$ (Fig. 20A) brain sections.

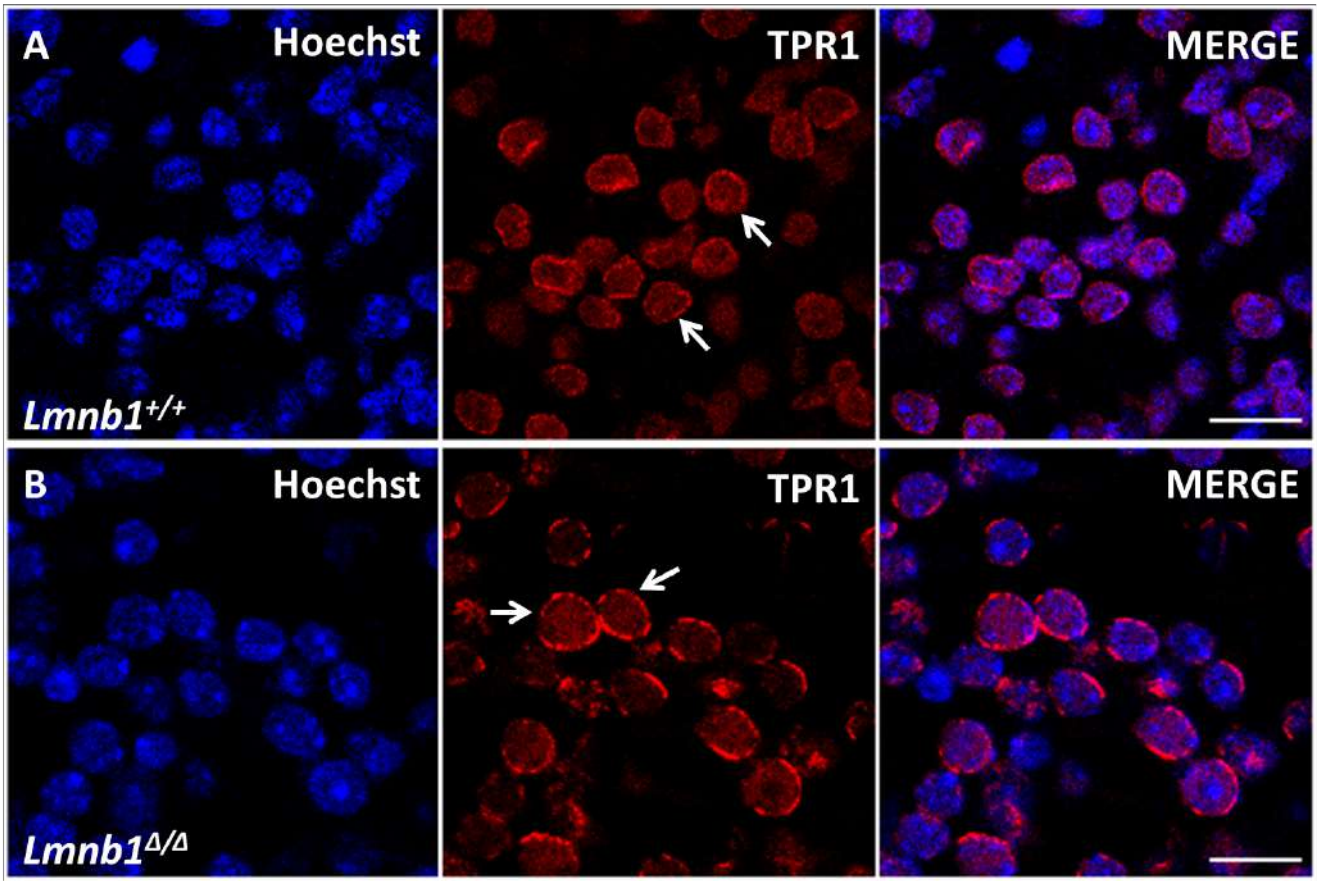

Figure 20. De-localization of TPR1 in E17.5 Lmnb1-deficient embryo sections.
A-B. Representative fluorescence confocal images for immunoreactivity for TPR1 (A-B; red) in *Lmnb1*$^{+/+}$ (A) and *Lmnb1*$^{\Delta/\Delta}$ (B) E17.5 embryo sections. Nuclei are counter-stained with Hoechst 33342 dye (blue). Scale bars 20 µm.

3.9 Lmnb1 deficiency has an effect on Notch signaling

However, it is important to understand whether any of the molecular pathways which are generally involved in differentiation are affected when Lmnb1 is absent, we decided to check the expression pattern of certain transcription factors downstream of the major molecular pathways involved. For this purpose, we decided to use DIV1 differentiated cells for both *Lmnb1*$^{\Delta/\Delta}$ and *Lmnb1*$^{+/+}$ along with their undifferentiated counterparts. We checked the expression pattern of transcription factors Hes1 and Hes5, which are downstream of Notch signaling pathway. It has been reported that Notch signaling pathway is essential for the proliferation and survival of progenitor cells as well as it promotes astrocyte differentiation and inhibits neurogenesis *(Grandbarbe et al, 2003, Mahajani et al, 2021)*. We observed a significant increase in the expression of Hes1 in *Lmnb1*$^{\Delta/\Delta}$ undifferentiated cells as compared to the *Lmnb1*$^{+/+}$ undifferentiated cells (Fig. 21A). At the same time, another downstream transcription factor of Notch signaling, Hes5 expression was observed to be significantly reduced in *Lmnb1*$^{\Delta/\Delta}$ undifferentiated cells as compared to the *Lmnb1*$^{+/+}$ undifferentiated cells (Fig. 21B). It has been reported that Hes1 promotes astrocyte differentiation, whereas Hes5 inhibits astrocyte and oligodendrocyte differentiation in neuroepithelial (NEP) cells *(Wu et al, 2003)*. The neurogenesis promoting transcription factor Neurogenin1 (Ngn1) was also observed to be significantly reduced in *Lmnb1*$^{\Delta/\Delta}$ differentiated cells as compared to the *Lmnb1*$^{+/+}$ differentiated cells (Fig. 21C). We also observed a significant increase in the expression of Sonic Hedgehog (Shh) in *Lmnb1*$^{\Delta/\Delta}$ differentiated cells as compared to the *Lmnb1*$^{+/+}$ differentiated cells (Fig. 21D). It has been known that Shh is required for ventral patterning of the neural tube in mouse *(Persson et al, 2002)*. Moreover, many in vitro protocols use Shh or agonist Purmorphamine to obtain GABAergic interneurons from human Induced pluripotent stem cells (iPSCs) *(Liu et al, 2013)*.

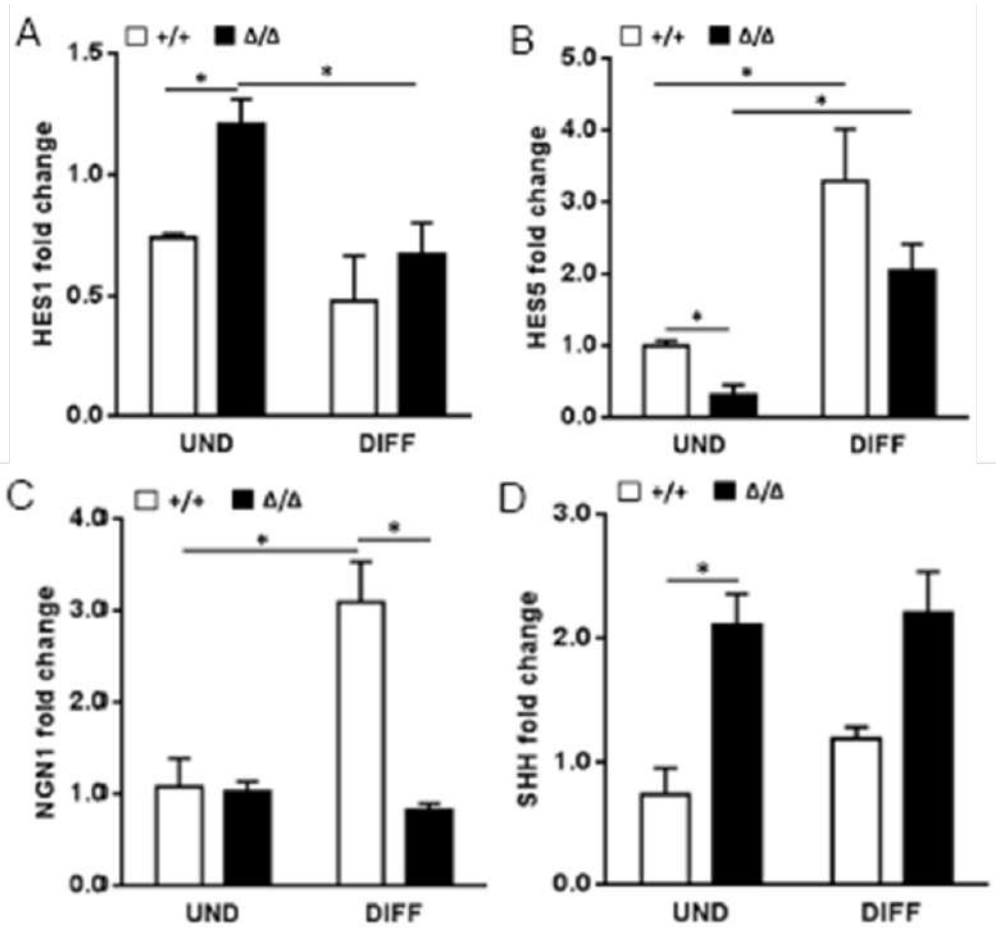

Figure 21. Lmnb1 deficiency alters Notch signaling in cultured NSCs.
A-D. Quantitative analysis of transcription factors. *Lmnb1*$^{+/+}$ and *Lmnb1*$^{\Delta/\Delta}$ undifferentiated and 1 DIV differentiated NSCs were analyzed for expression patterns of Notch signaling transcription factors HES1 (A) and HES5 (B) along with downstream bHLH transcription factor Neurogenin1 (NGN; C) and Sonic Hedgehog signaling (SHH; D), by qRT-PCR. Graph bars represent the average fold change ± SEM. *p<0.05 vs *Lmnb1*$^{+/+}$ at respective differentiation time, Student's t-test.

Expression patterns of Notch 2 mRNA along with other signaling pathways like Wnt-signaling pathway (β-catenin, Gsk3β, WNT), or JAK-STAT signaling pathway (STAT3) are not significantly affected when Lmnb1 is absent (Fig. 22A-E). These results indicate there is defective Notch signaling in Lmnb1 deficient NSCs.

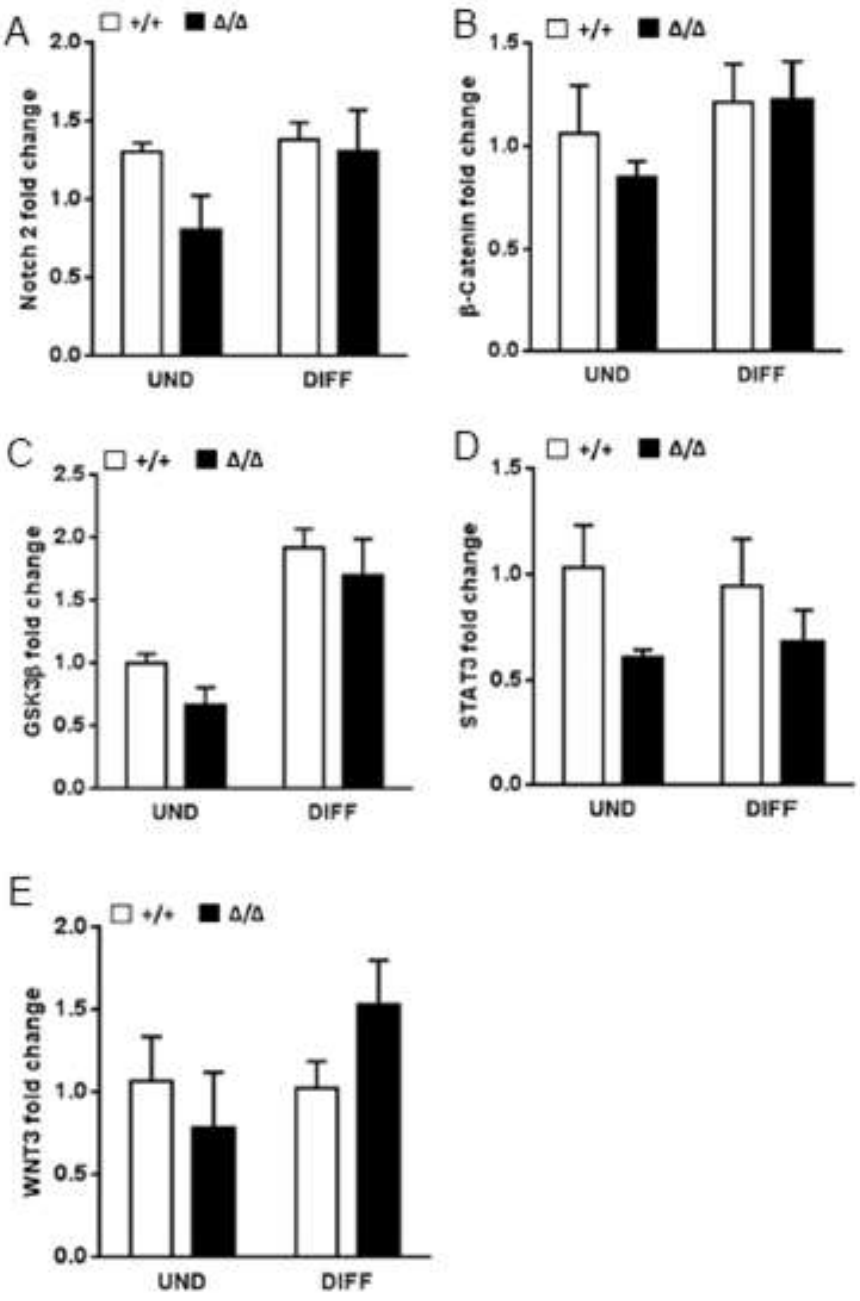

Figure 22. Lmnb1 deficiency does not affect other signaling pathways.
A-D. Quantitative analysis of transcription factors. *Lmnb1*$^{+/+}$ and *Lmnb1*$^{\Delta/\Delta}$ undifferentiated and 1 DIV differentiated NSCs were analyzed for expression patterns of Notch 2 (A) and other signaling pathways like β-Catenin (A), GSK3β (B), STAT3 (C) and WNT3 (D), by qRT-PCR. Graph bars represent the average fold change ± SEM.

We then activated Notch signaling using a ligand DLL4 in *Lmnb1*$^{+/+}$ NSCs (Fig. 23A-B) to observe its effect on the number of differentiated astrocytes. We found a significant increase in the number of astrocytes in DLL4 treated *Lmnb1*$^{+/+}$ cultures after 4DIV as compared to the untreated DLL4 *Lmnb1*$^{+/+}$ cultures (Fig. 23C; n=3; **p<0.01; Student's t-test). However, we did not observe a difference in the number of GFAP^{+} astrocytes at an early stage of differentiation i.e. 1DIV. We confirmed the increase in the number of astrocytes using Western blot analysis, and found a significant increase in the level of GFAP at 4DIV in DLL4 treated *Lmnb1*$^{+/+}$ cultures, but not at 1DIV as compared to their respective untreated *Lmnb1*$^{+/+}$ cultures (Fig. 23D-E; n=3; *p<0.05; Student's t-test).

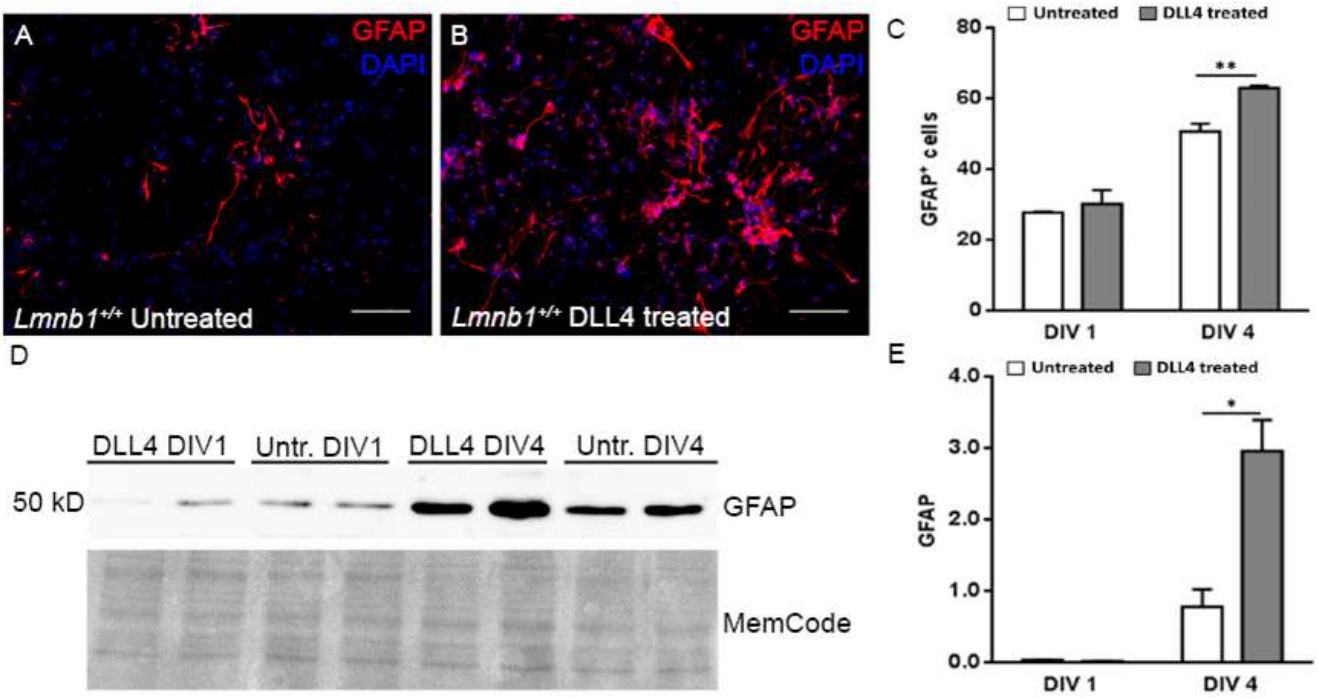

Figure 23. DLL4 induced Notch activation increases astrocytic number.

A-B. Representative fluorescence images of immunoreactivity for GFAP (A-B; red) in *Lmnb1*$^{+/+}$ NSCs either untreated (A) or DLL4 treated (B) at 4 DIV. Nuclei are counter-stained with DAPI (blue). Scale bars 100 µm.

C. Quantitative analysis of GFAP^{+} cells. The numbers of astrocytes (GFAP^{+}) were counted and expressed as percentage of the total number of cells identified by DAPI nuclear staining. Graph bars represent the average number of GFAP^{+}/DAPI^{+} ± SEM. **p<0.01 vs Untreated *Lmnb1*$^{+/+}$ differentiated cells at respective differentiation time, Student's t–test. Approximately, 1000 DAPI^{+} cells for each treatment condition were quantified in 3 independent experiments.

D. Western blot of GFAP in total lysates of *Lmnb1*$^{+/+}$ NSCs either untreated or DLL4 treated at 1 DIV or 4 DIV.

E. Quantitative analysis of GFAP expression. GFAP was normalized to MemCode. Graph bars represent the normalized values ± SEM. *p<0.05, vs untreated *Lmnb1*$^{+/+}$ differentiated cells at respective differentiation time, Student's t-test.

Next, we checked for the expression levels of full length Notch 1 and cleaved active Notch (NICD) in *Lmnb1*$^{+/+}$ and *Lmnb1*$^{\Delta/\Delta}$ E17.5 embryo brain lysates by Western blot analysis (Fig. 24A). Considering that the cells present in the brain at this age might be at different developmental stages, we observed no difference in the expression level of full length Notch 1 in *Lmnb1*$^{\Delta/\Delta}$ E17.5 embryo brain lysates as compared to the *Lmnb1*$^{+/+}$ (Fig. 24B). However, we did observe a significant reduction in the expression level of active NICD in *Lmnb1*$^{\Delta/\Delta}$ as compared to the *Lmnb1*$^{+/+}$ (Fig. 24C). When we quantified the rate of activation of NICD to full length Notch 1, we observed a significant decrease in *Lmnb1*$^{\Delta/\Delta}$ E17.5 embryo brain lysates as compared to *Lmnb1*$^{+/+}$ (Fig. 24D). We also performed quantitative analysis of the expression pattern of Notch 1 mRNA in in *Lmnb1*$^{+/+}$ and *Lmnb1*$^{\Delta/\Delta}$ undifferentiated and 1 DIV differentiated NSCs by qRT-PCR. We observed that during the course of differentiation, the expression level of Notch 1 mRNA showed significant increase in *Lmnb1*$^{\Delta/\Delta}$ differentiated cells as compared to the *Lmnb1*$^{\Delta/\Delta}$ undifferentiated NSCs (Fig. 24E). There was no significant change in the expression level of Notch 1 mRNA within *Lmnb1*$^{+/+}$ cells during differentiation.

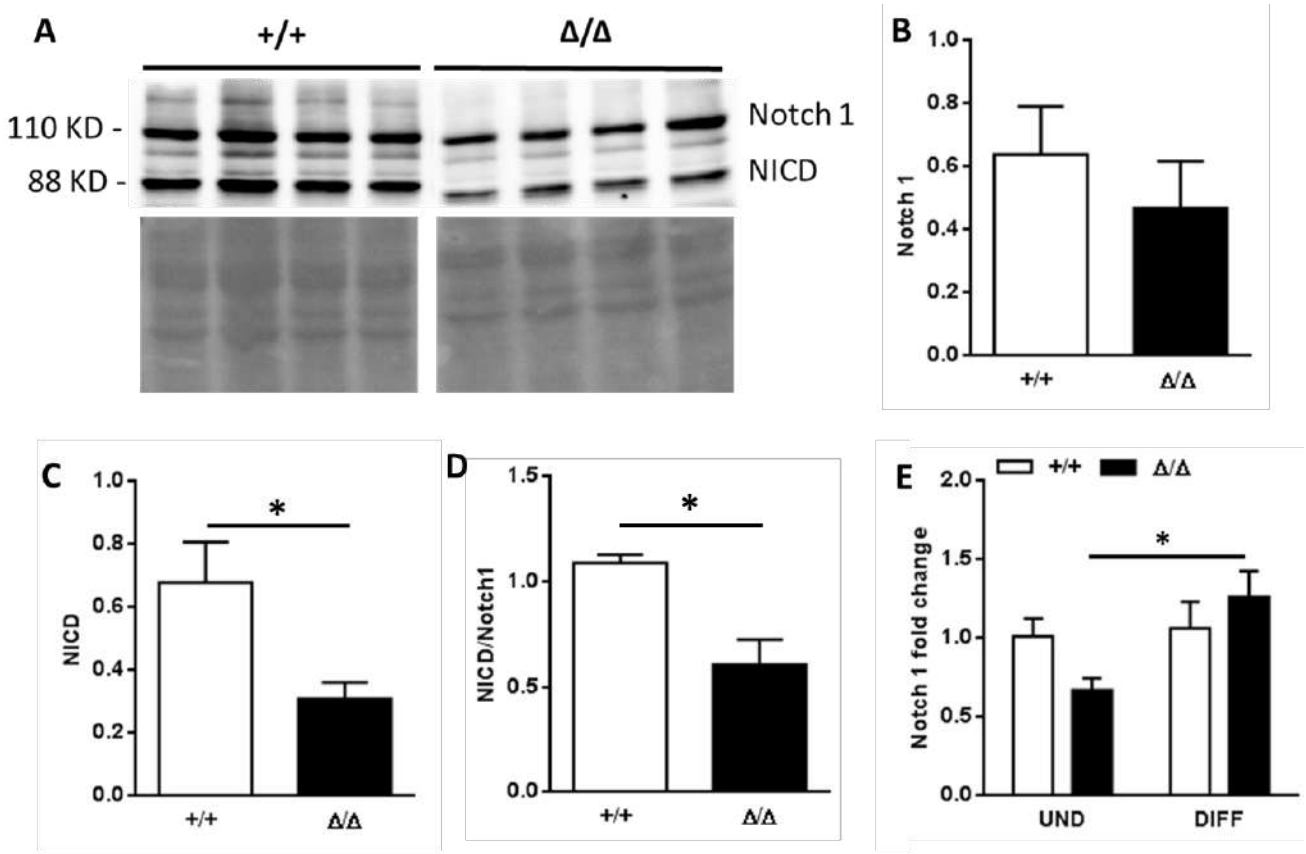

Figure 24. Lmnb1 deficiency reduces NICD expression and rate of Notch activation.

A-C. Quantification of expression levels of full length Notch 1 and NICD in *Lmnb1*$^{+/+}$ and *Lmnb1*$^{\Delta/\Delta}$ E17.5 embryo brain lysates. Normalization of Western blot was performed using MemCode. Graph bars represent the average expression levels of Notch 1 (B) or NICD (C) ± SEM. *p<0.05; Student's t-test.

D. Rate of activation determined by analyzing the ratio of expression levels of NICD to Notch 1 in *Lmnb1*$^{+/+}$ and *Lmnb1*$^{\Delta/\Delta}$ embryo brain lysates. Graph bars represent the average ratio of NICD to Notch 1 ± SEM. *p<0.05; Student's t-test.

E. Quantitative analysis of Notch 1 mRNA in *Lmnb1*$^{+/+}$ and *Lmnb1*$^{\Delta/\Delta}$ undifferentiated and 1 DIV differentiated NSCs by qRT-PCR. Graph bars represent the average fold change ± SEM. *p<0.05 vs *Lmnb1*$^{+/+}$ at respective differentiation time, Student's t-test.

We also checked for the expression of other genes by qRT-PCR (Fig. 25), however we did not observe any difference in their expression patterns in *Lmnb1*$^{+/+}$ and *Lmnb1*$^{\Delta/\Delta}$ undifferentiated and 1 DIV differentiated cells.

GENE	*Lmnb1*$^{+/+}$ UND	*Lmnb1*$^{+/+}$ DIFF	*Lmnb1*$^{\Delta/\Delta}$ UND	*Lmnb1*$^{\Delta/\Delta}$ DIFF
Actin	1.050 ± 0.245	1.459 ± 0.186	1.224 ± 0.332	1.165 ± 0.079
HPRT1	1.045 ± 0.200	0.706 ± 0.080	0.919 ± 0.250	0.866 ± 0.059
CBF1	1.013 ± 0.120	1.717 ± 0.105	0.767 ± 0.135	1.218 ± 0.125
HES3	1.039 ± 0.213	3.393 ± 0.459	1.159 ± 0.381	2.564 ± 0.294
NGN3	1.047 ± 0.221	1.631 ± 0.188	0.599 ± 0.071	2.739 ± 0.285

Figure 25. Expression levels of other transcription factors quantified by qRT-PCR.
Actin and HPRT1 was used as housekeeping genes throughout the qRT-PCR experiments.

DISCUSSION

4.1 Altered levels of Lmnb1 affects cell fate commitment

Lmnb1- deficient embryos show reduced cortical size and abnormal cortical layering. Various cortical layer specific markers were observed to be de-localized in *Lmnb1*$^{\Delta/\Delta}$ embryos *(Coffinier et al, 2011)*. However, the reason of reduced cortical size has not been reported. In our studies, we hypothesize that the reduction in cortical size and defect in cortical layering might be due to the defect in cell fate commitment during embryogenesis and/or defective neuronal migration. As it has been reported previously *(Molyneaux et al, 2007)*, neurogenesis starts around embryonic day 10.5-11 (E10.5-11) and finishes around E19-20 (time of birth). Moreover, glutamatergic and GABAergic neurons make up most of the cortical plate. Around 80% of the neurons observed in the cortical plate are glutamatergic in nature and the rest are GABAergic neurons *(Rakic, 2009)*. The glutamatergic neurons differentiate from the progenitor cells present in the sub-ventricular zone near the lateral ventricle and migrate upwards to make up the six layers of the cortical plate. However, the GABAergic neurons differentiate from the progenitor cells present in the Medial Ganglionic Eminence (MGE) and migrate tangential towards the cortical plate *(Molyneaux et al, 2007).*

We evaluated whether loss of Lmnb1 affect cell fate commitment using primary neural stem cell culture from Lmnb1-deficient embryos. After quantification for various cell types, we observed a significant increase in the number of differentiated astrocytes and a significant decrease in the number of differentiated neurons when Lmnb1 was absent. The number of differentiated oligodendrocytes were not affected in Lmnb1-deficient NSCs. This data could indicate that loss of Lmnb1 might promote astrocyte differentiation and inhibit neurogenesis in primary neural stem cells.

It has been reported that embryonic stem cells do not require Lmnb1 for self-renewal or pluripotency *(Kim et al, 2011)*. Consistent with previous reports, we did not observe any effect of loss of Lmnb1 on self-renewal property of NSCs. We also observed that Lmnb1-deficient does not cause apoptosis in these NSCs. Thereby, confirming that loss of Lmnb1 is not required for either survival or self-renewal of NSCs.

We also found that loss of Lmnb1 leads to changes in the gene expression pattern of cellular markers at a later stage of differentiation as compared to the undifferentiated state. Consistent with our results suggesting loss of Lmnb1 alters cell fate commitment, we observed a significant increase in the expression of GFAP mRNA and a significant reduction in βIII-tubulin mRNA levels in Lmnb1-deficient differentiated cells as compared to their respective counter-parts. After observing a reduction in the number of neurons, we decided to evaluate the expression level of doublecortin mRNA, which marks newly differentiated neurons. We observed that loss of Lmnb1 significantly reduces the expression of DCX mRNA in differentiated cells, suggesting that loss of Lmnb1 might delay neurogenesis. To confirm this, we quantified the expression pattern of Sox2, which marks the progenitor cells. Sox2 mRNA was significantly higher in Lmnb1-deficient differentiated cells as compared to the Lmnb1-deficient undifferentiated cells. This could suggest a defect in differentiation, as the number of progenitor cells should decrease in number during the course of differentiation, as observed in control differentiated cells compared to control undifferentiated cells.

Moreover, we found that LMNB1 overexpression affects cell fate commitment. After confirming that the pLMNB1-EGFP plasmid had the same transfection efficiency as the control, we transfected WT NSCs and observed a significant increase in the number of differentiated neurons when LMNB1 was overexpressed. No difference was observed in the number of astrocytes or oligodendrocytes

when LMNB1 was overexpressed. Considering the difference in cell fate commitment when Lmnb1 was either absent or overexpressed suggests that Lmnb1 might act as a switch between neurogenesis and astrocyte differentiation.

4.2 Altered Lmnb1 levels affect neuronal morphology

We thus evaluated whether Lmnb1 has any effect on the morphology of NSC-derived differentiated neurons. We observed a significant reduction in the axonal length of differentiated neurons when Lmnb1 was either absent or overexpressed. This could suggest that minute alteration in the level of Lmnb1 is detrimental to primary NSCs-derived neurons.

As Lmnb1 is responsible for providing structural integrity to the nucleus *(Vergnes et al, 2004)*, we evaluated the effect of altered levels of Lmnb1 to the nuclear size and shape of differentiated cells. We observed a significant reduction in the nuclear area and circularity in differentiated neurons when Lmnb1 was absent. We did not observe any change in the nuclear area and circularity in differentiated neurons when LMNB1 was overexpressed. We also did not observe any difference in the nuclear area or circularity in differentiated astrocytes or oligodendrocytes when Lmnb1 was either absent or overexpressed. This result suggests that normal level of Lmnb1 is essential to maintain proper nuclear size and shape, especially in neurons.

4.3 Lmnb1-deficient embryos show reduced cortical size due to reduction in the number of glutamatergic neurons

Confirming the previously published results *(Coffinier et al, 2011)*, we observed a significant reduction in the cortical thickness in Lmnb1-deficient embryos at E13.5, E15.5 and E17.5 as compared to the control. Moreover, we also observed a defective cortical plate to ventricular zone ratio in *Lmnb1*$^{\Delta/\Delta}$ E13.5 embryos as compared to control littermate. We further confirmed that this reduction in the cortical thickness was not due to the loss of progenitor cells present in the sub-ventricular as we did not observe any difference between *Lmnb1*$^{\Delta/\Delta}$ E13.5 embryos and control. However, we did observe a significant reduction in the number of neurons present in the cortical plate in Lmnb1-deficient E13.5 embryos as compared to the age matched control littermate. This could suggest that loss of Lmnb1 does not affect the survival of progenitor cells at an early stage of corticogenesis.

The cortical plate is made up of glutamatergic and GABAergic neurons *(Rakic, 2009)*. We, therefore, quantified the number of glutamatergic and GABAergic neurons present in a constant area per section of the cortex of *Lmnb1*$^{\Delta/\Delta}$ and *Lmnb1*$^{+/+}$ E19.5 embryos. We observed a significant decrease in the number of glutamatergic neurons and a significant increase in the number of GABAergic neurons in the cortical plate of Lmnb1-deficient embryos as compared to the control. As the cortical plate is majorly made up of glutamatergic neurons, the reduction in its number could explain the significant reduction in the cortical size of the *Lmnb1*$^{\Delta/\Delta}$ embryos. It has to be considered that the differentiation and migratory route of GABAergic neurons is different from that of the glutamatergic neurons.

To explain the increase we observe in the number of GABAergic neurons in the cortical plate of *Lmnb1*$^{\Delta/\Delta}$ E19.5 embryos, we hypothesized that reduction in the level of Lmnb1 could possibly

switch the fate of glutamatergic progenitor cells (present in the sub-ventricular zone) to GABAergic neurons which migrate into the cortical plate. Therefore, we decided to determine whether we observe any co-localization of Sh-Lmnb1 electroporation cells with GABA. However, we did not observe any co-localization of GABA neurons with $EGFP^{+}$ electroporated cells with either Sh-Lmnb1 or Sh-Scrambled. This data could indicate that there might be a defective GABAergic neuronal differentiation in the MGE or a defective GABAergic migration from the MGE to the cortical plate or a compensatory mechanism for the loss of glutamatergic neurons in the absence of Lmnb1.

As Lmnb1-deficient embryos show reduced cortical size, impaired cortical layering and reduction in the number of glutamatergic neurons in the cortex, we decided to analyze the number of progenitor cells in the cortical plate using Sox2 as the marker. During the course of differentiation the number of progenitor cells gradually decreases, as they differentiate into neurons which migrate into the cortical plate *(Rakic, 2009)*. However, we observed a significantly higher number of Sox2-positive cells in the cortical plate of Lmnb1-dificient E19.5 embryos as compared to its age matched control littermate. Consistent with previous reports *(Coffinier et al, 2011)*, this increase in the Sox2-positive cells was not observed in the cortical plate of E17.5 $Lmnb1^{\Delta/\Delta}$ embryos as compared to age matched control embryos. This could suggest that loss of Lmnb1 might lead to a delay in neuronal differentiation, and thereby increased number of Sox2-positive progenitor cells could still be observed at a later stage of development. This result is also in accordance with the increase in the expression level of Sox2 mRNA, which was observed in Lmnb1-deficient differentiated cells as compared to the Lmnb1-deficient undifferentiated cells.

4.4 Reduced Lmnb1 level *in vivo* increases the number of astrocytes

We have observed a significant decrease in the number of neurons when Lmnb1 was absent *in vitro* and *in vivo*. Further, we wanted to elucidate the effect of loss of Lmnb1 on the number of astrocytes *in vivo*. However, astrocytic differentiation starts postnatally and *Lmnb1*$^{\Delta/\Delta}$ embryos do not survive birth due to various lung and bone abnormalities *(Vergnes et al, 2004)*. We, therefore, used shRNA specific to LMNB1 to knockdown its expression *in vivo*. We observed approximately 50% reduction in the expression of Lmnb1 when Sh-Lmnb1 was transfected in N2A cells as compared to the empty (untransfected) or Sh-Scrambled transfected cells.

To evaluate the effect of reduced level of Lmnb1 on astrocytic differentiation *in vivo*, we performed in utero electroporation using Sh-Lmnb1 or Sh-Scrambled plasmids. After confirming that Sh-Lmnb1 does reduced the level of Lmnb1 *in vivo*, we quantified the expression of astrocytic marker GFAP in cortical plate of Sh-Lmnb1 electroporated brains as compared to the Sh-Scrambled electroporated brains at P7 of age. We observed a significant increase in the GFAP$^+$ area in the cortical plate of Sh-Lmnb1 electroporated brains. It is important to note that the increased GFAP$^+$ area is around the EGFP$^+$ Sh-Lmnb1 electroporated cells, but not with EGFP$^+$ Sh-Scrambled electroporated cells. This increase in GFAP$^+$ area provide further evidence that loss/reduction of Lmnb1 could promote astrocyte differentiation as compared to respective controls. Moreover, we also observed a significant increase in the expression of GFAP and a significant decrease in the expression of βIII-tubulin in Lmnb1-deficient E17.5 whole brain lysates as compared to the control by Western blot. However, it is essential to note that at E17.5 age of development, GFAP is known to mark progenitor cells as well as radial glial cells.

4.5 Altered level of Lmnb1 causes impaired neuronal migration *in vivo*

It has been previously reported Lmnb1-deficient embryos show defective cortical layering *(Coffinier et al, 2011)*, we evaluated the position of layer VI cortical layer markers Tbr1 and FoxP2 in Lmnb1-deficient embryos and observed them to be de-localized in the cortical plate of E17.5 *Lmnb1*$^{\Delta/\Delta}$ embryos as compared to the control. To elucidate whether this impaired cortical layering was due to defective neuronal migration when Lmnb1 levels are altered, we performed in utero electroporation using Sh-Lmnb1 (to knockdown Lmnb1) or pLMNB1-EGFP (to overexpress LMNB1) along with their respective controls in WT E14.5 embryos.

Upon knockdown of Lmnb1, we observed a significant impairment of neuronal migration *in vivo*. Majority of the Sh-Lmnb1 electroporated cells were located in the sub-ventricular zone or the sub-plate whereas majority of the Sh-Scrambled electroporated cells were situated in the layer V and VI of the cortical plate. This abnormal positioning of the Sh-Lmnb1 electroporated cells suggest a defective neuronal migration as the progenitor cells of the sub-ventricular zone are targeted during in utero electroporation.

After confirming that pLMNB1-EGFP does overexpress Lmnb1 *in vivo* after in utero electroporation, we used CTIP2 a layer V reference marker *(Molyneaux et al, 2007)*. After quantification of the position of electroporated cells with either pLMNB1-EGFP or control, we observed a significant decrease in the number of pLMNB1-EGFP^{+} electroporated cells within the CTIP2 layer as compared to the control. This suggests that either Lmnb1 knockdown or overexpression can also cause defective neuronal migration *in vivo*. It has also been reported that overexpression of LMNB1 in HEK293 and N2A cells mimics the mechanical phenotype of the nuclei from ADLD patient fibroblasts *(Ferrera et al, 2014)*. In ADLD patient fibroblasts, Lmnb1 is overexpressed at the nuclear lamina and specifically enhances nuclear stiffness. The authors also observed that altered levels of Lmnb1 in

ADLD patient fibroblasts alters nuclear mechanics and is linked to changes in nuclear signaling, which could help explain the pathogenesis of the disease *(Ferrera et al, 2014)*.

4.6 Absence of Lmnb1 causes de-localization of nuclear proteins

Along with providing structural integrity to the nucleus, Lmnb1 also plays a key role in maintaining proper organization of the nuclear protein on the membrane *(Vergnes et al, 2004)*. Lmnb1 deficiency also leads to de-localization of NPC in embryonic stem cell-derived fibroblast-like cells (EDFCs) and mouse embryonic fibroblasts (MEFs) *(Guo et al, 2014)*. Therefore, when we checked for localization of Nuclear Pore Complex (NPC) in cortical plate of $Lmnb1^{\Delta/\Delta}$ and $Lmnb1^{+/+}$ E17.5 embryos as well as in $Lmnb1^{\Delta/\Delta}$ and $Lmnb1^{+/+}$ derived NSCs, we observed a severe de-localization of NPC through the nuclear membrane of $Lmnb1^{\Delta/\Delta}$ E17.5 embryos or $Lmnb1^{\Delta/\Delta}$ derived NSCs as compared to their respective controls. The NPCs were irregularly spaced and often clusterized on the nuclear membrane in the absence of Lmnb1. As previously mentioned, NPCs play an important role in nuclear import and export of molecules from the cytoplasm *(Huenniger et al, 2010)*, we checked for the expression of certain nucleoporins (NUPs) which are present in the NPC. By Western blot analysis, we observed a significant decrease in the expression of Nup153 and Nup98, but not in Nup62 in Lmnb1-deficient whole brain lysates as compared to the control littermate. It has been reported that Lmnb1 interacts with Nup153, which is present in the inner ring of nuclear pore complex *(Jung et al, 2013)*. Therefore, this data suggests that loss of Lmnb1 not only causes de-localization of NPCs on the nuclear membrane but also reduces the expression of certain nucleoporins.

4.7 Notch signaling is specifically altered by loss of Lmnb1

Notch signaling has been reported to play a key role in stem cell proliferation and differentiation. According to previous studies, Notch signaling is important for proliferation of stem cells as well as it promotes astrocyte differentiation by inhibiting neurogenesis *(Grandbarbe et al, 2003)*. To understand the involvement of Notch signaling, we determined the expression pattern of its downstream transcription factors by qRT-PCR in *Lmnb1*$^{+/+}$ and *Lmnb1*$^{\Delta/\Delta}$ undifferentiated NSCs and early stage of differentiation (1DIV). After analysis, we observed a significant increase in the expression of HES1 in Lmnb1-deficient undifferentiated NSCs as compared to the control undifferentiated cells. HES1, a transcription factor activated directly by Notch, is reported to promote astrocyte differentiation *(Wu et al, 2003).* At the same time, the expression level of HES5 was observed to be significantly reduced in *Lmnb1*$^{\Delta/\Delta}$ undifferentiated NSCs as compared to its respective control. HES5, another transcription factor directly trigger by Notch signaling, is known to promote neurogenesis *(Wu et al, 2003)*. Neurogenin 1 (NGN1), is regulated by the expression of Notch transcription factors and is reported to promote neurogenesis in stem cells, was observed to be significantly reduced in *Lmnb1*$^{\Delta/\Delta}$ differentiated cells as compared to the control.

To determine whether loss of Lmnb1 affects other signaling pathways, we checked the expression patterns of Notch2, β-catenin WNT, JAK-STAT and GSK3β in *Lmnb1*$^{\Delta/\Delta}$ and *Lmnb1*$^{+/+}$ undifferentiated NSCs and differentiated cells. However, we did not observe any significant difference in the expression pattern of other signaling pathways during the course of differentiation when Lmnb1 was absent. Although, we did observe a significant increase in the expression of Sonic Hedgehog (SHH) mRNA in Lmnb1-deficient undifferentiated cells as compared to its respective control. SHH is reported to play a very essential role in the ventral patterning of neural tube during the course of development *(Persson et al, 2002).* It is also currently been used in the medium for *in vitro* culture of GABAergic neurons from embryonic stem cells *(Liu et al, 2013; Maroof et al, 2013).* This significant

increase in the expression of SHH mRNA in the absence of Lmnb1, could provide an indication as to why we observe a significant increase in the number of GABAergic neurons in the cortical plate of *Lmnb1*$^{\Delta/\Delta}$ E19.5 embryos as compared to the control.

Furthermore, we triggered endogenous Notch signaling using a ligand DLL4 in WT NSCs to observe the changes in the number of astrocytes after differentiation. Upon DLL4 treatment, we observed a significant increase in the number of astrocytes after 4 days of differentiation, but not after 1 day of differentiation as compared to the control untreated NSCs. Similar result was observed by Western blot where the expression of GFAP was significantly higher in DLL4 treated at 4 DIV, but not at 1DIV as compared to their respective untreated controls. This indicates that activated Notch promotes astrocyte differentiation in primary NSCs.

During this project, we observed that loss of Lmnb1 has an effect on cell fate commitment in vivo and in vitro, possibly via an impaired Notch signaling pathway. Loss of Lmnb1 is also detrimental to morphology of neurons more than astrocytes and oligodendrocytes. Reduction or overexpression of Lmnb1 impairs neuronal migration during corticogenesis.

CONCLUSION

It has been previously reported that loss of Lmnb1 can cause reduced cortical size and abnormal cortical layering during development. However, this defects could be due to either defective differentiation or impaired migration or both. Using murine primary neural stem cells, we observed a defective astrocytic vs neuronal differentiation in *Lmnb1*$^{\Delta/\Delta}$ NSCs. At the same time, we showed that the defect in cell fate commitment was due to an impaired Notch signaling in Lmnb1-deficient NSCs. We performed in utero electroporation in developing embryos to analyze the neuronal migration. We observed that the neuronal migration was affected when Lmnb1 was either absent or overexpressed. Therefore, we can conclude that loss of Lmnb1 affects cell fate commitment by promoting astrocyte differentiation over neurogenesis via a defective Notch signaling pathway and also impairs neuronal migration in developing mouse cortex.

REFERENCES

1. Al-Haboubi T, Shumaker D, Koeser J, Wehnert M and Fahrenkrog B (2011). Distinct association of the nuclear pore protein Nup153 with A- and B-type lamins. *Nucleus* **2**: 500-509.

2. Anderson J (2001). Stem cells and pattern formation in the nervous system. The possible versus the actual. *Neuron* **30**: 19-35.

3. Angevine J & Sidman L (1961). Autoradiographic study of cell migration during histogenesis of cerebral cortex in mouse. *Nature* **192**: 766–768.

4. Bartoletti-Stella A, Gasparini L, Giacomini C, Corrado P, Terlizzi R, Giorgio E, Magini P, Seri M, Baruzzi A, Parchi P, Brusco A, Cortelli P and Capellari S (2015). Messenger RNA processing is altered in autosomal dominant Leukodystrophy. *Human Molecular Genetics*: 1-11.

5. Bayer S & Altman J (1991) *Neocortical Development* 255 (Raven, New York).

6. Broers J, Machiels B, Kuijpers H, Smedts F, Kieboom R, Raymond Y, Ramaekers F (1997). A- and B-type lamins are differentially expressed in normal human tissues. *Histochemistry Cell Biology* **107**: 505-517.

7. Brussino A, Vaula G, Cagnoli C, Panza E, Seri M, Di Gregorio E, Scappaticci S, Camanini S, Daniele D, Bradac G, Pinessi L, Cavalieri S, Grosso E, Migone N and Brusco A (2010). A family with autosomal dominant Leukodystrophy linked to 5q23.2-q23.3 without lamin B1 mutation. *European Journal of Neurology* **17**: 541-549.

8. Caviness V & Takahashi T (1995). Proliferative events in the cerebral ventricular zone. *Brain Development* **17**: 159–163

9. Chen H, Chen X and Zheng Y (2013). The nuclear lamina regulates germline stem cell niche organization via modulation of EGFR signaling. *Cell Stem Cell* **13**: 73-86.

10. Coffeen C, McKenna C, Koeppen A, Plaster N, Maragakis N, Mihalopoulous J, Schewankhaus J, Flanigan K, Gregg R, Ptacek L and Fu Y (2000). Genetic localization of an autosomal dominant

Leukodystrophy mimicking chronic progressive multiple sclerosis to chromosome 5q31. *Human Molecular Genetics* **9**: 787-793.

11. Coffinier C, Jung H, Nobumori C, Chang S, Tu Y, Barnes R, Yoshinaga Y, Jong P, Vergnes L, Reue K et al (2011). Deficiencies in lamin B1 and lamin B2 cause neurodevelopmental defects and distinct nuclear shape abnormalities in neurons. *Molecular Biology of Cell* **22**: 4683-4693.
12. Colombi I, Mahajani S, Frega M, Gasparini L and Chiappalone M (2013). Effects of antiepileptic drugs on hippocampal neurons coupled to micro-electrode arrays. Frontiers in neuroengineering 6, 10.
13. Cordes V, Reidenbach S, Rackwitz H and Franke W (1997). Identification of protein p270/Tpr as a constitutive component of the nuclear pore complex-attached intranuclear filaments. *Journal of Cellular Biology* **136**: 515-529.
14. Couillard-Despres S, Winner B, Schaubeck S, Aigner R, Vroemen M, Weidner N et al (2005). Doublecortin expression levels in adult brain reflect neurogenesis. *European Journal of Neuroscience* **21**: 1-14.
15. Currle D, Hu J, Kolski-Andreaco A and Monuki E (2007). Culture of mouse neural stem cell precursors. *Journal of Visualized Experiments* **25**: 152.
16. Dauer W and Worman H (2009). The nuclear envelope as a signaling node in development and disease. *Developmental Cell* **17**: 626-638.
17. De Castro S, Malhas A, Leung K, Gustavsson P, Vaux D, Copp A and Greene N (2012). Lamin B1 polymorphism influences morphology of the nuclear envelope, cell cycle progression, and risk of neural tube defects in mice. *PLoS Genetics* **8**: e1003059.
18. Eldridge R, Anayiotos C, Schlesinger S, Cowen D, Bever C, Patronas N and McFarland H (1984). Hereditary adult-onset leukodustrophy simulating chronic progressive multiple sclerosis. *New England Journal of Medicine* **311**: 948-953.

19. Elkabetz Y and Studer L (2009). Human ESC-derived neural rosettes and neural stem cell progression. *Cold Spring Harbor Symposia on quantitative Biology* **73**: 377-387.

20. Espada J, Varela I, Flores I, Ugalde A, Cadinanos J, Pendas A, Stewart C, Tryggvason K, Blasco M, Freije J and Lopez-Otin C (2008). Nuclear envelope defects cause stem cell dysfunction in premature-aging mice. *The Journal of Cell Biology* **181**: 27-35.

21. Falcone C, Filippis C, Granzotto M and Mallamaci A (2015). Emx2 expression levels in NSCs modulate astrogenesis rates by regulating EgfR and Fgf9. *Glia* **63**: 412-422.

22. Ferrera D, Canale C, Marotta R, Mazzaro N, Gritti M, Mazzanti M, Capellari S, Cortelli P and Gasparini L (2014). Lamin B1 overexpression increases nuclear rigidity in autosomal dominant Leukodystrophy fibroblasts. **FASEB Journal 28**: 3906-3916.

23. Fuccillo M, Joyner A, Fishell G (2006). Morphogen to mitogen: the multiple roles of hedgehog signalling in vertebrate neural development. *Nature Reviews Neuroscience* **7**: 772-783.

24. Fukuda S, Abematsu M, Mori H, Yanagisawa M, Kagawa T, Nakashima K, et al (2007). Potentiation of astrogliogenesis by STAT3-mediated activation of bone morphogenetic protein-Smad signaling in neural stem cells. *Molecular Cell Biology* **27**: 4931-4937.

25. Giacomini C, Mahajani S, Ruffilli R, Marotta M and Gasparini L (2016). Lamin B1 protein is required for dendrite development in primary mouse cortical neurons. Molecular biology of the cell 27:35-47.

26. Grandbarbe L, Bouissac J, Rand M, Hrabé de Angelis M, Artavanis-Tsakonas S, Mohier E (2003). Delta-Notch signaling controls the generation of neurons/glia from neural stem cells in a stepwise process. *Development* **130**:1391-1402.

27. Guelen L, Pagie L, Brasset E, Meuleman W, Faza M, Talhout W, Eussen B, Klein A, Wessels L, Laat W and Steenesel B (2008). Domain organization of human chromosomes revealed by mapping of nuclear lamina interactions. *Nature* **453**: 948-951.

28. Guo Y, Kim Y, Shimi T, Goldman R and Zheng Y (2014). Concentration-dependent lamin assembly and its roles in the localization of other nuclear proteins. *Molecular Biology of Cell* **25**: 1287-1297.

29. Hatton B, Knoepfler P, Kenney A, Rowitch D, de Alborán I, Olson J, et al (2006). N-myc is an essential downstream effector of Shh signaling during both normal and neoplastic cerebellar growth. *Cancer Research* **66**: 8655-8661.

30. Hevner R, Daza R, Englund C, Kohtz J and Fink A (2004). Postnatal shifts of interneuron position in the neocortex of normal and reeler mice: evidence for inward radial migration. *Neuroscience* **124**: 605-618.

31. Hirsch C, Campano L, Wöhrle S, Hecht A (2007). Canonical Wnt signaling transiently stimulates proliferation and enhances neurogenesis in neonatal neural progenitor cultures. *Experimental Cell Research* **313**: 572-587.

32. Huenniger K, Kramer A, Soom M, Chang I, Kohler M, Depping R, Kehlenbach R and Kaether C (2010). Notch1 signaling is mediated by importins alpha 3, 4 and 7. *Cellular and Molecular Life Sciences* **67**: 3187-3196.

33. Hutton S and Pevny L (2011). Sox2 expression levels distinguish between neural progenitor populations of the developing dorsal telencephalon. *Developmental Biology* **352**: 40-47.

34. Jagatheesan G, thanumalayan S, Muralikrishna B, Rangaraj N, Karande A and Parnaik V (1999). Colocalization of intranuclear lamin foci with RNA splicing factors. *Journal of Cell Science* **24**: 4651-4661.

35. Jung H, Nobumori C, Goulbourne C, Tu Y, Lee J, Tatar A, Wu D, Yoshinaga Y, Jong P, Coffinier C, Fong L and Young S (2013). Farnesylation of lamin B1 is important for retention of nuclear chromatin during neuronal migration. *Proc Natl Acad Sci* **110**: E1928-E1932.

36. Kasai M, Satoh K, Akiyama T (2005). Wnt signaling regulates the sequential onset of neurogenesis and gliogenesis via induction of BMPs. *Genes Cells* **10**:777-783.

37. Kim Y, Sharov A, McDole K, Cheng M, Hao H, Fan C, Gaiano N, Ko M and Zheng Y (2011). Mouse B-type lamins are required for proper organogenesis but not by embryonic stem cells. *Science* **334**: 1706-1710.

38. Kole T, Tseng Y, Jiang I, Katz J and Wirtz D (2005). Intracellular mechanics of migration fibroblasts. *Molecular Biology of the Cell* **16**: 328-338.

39. Lai E (2002). Notch cleavage: Nicastrin helps Presenilin make the final cut. *Current Biology* **12**:200-202.

40. Lammerding J, Fong L, Ji J, Reue K, Stewart C, Young S and Lee R (2006). Lamins A and C but not lamin B1 regulate nuclear mechanics. *Journal of Biological Chemistry* **281**: 25768-25780.

41. Lin S and Fu Y (2009). miR-23 regulation of lamin B1 is crucial for oligodendrocyte development and myelination. *Disease Model Mechanisms* **2**: 178-188.

42. Lin S, Heng M, Ptacek L and Fu Y (2014). Regulation of myelination in the central nervous system by nuclear Lamin B1 and non-coding RNAs. *Translational Neurodegeneration* **3**: 4.

43. Liu Y, Liu H, Sauvey C, Yao L, Zarnowska E and Zhang S (2013). Directed differentiation of forebrain GABA interneurons from human pluripotent stem cells. *Nature Protocols* **8**: 1670-1679.

44. Louvi A, Artavanis-Tsakonas S (2006). Notch signaling in vertebrate neural development. *Nature Reviews Neuroscience* **7**:93-102.

45. Machon O, Backman M, Machonova O, Kozmik Z, Vacik T, Andersen L, et al (2007). A dynamic gradient of Wnt signaling controls initiation of neurogenesis in the mammalian cortex and cellular specification in the hippocampus. *Developmental Biology* **311**:223-237.

46. Mahajani S, Baehr M and Kuegler S (2021). Patterning inconsistencies restrict the true potential of dopaminergic neurons derived from human induced pluripotent stem cells. Neural regeneration research 16:692.

47. Mahajani S, Chavan S, Mahajani S and Raman K (2010). Biodiesel production from algae exposed to stressful conditions. Journal of Pure and Applied Microbiology 4: 339-342.

48. Mahajani S, Giacomini C, Marinaro F, Tonelli D, Contestabile A and Gasparini L (2017). Lamin B1 levels modulate differentiation into neurons during embryonic corticogenesis. Scientific reports 7:1-11.

49. Mahajani S, Raina A, Fokken C, Kuegler S and Baehr M (2019). Homogeneous generation of dopaminergic neurons from multiple hiPSC lines by transient expression of transcription factors. Cell death & disease 10: 1-15.

50. Malhas A, Lee C, Sanders R, Saunders N and Vauz D (2007). Defects in lamin B1 expression or processing affect interphase chromosome position and gene expression. *Journal of Cellular Biology* **176**: 593-603.

51. Mamber C, Kozareva D, Kamphuis W and Hol E (2013). Shades of gray: the delineation of marker expression within the adult rodent subventricular zone. *Progress in Neurobiology* **111**: 1-16.

52. Maroof A, Keros S, Tyson J, Ying S, Ganat Y, Merkle F, Liu B, Goulburn A, Stanley E, Elefanty A, Widmer H, Eggan K, Goldstein P, Anderson S and Studer L (2013). Directed Differentiation and Functional Maturation of Cortical Interneurons from Human Embryonic Stem Cells. *Cell Stem Cell* **12**: 559-572.

53. Marotta R, Catelani T, Pesce M, Giacomini C, Mahajani S and Gasparini L (2016). Role of Lamin B1 in structuring the cell nucleaus in eukaryotic cells. European Microscopy Congress 1011-1012.

54. Molyneaux B, Arlotta P, Menezes J and Macklis J (2007). Neuronal subtype specification in the cerebral cortex. *Nature Review Neuroscience* **8**: 427-437.

55. Okada T, Keino-Masu K and Masu M (2007). Migration and nucleogenesis of mouse precerebellar neurons visualized by in utero electroporation of a green fluorescent protein gene. *Neuroscience Research* **57**: 40-49.

56. Padiath Q and Fu Y (2010). Autosomal dominant Leukodystrophy caused by lamin B1 duplications a clinical and molecular case study of altered nuclear function and disease. *Methods in Cell Biology* **98**: 337-357.

57. Padiath Q, Saigoh K, Schiffmann R, Asahara H, Yamada T, Koeppen A, Hogan K, Ptacek L and Fu Y (2006). Lamin B1 duplications cause autosomal dominant Leukodystrophy. *Nature Genetics* **38**: 1114-1123.

58. Pajerowski J, Dahl K, Zhong F, Sammak P and Discher D (2007). Physical plasticity of the nucleus in stem cell differentiation. *PNAS* **104**: 15619-15624.

59. Pan H, Oliveria B, Saher G, Dere E, ….., Luehder F and Ehrenreich H (2019). Uncoupling the widespread occurrence of anti-NMDAR1 autoantibodies from neuropsychiatric disease in a novel autoimmune model. Molecular psychiatry 24: 1489-1501.

60. Persson M, Stamataki D, Welscher P, Andersson E, Bose J, Ruther U, Ericson J and Briscoe J (2002). Dorsal-ventral patterning of the spinal cord requires Gli3 transcriptional repressor activity. *Genes and Development* **16**: 2865-2876.

61. Peters A & Jones E (1984). Cellular Components of the Cerebral Cortex*. Plenum*, New York.

62. Pietro C, Brusco A, Brussino A, Giorgio E, Antonarakis S, … Mahajani S, Giacomini C and Gasparini L (2015). Clinical, neuroradiological and molecular investigation of Adult-onset Autosomal Dominant LeukoDystrophy (ADLD): dissection of Lamin B1-mediated

pathophysiological mechanisms in cellular and mouse models. XIII Scientific Convention 39-40.

63. Psol M, Darvas S, Leite K, Mahajani SU, Baehr M and Kuegler S (2021). Dementia with Lewy bodies – associated β-synuclein mutations V70M and P123H cause mutation-specific neuropathological lesions. Human Molecular Genetics 30, 247-264.

64. Raina A, Leite K, Guerin S, Mahajani SU, Chakrabarti K, …. and Kuegler S (2021). Dopamine promotes the neurodegenerative potential of β-synuclein. Journal of Neurochemistry 156: 674-691.

65. Raina A, Mahajani S, Baehr M and Kuegler S (2020). Neuronal trans-differentiation by transcription factors Ascl1 and Nurr1:induction of a dopaminergic neurotransmitter phenotype in cortical GABAergic neurons. Molecular neurobiology 57:249-260.

66. Rakic P (1974). Neurons in rhesus monkey visual cortex: systematic relation between time of origin and eventual disposition. *Science* **183**: 425–427.

67. Ramón y Cajal, S (1995). Histology of the Nervous System of Man and Vertebrates*. Oxford University Press*, New York.

68. Ribeiro A and Dahl K (2010). The nucleus as a central structure in defining the mechanical properties of stem cells. *Conf. Proc. IEEE Engg Med Bio Soc* : 831-834.

69. Robinson A, Partridge D, Malhas A, De Castro S, Gustavsson P, Thompson D, Vaux D, Copp A, Stanier P, Bassuk A and Greene N (2014). Is LMNB1 a susceptibility gene for neural tube defects in humans? *Birth Defects Research. Part A, clinical and molecular teratology* 97: 398-402.

70. Saito T (2006). In vivo electroporation in the embryonic mouse central nervous system. *Nature Protocols* 1: 1552-1558.

71. Smythe C, Jenkins H and Hutchinson C (2000). Incorporation of the nuclear pore basket protein nup153 into nuclear pore structures is dependent upon lamina assembly: evidence from cell-free extracts of Xenopus eggs. *EMBO Journal* **19**: 3918-3931.

72. Takahashi J, Palmer T and Gage F (1999). Retinoic acid and neurotrophins collaborate to regulate neurogenesis in adult-derived neural stem cell cultures. *Journal of Neurobiology* **38**: 65-81.

73. Takamori Y, Tamura Y, Kataoka Y, Cui Y, Seo S, Kanazawa T, Kurokawa K and Yamada H (2007). Differential expression of nuclear lamin, the major component of nuclear lamina, during neurogenesis in two germinal regions of adult rat brain. *European Journal of Neuroscience* **25**: 1653-1662.

74. Tang C, Maya-Mendoza A, Martin C, Zeng K, Chen S, Feret D, Wilson S and Jackson D (2008). The integrity of a lamin B1-dependent nucleoskeleton is a fundamental determinant of RNA synthesis in human cells. *Journal of Cell Science* **121**: 1014-1024.

75. Taylor M, Yeager K, Morrison S (2007). Physiological Notch signaling promotes gliogenesis in the developing peripheral and central nervous systems. *Development* **134**: 2435-2347.

76. Towbin B, Meister P and Gasser S (2009). The nuclear envelope – a scaffold for silencing? *Current Opinion in Genetics and Development* **19**: 180-186.

77. Tunnah D, Sewry C, Vaux D, Schirmer E and Morris G (2005). The apparent absence of lamin B1 and emerin in many tissue nuclei is due to epitope masking. *Journal of Molecular Histology* **36**: 337-344.

78. Vergnes L, Peterfy M, Bergo M, Young S and Reue K (2004). Lamin B1 is required for mouse development and nuclear integrity. *Proc Natl Acad Sci* **101**: 10428-10433.

79. Wakhloo D, Mahajani S, Tembe P and Raut A (2013). Lactobacillus plantarum shows more probiotic potential than S. cremoris. Journal of Pure and Applied Microbiology 7: 565-570.

80. Wakhloo D, Scharkowski F, Curto Y, … and Ehrenreich H (2020). Functional hypoxia drives neuroplasticity and neurogenesis via brain erythropoietin. Nature communication 11:1-12.

81. Wen S, Li H and Liu J (2009). Dynamic signaling for neural stem cell fate determination. *Cell Adhesion and Migration* **3**: 107-117.

82. Wu Y, Liu Y, Levine E and Rao M (2003). Hes1 but not Hes5 regulates an astrocyte versus oligodendrocyte fate choice in glial restricted precursors. *Developmental Dynamics* **226**: 675-689.

83. Yanagisawa M, Nakashima K, Taga T (1999). STAT3-mediated astrocyte differentiation from mouse fetal neuroepithelial cells by mouse oncostatin M. *Neuroscience Letters* **269**:169-172.

84. Yokota Y, Ghashghaei H, Han C, Watson H, Anton E (2007). Radial Glial Dependent and Independent Dynamics of Interneuronal Migration in the Developing Cerebral Cortex. *PLOS ONE* **8**: e754.

85. Yoon B, Jung H, Dwivedy A, O'Hare C, Zivraj K and Holt C (2012). Local translation of extracellular lamin B promotes axon maintenance. *Cell* **148**: 752-764.

86. Zechner D, Fujita Y, Hülsken J, Müller T, Walther I, Taketo M, et al (2003). Beta-Catenin signals regulate cell growth and the balance between progenitor cell expansion and differentiation in the nervous system. *Developmental Biology* **258**:406-418.